8426477

Shah, Jami Jamshed

NONLINEAR FINITE ELEMENT ANALYSIS OF ELASTIC AND ELASTIC-PLASTIC BUCKLING OF CYLINDERS UNDER COMPLEX COMBINED LOADS

The Ohio State University

PH.D. 1984

University Microfilms International 300 N. Zeeb Road, Ann Arbor, MI 48106

PLEASE NOTE:

In all cases this material has been filmed in the best possible way from the available copy. Problems encountered with this document have been identified here with a check mark __√__.

1. Glossy photographs or pages _____
2. Colored illustrations, paper or print _____
3. Photographs with dark background _____
4. Illustrations are poor copy _____
5. Pages with black marks, not original copy _____
6. Print shows through as there is text on both sides of page _____
7. Indistinct, broken or small print on several pages __√__
8. Print exceeds margin requirements _____
9. Tightly bound copy with print lost in spine _____
10. Computer printout pages with indistinct print _____
11. Page(s) __________ lacking when material received, and not available from school or author.
12. Page(s) __________ seem to be missing in numbering only as text follows.
13. Two pages numbered __________. Text follows.
14. Curling and wrinkled pages _____
15. Other ____

NONLINEAR FINITE ELEMENT ANALYSIS OF ELASTIC

AND ELASTIC-PLASTIC BUCKLING OF CYLINDERS UNDER

COMPLEX COMBINED LOADS

Dissertation

Presented in Partial Fulfillment of the Requirements
for the Degree of Doctor of Philosophy
in the Graduate School

by

Jami J. Shah, B.E.M.E., M.S. Met. E.

*****

The Ohio State University
1984

Reading Committee
Dr. J.A. Collins
Dr. K.J. Waldron

Approved By

Gary L. Kinzel
Dr. G.L. Kinzel

and

Henry R. Busby
Dr. H.R. Busby
Department of Mechanical
Engineering

THE BLIND MEN AND THE ELEPHANT

by John G. Saxe

It was six men of Indostan to learning much inclined,
    Who went to see the Elephant (though each of them were blind),
That each by observation might satisfy his mind.

The First approached the Elephant and happening to fall
    Against his broad and sturdy side, at once began to bawl:
"God bless me! but the Elephant is very like a wall!"

The Second, feeling of the tusk, cried, "Ho! what have we here
    So very round and smooth and sharp? To me 'tis very clear
This wonder of an Elephant is very like a spear!"

The Third approached the animal and happening to take
    The squirming trunk within his hands, thus boldly up and spake;
"I see," quoth he, "the Elephant is very like a snake!"

The Fourth reached out his eager hand, and felt about the knee.
    "What most this mighty beast is like is mighty plain," quoth he;
"'Tis clear enough the Elephant is very like a tree!"

The Fifth, who chanced to touch the ear, said "E'en the blindest man
    Can tell what this resembles most; deny the fact who can,
This marvel of an Elephant is very like a fan!"

The Sixth no sooner had begun about the beast to grope,
    Than seizing on the swinging tail that fell within his scope,
"I see," quoth he, "the Elephant is very like a rope!"

And so these men of Indostan disputed loud and long,
    Each in his own opinion exceeding stiff and strong,
Though each was partly in the right, and all were in the wrong!

TABLE OF CONTENTS

Acknowledgements

The author is extremely grateful to his Advisor, Dr. Kinzel, for his help and support. The project was his idea which was derived from the work done by him at Battelle Columbus Laboratories. The author is especially grateful to him for providing a VT100 computer terminal which the author installed in his home and connected to OSU's computing facilities. Without this terminal the task would have been considerably more difficult.

A very special thanks are due to Dr. Busby, who served as the author's co-adviser. He devoted considerable time to this project. The author found the discussions with him very useful. His willingness to help and to share his vast collection of books and papers is greatly appreciated.

The author is also indebted to Drs. Collins and Waldron for serving on the Committee. Lastly, the author thanks the Department of Mechanical Engineering for allowing unlimited use of the computers in the Advanced Design Methods Laboratory and the Instruction and Research Computer Center (inspite of its poor accessibility and 'User unfriendliness'). The cooperation of the ADML staff, especially Cliff Collins and George Jones is greatly appreciated. The author also apologizes to other users of these facilities for having inconvenienced them by running such large jobs on these computers.

Most of all, the author wishes to acknowledge the love and support of his parents and brothers and sisters, inspite of very difficult and trying times for the family.

VITA

Hometown: Karachi, Pakistan

Education

High School:	School Certificate, University of Cambridge, England, 1966
Undergraduate:	Bachelor of Engineering (Mechanical), N.E.D. Engineering College, Karachi, 1973
Graduate:	Master of Science (Metallurgical Engineering), University of Pittsburgh, 1976

Professional Experience

1973 - 1975	Graduate Engineer, Pakistan Steel, Karachi
1976 - 1978	Product Engineer, Pakistan Oxygen Limited, Karachi
1978 - 1980	Manager Production, Electrode Factory, Pakistan Oxygen Limited, Karachi
1981 - 1984	Teaching Associate, Department of Mechanical Engineering, The Ohio State University, Columbus

Honor Societies

Member, Sigma Xi

LIST OF FIGURES

I. INTRODUCTION

The many publications on the stability of shells demonstrates that uncertainties still exist in this area. It is well known that structures of this class often collapse at load levels which are less than those predicted by linear instability theory. The advent of the finite element method has drawn renewed interest in this area, since the inherent nonlinearities in buckling problems can be modelled effectively by this method.

Various types of instability phenomena are observed in practice, as shown by means of the Load - Displacement curves in Fig. 1. In (a), the path OB is the fundamental path and AC is the secondary or bifurcation path. The point at which the two paths intersect is known as the bifurcation point. The transition from the primary equilibrium path to the bifurcation path is called bifurcation buckling. The post buckling path may be ascending, as in (a), or descending, as in (b). These curves are valid for "perfect" structures. If the structure has initial imperfections, then the path followed would be indicated by the dashed lines. In these paths there is no bifurcation point. The structure with a rising postbuckling path will be able to endure loads higher than the bifurcation load. The imperfect structure in (b) will have lower strength. Structures of the latter type are termed "imperfection sensitive" and the maximum load attained is called the "limit point".

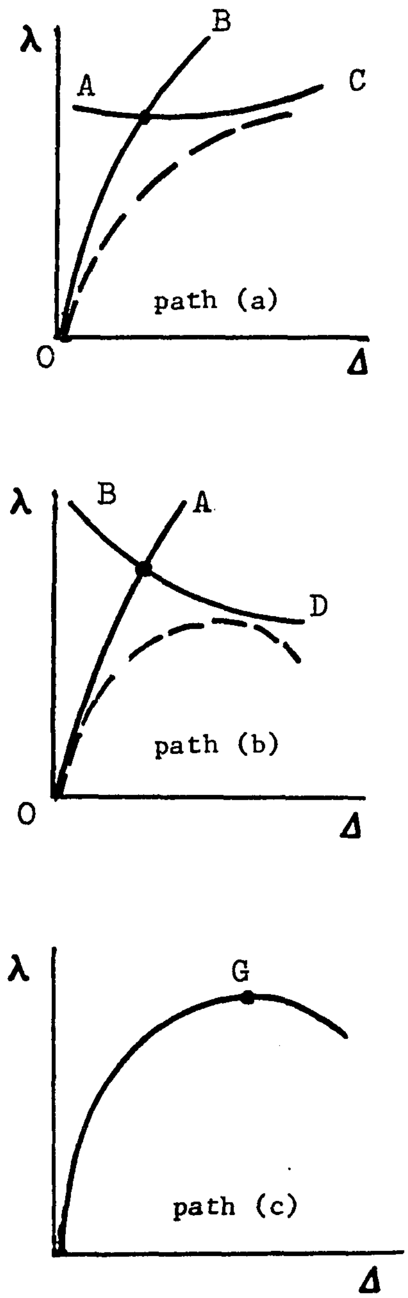

Figure 1 Load-displacement paths.

A non-bifurcating load-displacement behavior may also occur for structures devoid of imperfections, as shown by path (c) in Fig. 1. In such cases a limit point (G) is encountered.

The load-displacement curve is dependent upon material properties of the structure as well as its geometry. Inelastic material behavior, residual stresses, unknown boundary conditions, initial imperfections, and load interactions further complicate the problem of instability.

There are three types of buckling of thin cylinders corresponding to three types of membrane stresses: axial and circumferential normal stresses and shear stresses. To cause buckling the normal stresses must, of course, be compressive. Loading conditions that cause these stresses are axial compressive load, pure bending producing axial compressive stress and uniform circumferential stresses produced by uniform external pressure or internal vacuum, and uniform shear stresses produced by simple torsion. Combination of these stresses also occur such as during the laying operation of offshore pipelines, which involves external pressure, bending moment, and axial stress.

The present study is limited to unstiffened circular cylinders. The diameter to thickness ratio is a key factor in determining the buckling behavior of such structures. Thin shells buckle in the elastic range; the limiting D/t ratio for steel cylinders to buckle in the elastic range is not known accurately but is reported by some investigators to be in the vicinity of 250. Elastic buckling has been analyzed by classical shell theory. The most common approach was to use Donnel's, Timoshenko's or Flugge's equilibrium equations for thin shells and assume that the shape of the deformation curves could be modelled by trigonometric functions. In other words, solution of three partial differential equations in three unknowns: the displacements u,v,w. This approach was used in most classical works, and several loading cases have been treated in this manner, viz. axial loads, internal/external pressure, lateral pressure, and combined external pressure and axial load.

It was first pointed out by Brazier in 1927, that the cross-section of thin tubes subjected to bending, ovalizes before buckling. Therefore, these tubes collapse before developing their full moment. This also makes the moment-curvature relationship nonlinear. The D/t ratio at which significant ovalization takes place was determined experimentally by Ades [33]* to be in the range 10 - 50. Other studies disagree with this value [44].

Stresses in thick cylinders reach the plastic range before buckling occurs. The problem is further complicated by the fact that one part of the material may be unloading into the elastic range while another is loading beyond the yield point. This occurs if it is assumed that the axial load remains constant, after reaching the plastic range, while bending is initiated. In classical studies, Young's modulus was simply replaced by the tangent modulus or the reduced modulus in the formulae derived from elastic analysis. More recent studies used a flow rule and a hardening rule to relate stress to strain and substituted these

---

* numbers in square brackets are reference numbers listed at the end of this dissertation

relations in the equilibrium relations used for deriving the modified Donnel equations.

Another mode of failure that becomes important at very high D/t ratios is local buckling. The final buckled configuration involves a localized deformation pattern (as shown in the Fig. 2) in contrast with a periodic deformation pattern over the entire structure that is associated with the gross buckling of the entire column.

The problem of buckling involves large displacements, large strains, and nonlinear material behavior. It is difficult to take these nonlinearities into account by using analytical methods. One must then resort to numerical methods. In the last decade, there has been a considerable amount of work done in the area of nonlinear finite element analysis. However, when formulating the finite element problem one must keep computational capability and efficiency in mind. Reliable and efficient representations of the curved shell element are first required and this has not been an easy task due to conditions such as interelement displacement continuity.

Nonlinear finite element analysis can be divided into three categories: (i) materially nonlinear problems only, (ii) large displacements but small strains, (iii) large displacements and large strains. Most buckling problems are a combination of the first two. Nonlinear problems can be formulated in three different ways: generalized potential energy, hybrid stress, and mixed formulations. In the generalized potential energy approach, the element stiffness

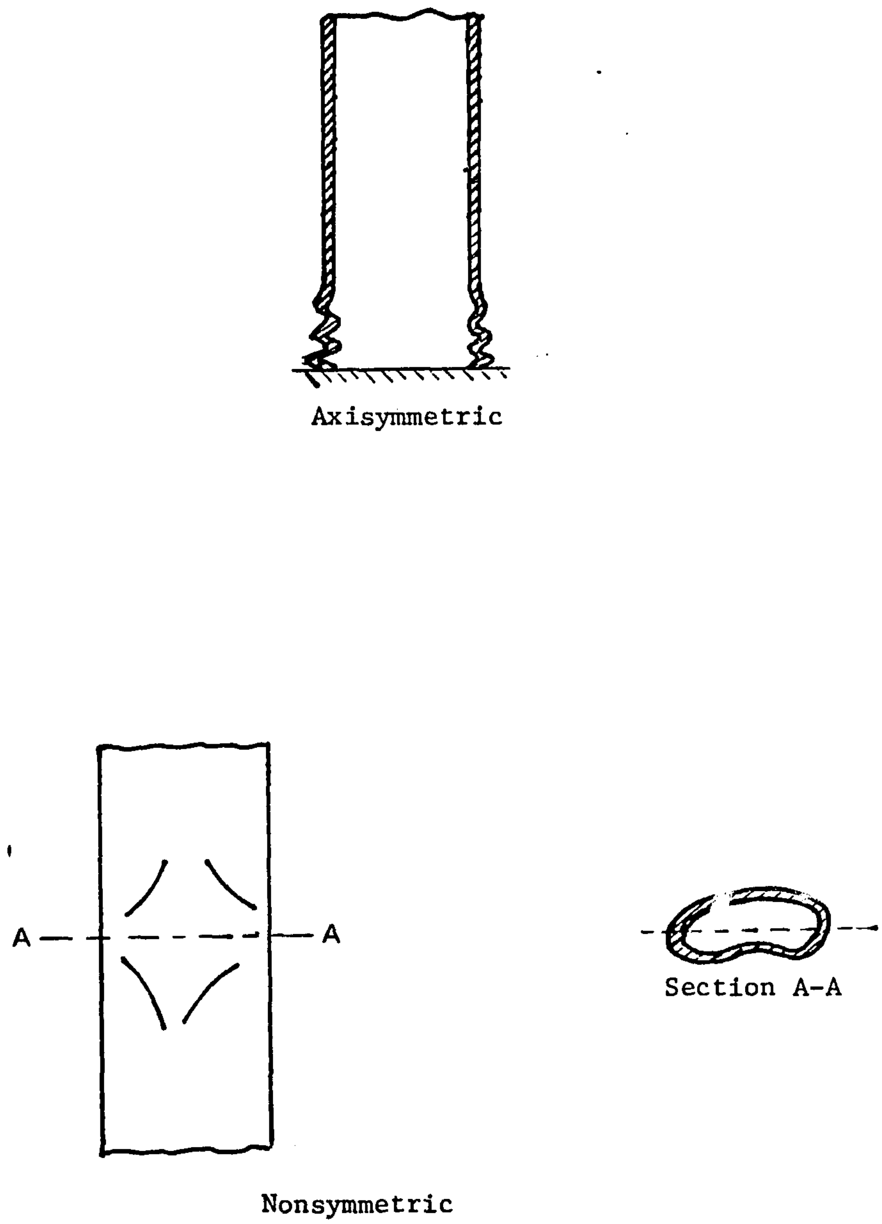

Figure 2 Localized buckling patterns.

matrices are formed and summed to give a global stiffness matrix, but without specific attention to the conditions of interelement continuity of displacement. Constraint conditions are then written, whose purpose it is to enforce the requirements of interelement displacement continuity. The constraint conditions are added to the potential via Lagrange multipliers or penalty functions. Mixed variational principles are functionals written in terms of two or more fields of structural mechanics. They permit the independent approximation of the respective fields which appear in the variational integral. Each field is approximated in terms of its physical values at the node points, such as stresses or displacements. Hybrid element formulations are special forms of energy functionals. They are developed from the conventional energy functionals by treating the element as an isolated, complete structure during the formulative phase. One or more of the structural behavior parameters (e.g. stress, displacement) is approximated in terms of generalized parameters (non physical) while the others are approximated in terms of node point physical parameters, such as forces or displacements. The generalized parameters are eliminated at the element level through application of the stationary condition.

Few analytical studies have included the effect of combined loads. Some authors have suggested that the critical buckling stress be calculated for each mode separately and then the interaction of these loads determined by means of empirical formulae. With the finite element method, it is possible to consider complex loading. However, most researchers have assumed a specific order in which the loads are applied.

II. OBJECTIVES OF STUDY

The objective of this study was to determine the maximum allowable safe loads for cylinders, subjected to complex combined loads, using the nonlinear finite element method. The study is restricted to straight, hollow cylinders of circular cross-section, ranging in D/t ratio from 5 to 250. The formulation should include linear elastic as well as elastic-plastic material behaviors, which can be encountered in the D/t range given above. Few studies have dealt with combined loads and none have studied the influence of the order of loading and nonproportional or nonlinear loads. This study presents a formulation which can model any combination of external/internal pressure, axial loads, bending moments, and uniformly distributed lateral pressure. All loads can vary in any manner, can increase or decrease, linearly or nonlinearly, independently of each other. It is known that the load-displacement relationship is nonlinear for large displacements and nonlinear material behavior. Therefore, the loading history can have a considerable influence on the failure mode and limit point loads. It is here that this study makes its most important contribution.

The study also develops an elastic-plastic, large displacement, degenerated cylindrical shell element by extending the work of Bathe and Bolourchi [71].

There are no 'fool proof' solution techniques for nonlinear elements that guarantee convergence for all problems. This is especially true in the vicinity of limit points. This study examined some of these methods and used a combination of two commonly used methods. Various measures and indices were defined and used for speeding convergence, sensing the approach of limit points, and detecting the limit points.

III. OVERVIEW OF ANALYSIS TECHNIQUES

In the present study, the variational formulation of the Potential Energy principle is used. The load is assumed to be applied in several steps, thereby allowing linearization of the above governing equation in each loadstep. Coordinates and displacements are measured in a Total Lagrangian coordinate system. An iterative solution procedure is used in each loadstep to obtain convergence. Use of the Second Piola-Kirchhoff stress tensor and the Green-Lagrange strain tensor permits large rotations.

Many shell elements have been developed by previous investigators. In this study the degenerated shell element developed by Bathe and Bolourchi at MIT [71] is modified and extended to yield a large displacement, degenerated, elastic-plastic, cylindrical shell element. The element is parabolic (eight nodes per element) with five degrees of freedom per node (three translational, two rotational). Gauss quadrature is used to perform reduced numerical integration. These elements are based on the continuum strain-displacement relations and are degenerated using Kirchhoff's assumptions for shells; they are very general as no specific shell theory has been used. The elements can model linear-elastic or elastic-plastic deformations under membrane as well as bending stresses. A comparison of non-degenerated continuum elements was made with degenerated shell elements under various types of loads.

A quasi-Newton scheme is used for solving the nonlinear equations, with the stiffness matrix being updated only once per loadstep to reduce computations. The linear equation solver is based on LDL^T decomposition; a skyline algorithm is used [46].

Several alternative measures of structural 'softening' have been proposed here and tried. These are used to predict the approach of limit points so that solution strategy may be changed before the solution goes unstable. A new use for these softening parameters is also proposed: when the softening parameter is below a certain linearity index the problem may be treated as linear, eliminating the need for unnecessary iterating. Once the stiffness parameter falls below a critical value (stability criterion), displacement control may be used to find the limit point. A necessary condition for this is that the determinant of the stiffness matrix change sign. This indirect method can be used, with displacement control, to find the limit point.

Plasticity relations are based on the von Mises yield criterion, isotropic hardening rule, and the incremental theory of plasticity. These choices were made because the primary aim is to model buckling behavior of steel pipes.

A computer-program, called 'BUCKS.OSU' was written to validate the above ideas. A special purpose mesh generation program 'PREP' and a graphics model checking program 'DSPLAY' are used for preparing the data input. The hardening indices, required in elastic-plastic analysis, can be obtained from curve-fitting experimental data of a tension test.

This may be done using program 'SSCURV' for the three material models used: Bilinear, Exponential, and Ramberg-Osgood.

Runs of the above program were made under various combinations of loads. First, single loads were considered this included stability analysis under pure pressure and under pure bending. Combinations of external pressure and bending moments were also considered and the results compared to Battelle's experiments [43].

IV. LITERATURE REVIEW

Investigators have used many different tools for studying the complex problem of shell stability. Some of these are:

i) analytical

ii) experimental

iii) finite elements

A survey of each of these follows.

Analytical Studies

Classical works, such as [2]-[4] have considered the buckling of beam-columns i.e. columns under combined axial load and lateral distributed load. Euler's formula is a special case of this. Buckling of thin shells has been analyzed as follows: some form of shell equilibrium equations are written for a given mode of loading. Substituting linear elastic constitutive relations and kinematic relations into the equilibrium equations yields a set of partial differential equations in the dependent variables u, v, w, the translational displacements.

As an example, Flugge's shell equations [10] can be written as (neglecting curvature effects)

$$\frac{\partial^2 u}{\partial x^2} + \frac{1-\nu}{2}\frac{\partial^2 u}{\partial \phi^2} + \frac{1+\nu}{2}\frac{\partial^2 v}{\partial x \partial \phi} + \nu\frac{\partial w}{\partial x} + \frac{p_x R^2}{D} = 0$$

$$\frac{1+\nu}{2}\frac{\partial^2 u}{\partial x \partial \phi} + \frac{\partial^2 v}{\partial \phi^2} + \frac{1-\nu}{2}\frac{\partial^2 v}{\partial x^2} + \frac{\partial w}{\partial \phi} - k\left(\frac{\partial^3 w}{\partial x^2 \partial \phi} - \frac{\partial^3 w}{\partial \phi^3}\right) + \frac{p_\phi R^2}{D} = 0$$

and

$$\nu\frac{\partial u}{\partial x} + \frac{\partial v}{\partial \phi} + w + k\left(\frac{\partial^4 w}{\partial x^4} + \frac{2\,\partial^4 w}{\partial x^2 \partial \phi^2} + \frac{\partial^4 w}{\partial \phi^4}\right) - \frac{p_r R^2}{D^2} = 0 \qquad (4.1)$$

where x , r ϕ are the cylindrical coordinates

R = shell radius of curvature

t = shell thickness

ν = Poisson's ratio

E = Young's modulus

k = $t^2/12R^2$

D = $Et/(1 - \nu^2)$

p_i = components of normal pressures

These equations are solved for a given set of boundary conditions. In most cases, the solution is assumed as a trignometric function of the form

$$u_i = f(x_i) \cos m\phi \quad \sin n\phi \tag{4.2}$$

where u_i are the displacements, x_i the coordinates, ϕ the angle in cylindrical coordinates, and m, n are constants.

Examples of the above approach can be found in Timoshenko and Gere [2] where solutions for a few simple cases are presented. These include pure axial load, pure external/internal pressure, and lateral distributed load. Brush and Almroth [3] also present a similar approach using Donnel's shell equations. For combined external pressure and axial load, Brush and Almroth [3] used membrane equations and trignometric deflection functions to obtain the critical load.

Brazier [8] was one of the first to study the effect of second order terms on the flexure of thin cylindrical shells. He pointed out that St. Venant's solution was not valid for large displacements and that the moment-curvature relation becomes nonlinear at higher loads (Fig. 3). This happens because the cross-section of an initially circular shell ovalizes as shown in Fig. 4. The structure is, therefore, subject to limit point buckling. Brazier obtained an expression for the limit point load and ovalization by differentiating the strain energy with respect to the midsurface curvature, assuming circumferential inextensionality i.e.

$$w = \frac{dv}{d\phi} \tag{4.3}$$

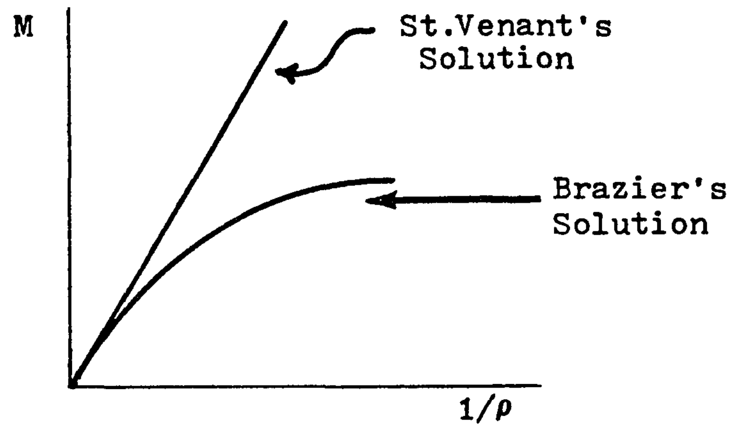

Figure 3 Moment-curvature relation.

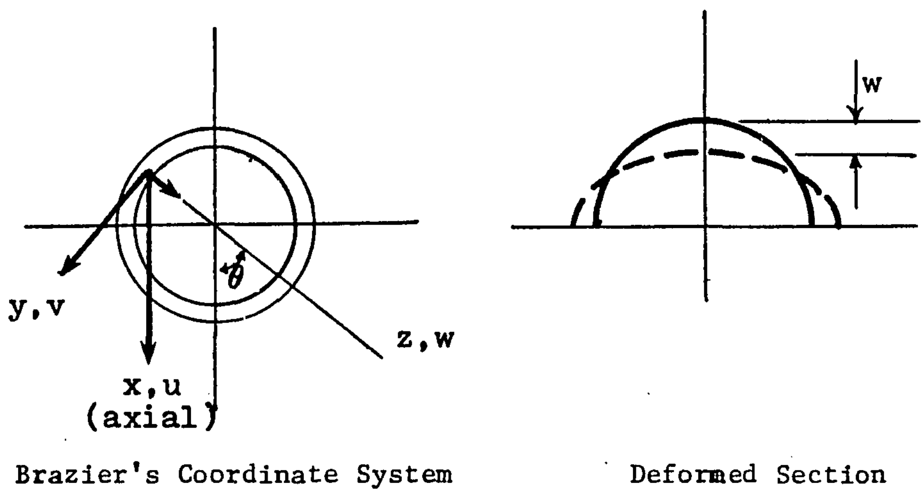

Figure 4 Ovalization.

The analysis was limited to the elastic range.

Stresses in thick shells can reach the plastic region before the onset of buckling. Thus, the equations discussed so far would not be applicable. Engesser was the first one to address this problem back in 1889. He suggested that Young's modulus be replaced by the Tangent Modulus in Euler's formula. This was criticized for not taking into account the unloading due to bending in a column that was under pure compression until it reaches the plastic range. This appears to have been an important issue three decades ago and a great deal of discussion can be found on this subject. A compromise was found in the 'Reduced Modulus' formula. Shanely [24] shows that the Engesser load represents a lower bound since no bending is assumed to take place and that the Reduced Modulus formula represented an upper bound, since it requires infinite lateral deflection.

In a later paper, Shanely [14] developed an inelastic column theory based on the assumption that bending takes place simultaneously with increase in axial load. Thus, it is possible to have bending without strain reversal. Derivation of the equation was based on a two-flange column and the results obtained were generalized. It was concluded that the tangent modulus formula gives the maximum load at which an initially straight column will remain straight; the column load may exceed this limit but it cannot be greater than the reduced modulus load.

Gerard [26] derived an expression for the buckling load of thin cylindrical shells based on linearized Donnel equations and the deformation theory of plasticity. These were valid for axial loads only. Batterman [27] used an incremental J_2 plasticity theory instead, to determine the axial buckling loads.

Croll [11] has analyzed the elasto-plastic buckling of cylinders under combined external pressure and axial load. An expression for the hoop strain was derived from membrane theory and substituted into the Donnel equilibrium equations. Von Mises criterion was used to predict yielding. A numerical technique was used to calculate a lower bound for the critical pressure.

Reddy [15] considered the plastic buckling of cylindrical shells under pure bending. The incremental J_2 theory was used assuming isotropic hardening. Reddy contended that pre-buckling ovalization is negligible in the plastic range*, so a linear variation of axial strain was assumed. The stress-strain relations were substituted in the uncoupled Donnel equations to give the following differential equation in the unknown w, the axial displacement:

$$L \left\{ \frac{Et^2}{12} \left[C_{11} \frac{\partial^4 w}{\partial x^4} + 2(C_{12} + C_{13}) \frac{\partial^4 w}{r^2 \partial x^2 \partial \theta^2} + C_{22} \frac{\partial^4 w}{r^4 \partial \theta^4} \right] - \sigma_{xo} \frac{\partial^2 w}{\partial x^2} \right\}$$

$$+ \frac{E}{r^2} (C_{11} C_{22} - C_{12}{}^2) \frac{\partial^4 w}{\partial x^4} = 0$$

where $$L = C_{11} \frac{\partial^4}{\partial x^4} + \frac{1}{C_{33}} (C_{11} C_{22} - C_{12}{}^2 - 2 C_{12} C_{33}) \frac{\partial^4}{r^2 \partial x^2 \partial \theta^2}$$

$$+ C_{22} \frac{\partial^4}{r^2 \partial \theta^4} \qquad (4.4)$$

---

* This is supported by references cited in [15]

where Cij are the elements of the constitutive matrix evaluated from

$$C_{ijkl} = \frac{E}{1+\nu}\left[\left[\frac{1}{2}\left(\delta_{ik}\,\delta_{jl} + \delta_{il}\,\delta_{jk}\right) + \frac{\nu}{1-2\nu}\,\delta_{ij}\,\delta_{kl} - f\left(\frac{S_{ij}S_{kl}}{\sigma_e^{2}}\right)\right]\right.$$

$$f(\sigma_e) = \begin{cases} 0 & \text{for } \sigma_e < \sigma_y \\ \dfrac{3(E/E_t - 1)/2}{E/Et - (1-2\nu)/2} & \text{for } \sigma_e \geq \sigma_y \end{cases} \tag{4.5}$$

r = radius of cylinder

x,θ = cylindrical coordinates

A trignometric function was assumed for w and the equation solved by an iterative technique.

Tamano, et al [19] developed a theoretical analysis for the evaluation of the plastic collapse of ideal pipes under pressure. Statistical regression analysis was used to obtain an empirical formula from the experimental data.

Malik, et al [23] used Flugge's equations instead of Donnel's. A mixed displacement function was used to solve the equation thus removing the restrictions placed by pure sine or cosine functions on boundary conditions. However, the only load case considered was of lateral pressure.

Bynum [28] surveyed several analytical formulae for elastic and plastic shell buckling. It may be noted here that none of the formulae surveyed were for combined loads.

Tugcu and Schroeder [32] considered the plastic buckling of pipes under pure bending. The material was modelled as rigid, linear work - hardening, using the deformation theory of plasticity. Thin shell theory assumption of zero radial stress was used. The strain energy was expressed in terms of the strains only by using the constitutive model developed in the paper. By using nonlinear shell theory, the strain energy was expressed exclusively in terms of the displacements. The strain energy integral was set equal to the virtual work and differentiated. The assumed displacement functions allowed for variation of the displacement u in the axial direction, by using the form

$$u = A[1 - \cos \frac{k\pi z}{\ell}] \cos \phi - C \cos 2\phi \; [\cos \frac{2n\pi z}{\ell} + 1] \qquad (4.6)$$

The displacement function for v was selected on the assumption that the hoop strain is due to bending only, thus it vanishes at the midsurface. Displacement w was constructed such that for linear terms only, the shear strain in the r - z plane vanishes.

Hangai and Kawamata [113] extended Koiter's method for solving nonlinear problems by the perturbation technique [91]. They have shown that it is possible to distinguish between a limit point and a bifurcation point by this method.

Ades [33] extended Brazier's work on ovalization, to the plastic range for pure bending. An expression for the strain energy was derived in terms of the longitudinal and transverse stresses and strains, assuming circumferential inextensionality and the stress in the radial direction to be zero. The differential equations were obtained using the following condition:

$$\frac{\partial w}{\partial (a/r)} = 0$$

where w = work per unit length

a = semi-major axis

r = original radius

A closed form solution could not be obtained for this case. Numerical integration was used to obtain w as a function of (a/r). By plotting the critical moment against D/t (Fig. 5) for both ovalized and non-ovalized sections, the critical failure mode can be predicted.

Shells of very large D/t ratios may buckle locally. Timoshenko [2] considered the symmetric buckling of thin cylinders under uniform axial compression. Schilling [34] surveyed information available until the year 1965, on the buckling of tubes. He cited a reference by Gerard that classified tubes into three categories, on the basis of the following parameter

$$Z = \left(\frac{R}{t}\right) \left(\frac{L}{R}\right)^2 \left(1 - \nu^2\right)^{1/2} \tag{4.8}$$

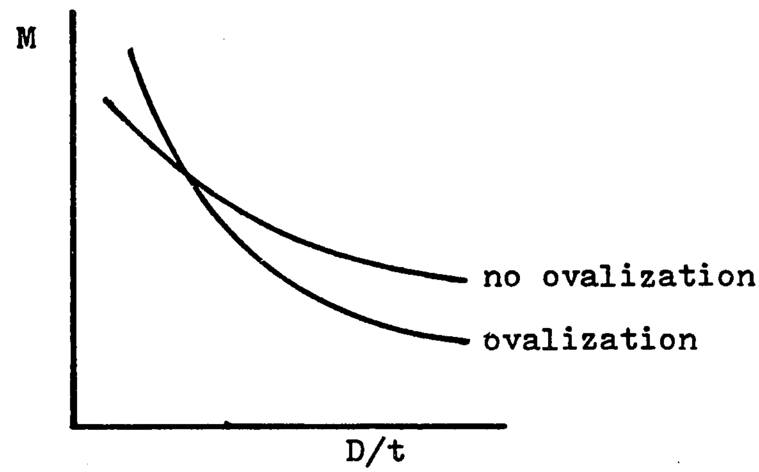

Figure 5 Effect of ovalization on buckling moment

For Z $\geq$ 2.85, local buckling was important and various empirical formulae were given for calculating buckling strength under different types of loads acting independently.

Ramsey [37] used the J_2 incremental theory for a rigid-plastic material to derive a linear partial differential equation for axisymmetric buckling of moderately thick shells under axial compression. The equations were solved using asymptotic series. In a later paper [39], Ramsey extended his study to buckling deformations caused by local axisymmetric imperfections.

Tvergaard and Needleman [38] looked at the localization of buckling patterns from a broad perspective. It was observed that the load-deflection curve (Fig. 6) for structures prone to local buckling, displays a maximum load point. In realistic structural models there is a delay between the maximum load point and the point of bifurcation that leads to localization. The authors compared the localizing of buckling patterns to necking in a tension test and found the two anologous.

Between 1969 and 1976, Battelle Columbus Laboratories conducted a study of buckling of offshore pipelines during the pipe-laying operation. The study considered both gross and local buckling under a combination of loads: tension, bending, and external pressure. Details of the study can be found in [7], [42] - [45]. A summary of the study is given below.

The analysis was divided into two parts: collapse due to ovalization and bifurcation buckling. A specific order of loading was assumed - pressure was applied first, followed by axial loading and

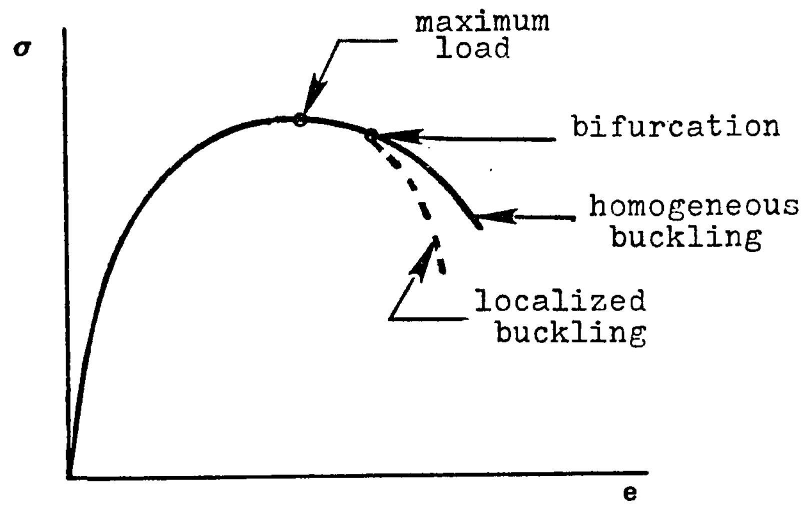

Figure 6 Stress-strain curve for localized buckling.

bending. It was assumed that the pipe does not ovalize until after the bending moment and axial forces are applied. The constitutive relations were derived using the deformation theory of plasticity. The total strains were composed of

a) strains due to the external pressure

b) strains due to axial force, F

c) strains due to bending moment, M

d) circumferential strains due to ovalization

The strains due to external pressure were calculated from the membrane equations (thin walled pressure vessel) i.e.

$$\sigma_1 = \sigma_r = 0$$

$$\sigma_2 = \sigma_\theta = \frac{pr_o}{t}$$

and

$$\varepsilon_\theta = \begin{cases} \sigma/E & \text{for} \quad |\sigma| \leq \sigma_y \\ \pm \dfrac{\sigma_y}{E}\left[n^{-1}\left(\dfrac{|\sigma|}{\sigma_y}\right)^n + 1 - n^{-1}\right] & \text{for} \quad |\sigma| > \sigma_y \end{cases} \tag{4.9}$$

The strains due to the force were taken to be constant along the length.

$$\varepsilon_{1a} = \varepsilon_a$$

$$\varepsilon_{2a} = -\mu\varepsilon_a \tag{4.10}$$

The bending strains at any point z from the midsurface were calculated from

$$\begin{aligned} \varepsilon_{1b} &= \frac{-1}{\rho}\,(y + Z\cos\phi) \\ \varepsilon_{2b} &= -\mu y/\rho \end{aligned} \qquad (4.11)$$

where ϕ is the angle from the vertical

The circumferential strains due to ovalization were written as

$$\varepsilon_{2c} = \gamma_2 + \frac{Z}{r_o}\,\frac{\partial\psi}{\partial\phi} \qquad (4.12)$$

where γ_2 = hoop strain of mid-surface

ψ = rotation due to load

Strain energy density was written in terms of the strains only and the above expressions substituted. The strains at any point can be related to the mid-surface displacement. The total strain energy was found by integrating the expression over the whole body.

The potential function was written as

$$\pi = U - W_p = \pi(w_o) \qquad (4.15)$$

where W_p is the work done by the external loads.

w_o is the flattening due to the moment

U is the strain energy of the body

π was minimized with respect to w_o, using an iterative numerical technique. Once W_p was found all strains could be calculated.

The second part of the analysis dealt with bifurcation buckling i.e. given the equilibrium position from the ovalization analysis, determine if another equilibrium point exists in the neighboring region. Such a point would be defined by the stress field $\sigma_{ij} + \dot{\sigma}_{ij}$ and strain field $\varepsilon_{ij} + \dot{\varepsilon}_{ij}$, where $\dot{\sigma}_{ij}$ and $\dot{\varepsilon}_{ij}$ are perturbations about σ_{ij} and ε_{ij} respectively. Equations relating shell deformations at the middle surface to the loading conditions are developed from the stress-strain constitutive relations (J_2 deformation theory), the kinematic equations relating the strains to the deformations, and the equilibrium relations for the shell. The resulting Partial Differential Equations involve functions of the quantities σ_{ij}, ε_{ij} and $\dot{u},\dot{v},\dot{w}$ as unknowns. By separation of variables, the Partial Differential Equations were transformed to a set of Ordinary Differential Equations. The finite difference technique was used to solve these equations.

Most buckling analyses surveyed in the previous sections have been restricted to only one type of loading, i.e. either buckling under pure bending or pure axial pressure or pure external/internal pressure. Although some studies, such as the Battelle study, considered combined loading, several researchers have suggested that critical loads be calculated separately for each type of loading and then the loads be superimposed using an interaction formula.

Interaction formulae are derived semi-empirically. The first step is to plot a failure surface by taking each type of loading to be represented by non-dimensional ratios e.g.

$$X = \frac{\sigma}{\sigma_{cr}} \qquad Y = \frac{p}{p_{cr}} \qquad Z = \frac{M}{M_{cr}} \tag{4.16}$$

where σ_{cr}, p_{cr}, M_{cr} are the values of the axial compressive stress, external pressure, and bending moment, respectively, at failure if each of these acted independently. The curve will intersect each of the axes at $X = 1$, $Y = 1$, $Z = 1$. Donnel [18] has shown that the general equation would be of the form

$$X^{m} + Y^{\bar{m}} + Z^{n} = 1 \tag{4.17}$$

The exponents may be evaluated from curve fitting experimental data. For combined torsion and axial compression, Donnel suggested the following equation

$$\left(\frac{\sigma}{\sigma_{cr}}\right) + \left(\frac{\tau}{\tau_{cr}}\right)^{3} = 1 \tag{4.18}$$

Schilling [34] suggested different exponents

$$\left(\frac{\sigma}{\sigma_{cr}}\right) + \left(\frac{\tau}{\tau_{cr}}\right)^{2} = 1 \tag{4.19}$$

Furthermore, Schilling claimed that if both bending and axial loads are present, it would be safe to simply add the axial (direct) stresses due to each load and then substitute into the above equation. However, the following equation for the direct stress was found to be less conservative.

$$\sigma = \sigma_{axial} + \frac{\sigma_{bend}}{1 \cdot 3} \tag{4.20}$$

Donnel [18] suggested that σ_{cr} in bending be taken as 1.4 times σ_{cr} in axial compression. Battelle's researchers [44] suggested a linear formula for combined bending moment and external pressure:

$$\frac{p}{p_{cr}} + \frac{M}{M_{cr}} = 1 \tag{4.21}$$

Experimental Studies

Numerous experimental studies have been conducted to determine buckling strength of cylinders. The following is not, by any means, a complete survey. Only a few studies are cited, the results of which will be compared to the results from BUCKS.OSU.

To validate the analytical method discussed in the previous section, Battelle conducted experimental tests on 1020 steel cylinders under combined bending moment and external pressure [43]. D/t ratios of 40, 20, and 16 were used with L/D ranging from 10 to 25. Some full size tests were also conducted on pipes of 20-inch diameter and 24 feet length. The test apparatus consisted of a four-point bending mechanism within a pressure vessel. From this study, the moment-pressure interaction curve was validated. It should be mentioned, however, that because of limitations on maximum pressure and specimen size, a relatively small portion of the curve could be validated.

TRW conducted experiments on Mylar cylinders and cones under combined axial compression and lateral external pressure [143]. R/t of 150 to 400 and Z ranging from 30 to 740 was used. Interaction curves were obtained based partly on the experimental results.

Sobel and Newman [22] tested 304 stainless steel cylinders in axial compression. D/t ranges were chosen so as to get localized axisymmetric buckling in the plastic range.

Mesloh, et al [42] coined the term "propagating buckle" to describe a local transverse buckle that occurs in pipes subjected to external pressure and bending. Once initiated, this buckle may propagate along the pipe. From experiments it was observed that this type of buckle forms in pipes having the range of D/t between 20 and 100. Empirical relations were derived for the initiation and propagation pressures required to get this kind of buckling.

Kyriakides, et al [41], conducted extensive experimental studies on the propagating buckle. The problem was examined parametrically, and the results presented in graphical form.

Finite-Element Studies

Variational formulations of finite element methods are derived from energy principles and can be divided into the following categories:

1. Potential Energy Formulation
2. Mixed Formulation
3. Hybrid Formulation

For linear structural problems, the first method is the most popular one. In the displacement based method, the variation in potential energy is written as an algebraic sum of the virtual work done by the internal and external forces on a body. By using force-stress relations, followed by constitutive and then kinematic relations, the equations thus obtained can be written entirely in terms of the known forces and the unknown displacements. These equations are then discretized.

$$\delta\pi = \int_V \delta\underline{e}^T \sigma dV - \int_V \delta\underline{U}^T \underline{b}\, dV - \int_S \delta\underline{U}^T \underline{t}\, dS \tag{4.21}$$

$$\delta\pi = 0 \text{ (minimize potential energy)}$$

$$\underline{KU} = \underline{R} = 0 \text{ (descretized)}$$

In the above expressions

π = Potential

$\underline{e}^T\underline{\sigma}$ = Strain energy/unit volume

$\underline{U}^T\underline{b}$ = Virtual work of body forces

$\underline{U}^T\underline{t}$ = Virtual work of surface tractions

$\underline{K}$ = Stiffness matrix

$\underline{R}$ = Load vector

$\underline{U}$ = Displacement vector

V = Volume of body

S = Surface area

Mixed formulations are based on the Reissner-Hellinger Principle described in [102] by Washizu. In this case, stresses and displacements are considered independent but compatability is forced on strains and the boundary conditions are assumed to be satisfied. This is a specialization of the Generalized Potential Energy Principle. (Zienkiewicz [47].

$$\pi = \int_V \underline{\sigma}^T \underline{e}\, dV + \int \underline{U}^T (\underline{L}^T \underline{\sigma} + b) dV - \int_S \underline{U}^T (\underline{G\sigma} - \underline{t}) dS \qquad (4.22)$$

where operator $\underline{L}^T = \left[\frac{\partial}{\partial x} + \frac{\partial}{\partial y} + \frac{\partial}{\partial z}\right]$

and G is the operator linking stresses to tractions

It can be observed that displacements have to preserve the same continuity as strains because of the operator $\underline{L}$ but since the stresses do not have to be differentiated they can be discontinuous. Thus, the mixed method relieves continuity requirements on interpolating functions [47], [102], [103].

Hybrid methods are discussed in [47, 87, 95, 98, 99, 101, 103, 104]. The formulation was introduced by Pian to alleviate continuity problems even further. The method is based on the Complimentary Energy Principle. Each element is considered to be a separate structure. A compatible (or equilibriating) field of strains (or stress) is defined inside each element without ensuring inter-element compatibility (or equilibrium), which is imposed by Lagrangian multipliers defined only at the interfaces.

$$\text{Potential:} \quad \pi = \pi\,(\underline{\phi})$$

$$\text{Constraint:} \quad \underline{E}\,(\phi)^1 - E(\phi)^2 = 0 \text{ on } \Gamma_1 \qquad (4.23)$$

where $\underline{E}$ is a linear operator

Γ_1 is the inter-element boundary

$\underline{\phi}$ is the assumed field

This is a relatively new method and elements based on it are under development.

In surveying the analytical studies some of the difficulties encountered in using this approach for shell buckling were obvious. The shell partial differential equations, that form the basis of these methods, can only be solved for a few cases, even with assumed displacement modes. When combined loads are considered, or non-linear shell theories used (for large displacements) or when elastic-plastic stress-strain relations are used, it becomes impossible to use this approach. For this reason, numerical methods such as finite differences and finite elements have been used. Although, there are nonlinear finite difference programs available, such as Lockheed's STAGS [22] and Bushnell's BOSOR [84], it was decided 'a priori' to consider only the finite element method for this study.

If one considers the governing equation of the displacement-based finite element method given earlier as

$$\underline{K}\,\underline{U} = \underline{R}$$

or $$(\underline{B}^T\underline{C}\,\underline{B})\underline{U} = \underline{R}$$

where $\underline{B}$ = strain-displacement matrix

$\underline{C}$ = constitutive matrix

and $\underline{K}$ and $\underline{R}$ are constant, we have a linear set of equations. This requires that (a) the loads be independent of displacements, (b) the strain-displacement matrix $\underline{B}$ should be constant, which is true for small displacements only, (c) the constitutive matrix $\underline{C}$ be constant, which is valid only for linear-elastic materials. If any of the above three conditions are violated, the set of equations would be nonlinear. Therefore, one can divide nonlinear analyses into three categories:

1. Materially non-linear ($\underline{C}$ is nonlinear)
2. Large displacements but small strains ($\underline{B}$ is nonlinear)
3. Large displacements and large strains ($\underline{B}$ and $\underline{C}$ are nonlinear)

For nonlinear problems, a common approach is to apply the loads in several small steps and to linearize the equations in each load step [46, 47]. A time variable is used to describe the loading and the motion of the body, i.e. the loads and configuration of the body change in discrete intervals by discrete amounts, from the original loads and configuration to the final ones.

For large displacement problems, it is better to employ a Lagrangian formulation (moving coordinate system) rather than a Eulerian formulation (stationary coordinate system). Two approaches are generally used: the Total Lagrangian (T.L.) and the Updated Lagrangian (U.L.) formulations. The former was introduced by Oden [92] and Yaghmai [93] and the latter is described by Bathe in [46]. In the T.L. formulation, all static and kinematic variables are referred to the initial configuration at time zero. In the U.L. formulation all variables are referred to the configurations at time t.

Just as in linear analyses, isoparametric elements can be used in nonlinear analysis i.e. the 'shape functions' employed for interpolating the coordinates can also be used for interpolating the displacements. Either continuum or structural elements may be used.

Sandia Laboratories report on Nonlinear Finite Elements [54] compares various non-linear formulations with respect to computational efficiency and accuracy. The survey was limited to material - geometric non-linearities and small strains. As such the conventional Cauchy stress and strain tensors were the only measures considered. Formulations based on the incremental law of plasticity were deemed to be most accurate. The study recommended not sparing any effort in computing the element stiffness matrix for the sake of reduction in computing cost. It also concluded that it is more efficient to use simplifying assumptions for the nonlinear terms and a large number of elements than to use a few complex elements. As the geometric nonlinear terms depend only on the midsurface strains and rotations, they should be computed using elements that can compute these to a sufficient degree of accuracy. Since this report was published in 1972 and is restricted to small displacement problems, it is a bit outdated and somewhat less comprehensive than Bathe's [46] which was published in 1982.

Shell stability analysis using Finite Elements can be divided into two classes [106]: 'classical' concept and 'degeneration concept'. In the former, nonlinear shell equations are introduced into the field equations for a 3-D continuum. In most cases, Kirchhoff-Love assumptions are used. Either curved elements (e.g. Gallagher [63]) or flat elements (Wennerstrom [111]) are used. Generally, C^1 continuity requirement has to be satisfied. The second method directly discretizes the 3-D field equations in terms of the midsurface variables, i.e. displacements and rotations are independent variables so only C^0 continuity is required.

In geometrically nonlinear analysis either a total or an updated Lagrangian formulation is used. In shell analysis no preference for one over the other can be observed [106]. Argyris [123] presented the corotational formulation, in which an initially flat element deforms to a curved shape. The element variables are referred to a local coordinate system which undergoes rigid body motions. The geometric nonlinear effects enter through the rigid body kinematics.

The bifurcation point and the limit point, though different in meaning physically, can be found in the same way, i.e. by setting the determinant of the stiffness matrix to zero.

Material nonlinearity can be introduced in three ways: (1) If solid elements are used, each element will have a certain stress state which can be used to calculate the constitutive matrix for each increment. The procedure is simple but costly. (2) If shell elements are used, a layered model could be used, i.e. using the same constitutive matrix for each layer, thus reducing the expense. (3) In the integral model the material law is defined in terms of the stress resultants instead of the stresses. This requires the use of integral material laws in the formulation [106].

Ramm [106] used the Lagrangian formulation to investigate the buckling of axially loaded cylindrical shells and panels under various boundary conditions. Degenerated isoparametric elements were used and the layered plasticity model was employed to model material nonlinearity. An interative solution method was used.

Wennerstrom [111] developed a nonlinear flat shell element, primarily for use in metal forming analysis, but the procedure was also applied to cylindrical shells under internal pressure and axial tension. The membrane strains and bending curvature were assumed constant within each of the two triangular sub-elements that composed a quadrilateral element. Six stress resultants were considered. Cauchy stress and strains were used. The constitutive relations were based on von Mises criterion and Prandtl-Reuss flow rule. Newton-Raphson solution procedure was used.

Brendel and Ramm [60] used a two-dimensional discretization, the total Lagrangian formulation with the 2nd Piola stress tensor and the Green-Lagrange strain tensor, an incremental solution procedure, and the Newton-Raphson iteration method for the stability analysis of cylinders (of open and closed cross-sections). The loading cases for which the problem was solved were external pressure, transverse distributed load, transverse concentrated loads. Each load case was considered separately. Degenerate isoparametric shell elements (superparametric) with 9 and 16 nodes were used. The lowest eigenvalue of the tangent stiffness matrix gives the ultimate load (arbitrary mth iteration)

$$\det \underline{K}^{m} = 0 \qquad (4.25)$$

Neither combined loading was considered nor large strains; the material was assumed to be linear elastic.

Civil and Aeronautical engineers have applied the F.E. method to predict the buckling behavior of frame structures. Akkoush et al [59] developed a procedure for analyzing complex structures by dividing it into three-dimensional beam elements and thin rectangular plate elements. Cauchy tensors were used so the analysis was limited to small strains. Only geometric non-linearity was taken into account. The elasticity matrix was assumed constant throughout the loading process. The problem was reduced to an eigenvalue problem and an incremental solution was used. The method can be applied to thick walled cylinders or solid circular rods.

The Finite Element Method was applied to the local buckling of large diameter pipelines by Row et al [40]. The study is divided into two parts: axisymmetric and bending analysis. It is assumed that an axisymmetric wrinkle forms at the middle of the pipe, which leads to buckling. A total Lagrangian formulation was used in conjunction with an 8-node axisymmetric solid finite element. An anisotropic hardening behavior was assumed for the material. Imperfection sensitivity was considered also by examining two types of imperfections: 'bulge' and 'offset'. The combined effect of internal pressure and axial compression was based on the assumption that the pressure was applied first, before the axial compression was imposed. The effects of pipe ovalling on the buckling limit were also considered. This was found to be the most comprehensive study on local buckling using the finite element method.

Kasar [57] applied the F.E. Method to Inelastic Buckling of thin-walled structural systems. The members of the space frame were assumed to be of open cross-section. Elastic-perfectly plastic material behavior was assumed and an incremental formulation was used to accomodate large displacements. The failure modes considered were (1) local failure of a part of the cross-section of a member, (2) failure of the entire member. Both torsional and lateral buckling were considered. The shifting of the elastic centroidal and shear center axes, after initiation of yielding, was considered. Strain reversal and residual stresses were also included.

Mau and Gallagher [66] recommended the following general procedure for nonlinear buckling problems. Use a Lagrangian frame of reference to give the following general equation

$$[\underline{K}]\{\Delta\} + [\underline{N}_1(\Delta)]\{\Delta\} + [\underline{N}_2(\Delta)]\{\Delta\} = \lambda\{\underline{P}\} \tag{4.26}$$

where K = linear stiffness matrix

N_1, N_2 = are first and second order nonlinear matrices

P, Δ = are loads and displacements respectively

It is claimed that the Newton-Raphson method fails in the vicinity of bifurcation point so a direct iterative method is used, the load is increased in discrete steps. All loads must increase in the same proportion. Also, one can conclude from the above equation that the formulation is limited to geometric nonlinearities only. The bifurcation point is determined in the usual way, i.e. the second variation of the potential energy should be zero. This results in the following eigenproblem:

$$\text{Det}\ [\underline{K} + 2\underline{N}_1(\Delta) + 3N_2(\Delta)] = 0 \qquad (4.27)$$

Therefore, Gallagher's method does not represent any major deviations from Bathe's method discussed before.

In a later paper [63] Gallagher presented a nonlinear curve thin shell element to overcome the problems associated with interelement continuity that were inherent in other elements of this kind developed earlier.

Krakeland [64] used an updated Lagrangian formulation with the Kirchhoff stress and Green strain tensors. The element used was the degenerate isoparametric shell element, parabolic type i.e. eight noded.

The material was modelled by using the von Mises yield criterion and Prandtl-Reuss flow theory. Two types of hardening were considered: isotropic and "overlay". The computer program developed was applied to several numerical problems, including a cylindrical concrete shell with axial load and hydrostatic pressure.

Yamada [112, 115] has been the principal user of the updated Lagrangian formulation for nonlinear analysis. Yamada has compared the results obtained from using different stress tensors (Lagrange, Euler, Kirchhoff, and Cauchy) with the same type of element (plane stress). It was observed that the choice of the stress tensor influenced the results significantly [112].

In recent years, a great deal of effort has been focused on mixed and hybrid methods. The hybrid method was developed by Pian [90, 98, 110, 122, 124] and Tong [95, 103] and Atluri et al [99]. The mixed method has been used by Altman and Igut [94]. In the mixed formulation, both stresses (or internal forces) and displacements are treated as independent variables, as opposed to only the displacements being independent in the displacement based method or only internal forces being independent in the force based method. Thus, only constitutive relations must be assumed but compatibility conditions are relaxed (only approximately satisfied). On the other hand, hybrid methods assume an equilibriating stress within each element and compatible displacements along interelement boundaries. This relaxes continuity requirements on stress distributions.

In order to take shear deformation into account for thick shells, the conventional method requires adding rotations of the surface normals as additional nodal displacements which are independent of u, v, w. Thus, there is an increase in degrees of freedom when compared to elements based on Kirchhoff theory. Also, in the limiting case of thin shells, this scheme would fail because of near zero shear deformations. A hybrid thick shell element may be described in exactly the same manner as Kirchhoff's hypothesis [122].

Atluri [99] presented a unifying theory for all hybrid elements. Both total and updated Lagrangian approaches were considered. Modifications were made to the general expressions for the purpose of developing an element suitable for nonlinear elastic solids. Horrigmoe and Eidsheim [101] developed hybrid stress models suitable for elastic-plastic analysis of plates in bending and strain problems. Barnard and Sherman [104] developed plane stress, plate bending, and 3-D solid hybrid elements for elastic-plastic analysis.

Pian and Boland [110] derived hybrid principles for large deflection of shallow shells and incremental analysis. The Finite Element formulation was based on the interpolation of both interior and boundary displacements for an element and an assumption of an element stress distribution. However, the resulting matrix contained only nodal displacements as unknowns.

Horrigmoe [73] used the hybrid formulation to perform buckling analysis of cylindrical and spherical shells. As with other studies, an incremental form of the Hellinger-Reissner principle was employed.

Simple flat triangular and quadrilaterial elements were used. It was claimed that this procedure was more efficient and accurate than the conventional method. One of the problems solved by this method was the axisymmetric loading of a cylinder under tension and internal pressure. Convergence was studied for both types of elements.

Altman and Iguti [94] used a mixed formulation to derive a thin cylindrical shell finite element. All stress resultants (except shear loads) and displacements were treated as independent variables. Linear theory of shells was used. The method was applied to thin cylindrical shells under a lateral concentrated load (pinched load).

Nonlinear equations may be solved by any of the following groups of methods:

1. Iterative Methods (classical)
2. Incremental Methods (Argyris, Gallagher)
3. Incremental-iterative methods (Conner, Fellipa)
4. Self-correcting methods (Oden, Haisler, Stricklin)
5. Search methods

All these methods attempt to solve the nonlinear equation

$$\underline{K}\ (\underline{U})\ \underline{U} = \underline{R}$$

$\underline{R}$ may also be a function of $\underline{U}$ or it could be constant. These methods are discussed in Refs. [133-137, 116, 105, 82, 83, 46-50]. Some of the popular ones are briefly discussed below.

The direct iteration method, shown schematically in Fig. 7, uses an assumed starting value of $\underline{U}$ to calculate $\underline{K}$ and $\underline{R}$. These are substituted in the above equation to get a new value of $\underline{U}$. This new value is used

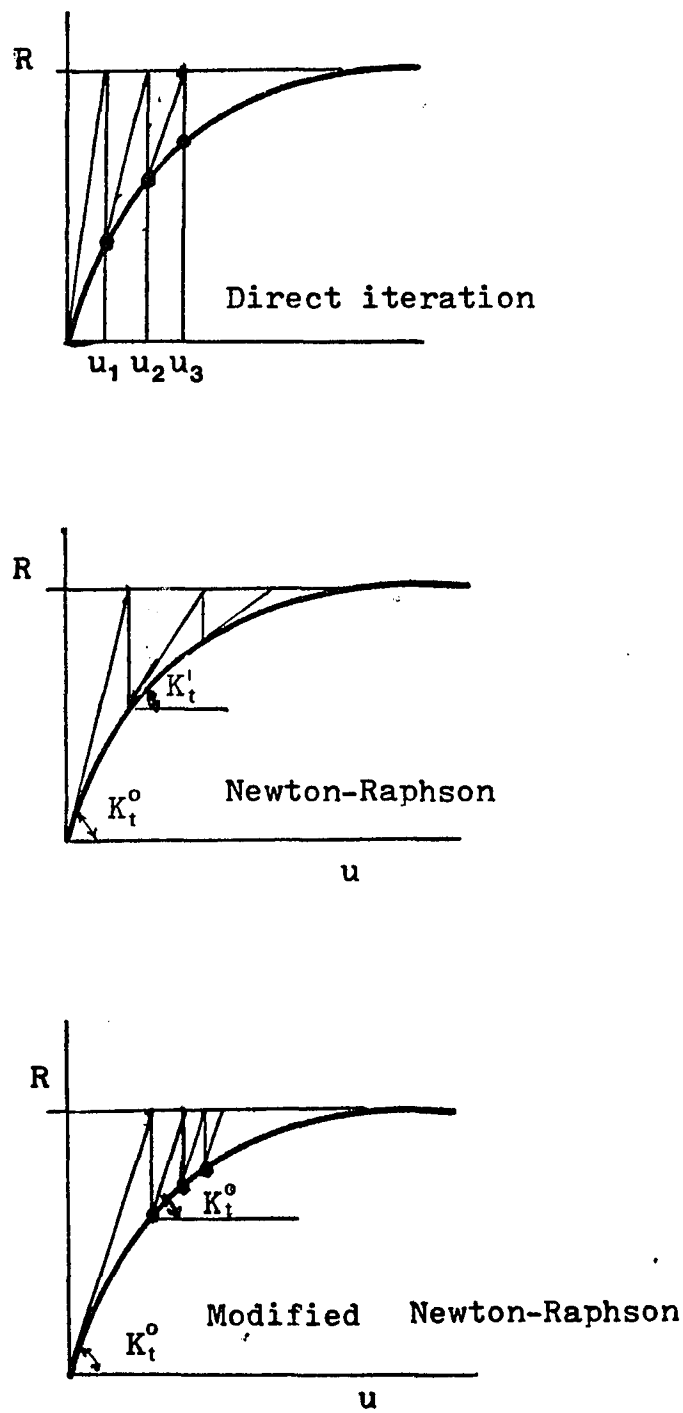

Figure 7 Solution techniques.

in the next iteration and so on until the error (difference in $\underline{U}$ between consecutive iterations) falls below some specified value. This involves inversion of the stiffness matrix in each interation. Also, convergence is not guaranteed.

The Newton-Raphson scheme is an iterative technique in which the stiffness matrix is updated in every iteration and the resulting linear equations solved. This is time consuming but very accurate. Several modifications are used. One method, called the Modified Newton-Raphson method, uses the initial tangent matrix throughout all iterations. This is not suitable for all nonlinear problems, since convergence is not guaranteed. Other quasi-Newton schemes, that fall in between the two methods mentioned above are also used; the stiffness matrix is updated periodically. This method has been used by Gallagher [63] and Krakeland [64].

In incremental methods, each load step is linearized, thus no interation is necessary. This is suitable for problems where the non-linearities are of a relatively lower order. However, this method is known to be unreliable. An improvement is to use equilibrium constraints at the end of each load step, as proposed by Hoffmiester [137].

In incremental-iterative methods, the load is applied in increments and the solution obtained by iteration within each increment, treating the load increment as the final load.

The BFGS method (Broyden-Fletcher-Goldtarb-Shanno) is described in [140]. It belongs to a class of quasi-Newton methods and represents a compromise between the cost effectiveness of Modified Newton method and the accuracy of Newton-Raphson method. The method has been introduced as recently as 1979, but is already being acclaimed as the fastest and most reliable method. In this method the inverse of the coefficient matrix is updated to provide a second approximation from iteration (i-1) to i.

Another self correcting method is the mean stiffness method of Argyris, Fellipa, and Akyz.

Search or Gradient Methods were introduced by Cauchy [105] but are used in more sophisticated forms now. The basic idea is that starting from an arbitrary point in the solution space, a stationary point can be reached by moving in the direction of the minimum (maximum) slope (gradient). This is replaced in steps until the stationary point is found.

$$\text{Potential} \quad \pi = \pi(x_1, x_2 \ldots x_n)$$

$$\text{Step Size} \qquad \frac{\Delta x_i}{\Delta x_1} = \frac{\Delta\pi_i/\Delta x_i}{\Delta\pi_1/\Delta x_1} \tag{4.29}$$

Since the variables may be of different orders of magnitude, it is more efficient to work with normalized variables. The conventional gradient method converges slowly and may become stalled at saddle points or ridges. Powell and Fletcher [82, 86] introduced the conjugate gradient method which improves convergence. The same equation can be written as

$$\Delta x_i = \lambda C_i^j$$

where $\lambda = \Delta x_1/(\Delta\pi_1/\Delta x_1)$

and $C_i^j = f(\Delta U/\Delta x_i)$ for the jth iteration (4.30)

An iteration is defined here as the sequence of steps along the line of a given direction until a minimum is reached on that line. The value of C is reset after each iteration using either the Fletcher-Reeves [86] or the Fletcher-Powell [82] formulae.

Irons and Elsawaf [83] presented a new method that is a compromise between the Newton method and the conjugate gradient method; it was labelled as the conjugate-Newton Algorithm. It is claimed by the researchers that this method guarantees convergence even for ill-conditioned non-linear equations and uses less core and backup storage.

V. THEORY AND FORMULATION

Variational Formulation:

As evidenced from the literature review, the following variational formulations could be used for stability problems of thin/thick shells.

1. Potential Energy formulation in the form of the displacement-based method.
2. Mixed formulation in terms of stresses and displacements or stress resultants and displacements.
3. Hybrid formulations with assumed stress distribution within the element and Lagrangian multipliers defined on the inter-element surface only. Subsequent elimination of one set of variables to enable use of standard solution techniques.

It is the opinion of the author that mixed methods create unnecessary problems by increasing the number of field variables thus increasing the size of the matrices and requiring more CPU time for the solution without yielding significant benefits. Therefore, this formulation was not considered.

The displacement method derived from the potential energy formulation may be regarded as a 'classical' finite element technique in the sense that it has been around since the inception of the finite element method. A great deal of literature exists on it, and it would be relatively simple to formulate the proposed problem along these lines. On the other hand, hybrid methods were introduced very recently, although a great deal of work has been done on the stress-hybrid element in the last five years. Because of the availability of reliable large displacement elements based on the potential energy formulation, it was decided to use this method.

The potential energy method is based on the Principle of Virtual Work, which states that for a system in static equilibrium, the sum of the virtual work done by the external and internal forces acting on the system is zero:

$$\delta\pi = \delta(U - V) = 0 \tag{5.1}$$

where π = Potential of system

U = Internal energy (strain energy)

V = Virtual work of applied forces

δ implies 'variation in'

Washizu [102] derived the generalized potential energy principle for elasticity and plasticity problems (neglecting second order terms; these will be included later), as

$$\pi = \iiint_V [A(e_x e_y \; \ldots \; \tau_{xz}) - (b_x u + b_y v + b_z w)]dV$$

$$-\iiint_V [(e_x - \frac{\partial u}{\partial x})\sigma_x + (e_y - \frac{\partial v}{\partial y})\sigma_y + (e_z - \frac{\partial w}{\partial z})\sigma_z$$

$$+ \left(\gamma_{yz} - \frac{\partial w}{\partial y} - \frac{\partial v}{\partial z}\right) \tau_{yz} + \left(\gamma_{zx} - \frac{\partial u}{\partial z} - \frac{\partial w}{\partial x}\right) \tau_{zx}$$

$$+ \left(\gamma_{xy} - \frac{\partial v}{\partial x} - \frac{\partial u}{\partial y}\right)\tau_{xy}]dV$$

$$- \iint_{\Gamma_1} (T_x u + T_y v + T_z w)\, d\Gamma$$

$$- \iint_{\Gamma_2} [(u - \overline{u})p_x + (v - \overline{v})p_y + (w - \overline{w})p_t]\, d\Gamma_2 \qquad (5.2)$$

where x,y,z are the Cartesian coordinates

$e_x \ldots \gamma_{xz}$ are the components of strain

$\sigma_x \ldots \tau_{xz}$ are the components of stress

u,v,w are the displacements

T_i are surface tractions on surface Γ_1

p_i are surface tractions on surface Γ_2

b_i are the components of body forces

The terms $(u-\overline{u})$ result from not satisfying the boundary conditions exactly. If it is assumed that the boundary conditions are satisfied exactly, the last term will disappear. If a kinematic relation can be found between strains and displacements, the second term will disappear. For static problems, if gravity forces are neglected, we get

$$\pi = \iiint_V A(e_x, e_y \ldots \gamma_{xz})dV - \iint_{\Gamma_1} (T_x u + T_y V + T_z w)d\Gamma \qquad (5.3)$$

For elastic-plastic problems, it has been shown (Washizu [102]) that A represents the strain energy. If constitutive relations are used, stresses can be eliminated from the above equation and using kinematic relations, the potential can be expressed entirely in terms of the displacements and applied forces.

$$\delta\pi = 0$$

$$\text{or} \qquad \iiint_V \delta e_{ij}\sigma_{ij}\, dV - \int_\Gamma \delta u_i{}^T T_i d\Gamma = 0 \qquad (5.4)$$

This is the governing variational equation for elastic-plastic problems for static structures.

Stress and Strain Tensors

The stress and strain measures must satisfy the following two conditions. First, they must be energetically conjugate (their product should give a measure of strain energy) since the formulation is based on potential energy. Second, the stress and strain tensors must be invariant under rigid body motions, which can be large in buckling problems.

There are many such pairs available, as evidenced by the literature on continuum mechanics. The pair chosen for this study is the 2nd Piola-Kirchhoff stress tensor and the Green-Lagrange strain tensor. These measures cannot be given any physical meaning but were chosen because not only do they satisfy the two conditions stated above, but they can be converted to Cauchy measures through simple tensor transformations; i.e. they do not require an integration over the loading path to obtain Cauchy stresses.

The second Piola-Kirchhoff stress at time t_1 is defined as (measured in coordinate system at time t_o)

$$ {}^{t_1}P_{ij} \triangleq \frac{{}^{t_o}\rho}{{}^{t_1}\rho} \frac{\partial\, {}^{t_o}x_i}{\partial\, {}^{t_1}x_i} \, {}^{t_i}\sigma_{kl} \, \frac{\partial\, {}^{t_o}x_j}{\partial\, {}^{t_1}x_l} \qquad (5.5) $$

where ${}^{t_o}\rho$ = density at time t_o

${}^{t_1}\rho$ = density at time t_1

${}^{t_1}\sigma_{kl}$ = Cauchy stresses at t_1

${}^{t}x_i$ = coordinates at time t

The Green-Lagrange strains are defined as

$$ {}^{t_1}G_{ij} \triangleq \frac{1}{2}\left[\frac{\partial\, {}^{t_1}u_i}{\partial\, {}^{t_o}x_j} + \frac{\partial\, {}^{t_1}u_j}{\partial\, {}^{t_o}x_i} + \left(\frac{\partial\, {}^{t_1}u_k}{\partial\, {}^{t_o}x_i}\right)\left(\frac{\partial\, {}^{t_1}u_k}{\partial\, {}^{t_o}x_j}\right)\right] \tag{5.6} $$

Lagrangian Incremental Equations

As discussed in Chapter IV, two approaches can be used for large displacement problems: the Total Lagrangian (T.L.) and Updated Lagrangian (U.L.) formulations. Both yield the same final solution. The T.L. formulation involves more computations because of an additional term resulting from referring all kinematic variables to the original coordinate system. The U.L. approach is slightly more complex to formulate. In this study, the T.L. approach is being used.

In large displacement problems, the load-displacement path is nonlinear. Therefore, it is assumed that the load increases in small steps from its initial value to its final value, in a quasi-static manner (dynamic effects are neglected in this study). The variational equation (5.4) is written for each step and linearized.

Figure 8 shows the motion of a body in steps from the original position at time t_o to the position at time t_1. The variational equation is written in incremental form between adjacent positions. The solution of this equation in each step gives the incremental displacements, measured in the coordinate system for which the solution was obtained in the previous step. The coordinates, stresses, and

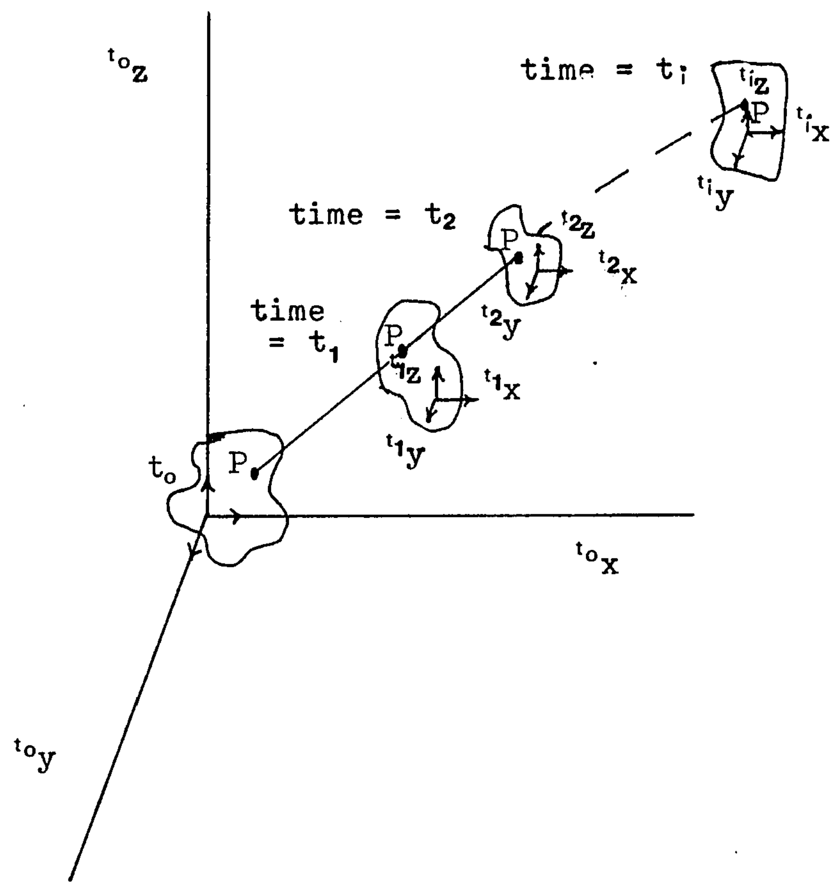

Figure 8 Motion of a body in a Lagrangian frame.

strains are updated and the procedure repeated: For example, between steps t_1 and t_2, the coordinates are updated as follows.

$$
\begin{aligned}
{}^{t_2}x &= {}^{t_1}x + {}^{t_1t_2}\Delta u \\
{}^{t_2}y &= {}^{t_1}y + {}^{t_1t_2}\Delta v \\
{}^{t_2}z &= {}^{t_1}z + {}^{t_1t_2}\Delta w
\end{aligned}
\tag{5.7}
$$

The displacements, referred to the original coordinates ${}^{t_o}x$, ${}^{t_o}y$, ${}^{t_o}z$ are

$$
{}^{t_2}u = {}^{t_1}u + {}^{t_1t_2}\Delta u \quad \text{, etc.} \tag{5.8}
$$

and the stresses and strains at the end of t_2 are

$$
{}^{t_2}G_{ij} = {}^{t_1}G_{ij} + \Delta G_{ij} \tag{5.9}
$$

$$
{}^{t_2}P_{ij} = {}^{t_1}P_{ij} + \Delta P_{ij} \tag{5.10}
$$

Equation (5.4) for the position t_2 can be written as

$$
\int_V {}^{t_2}P_{ij} \; \delta \; {}^{t_2}G_{ij} \, dV = \int_\Gamma {}^{t_2}T_i \, \delta u_i^s \, d\Gamma
$$

$$
\int_V ({}^{t_1}P_{ij} + \Delta P_{ij}) \, \delta (\Delta e_{ij} + \Delta\eta_{ij}) dV = \int_\Gamma {}^{t_2}T_i \, \delta u_i^s \, d\Gamma \tag{5.11}
$$

where Δe_{ij} = linear component of ΔG_{ij}

$\Delta \eta_{ij}$ = nonlinear component of ΔG_{ij}

u_i^s = displacements caused by tractions T_i

Multiplying out, one gets

$$\int_{V_o} {}^{t_1}P_{ij}\ \delta\Delta e_{ij}\ dV_o + \int_{V} {}^{t_1}P_{ij}\ \delta\Delta\eta_{ij}\ dV_o + \int_{V_o} \Delta P_{ij}\ \delta\Delta e_{ij} dV_o$$

$$+ \int_{V_o} \Delta P_{ij} \delta\Delta\eta_{ij} \cdot dV_o = \int_{\Gamma} {}^{t_2}T_i\ \delta u_i^s d\Gamma \qquad (5.12)$$

In linearizing the interval, the fourth term may be dropped and one may also write the approximate constitutive relation

$$\Delta P_{ij} = {}^{t_1}C_{ijrs}\ \Delta e_{rs} \qquad (5.13)$$

where ${}^{t_1}C_{ijrs}$ = elements of constitutive matrix at time t_1

$$\int_{V_o} {}^{t_1}P_{ij}\ \delta\Delta e_{ij} dV_o + \int_{V_o} {}^{t_1}P_{ij} \delta\Delta\eta_{ij} dV_o + \int_{V_o} \Delta P_{ij}\ \delta\Delta e_{ij} dV_o$$

$$= \int_\Gamma {}^{t_2}T_i\ \delta u_i^s\ d\Gamma$$

$$\int_{V_o} {}^{t_1}C_{ijrs}\ \Delta e_{rs}\ \delta\Delta e_{ij} dV_o + \int_{V_o} {}^{t_1}P_{ij} \delta\Delta\eta_{ij} dV_o$$

$$= \int_\Gamma {}^{t_2}T_i\ \delta u_i^s\ d\Gamma - \int_{V_o} {}^{t_1}P_{ij}\ \delta\Delta e_{ij}\ dV_o \tag{5.14}$$

This is the incremental equation of motion for a total Lagrangian system.

Discretization

Equation (5.14) has been derived for a continuum. The next step is to divide the body into discrete elements and write this equation for each element separately. Summing up the left and right hand sides of the individual equations gives the system energy balances i.e.

$$\sum_{i=1}^{NE} \int_{V_e} {}^{t_1}C_{ijrs}\ \Delta e_{rs}\ \delta\Delta e_{ij} dV_e + \sum_{i=1}^{NE} \int_{V_e} {}^{t_1}P_{ij}\ \delta\Delta\eta_{ij} dV_e$$

$$= \sum_{i=1}^{NE} \int_{\Gamma_e} {}^{t_2}T_i\ \delta u_i^s\ d\Gamma_e - \sum_{i=1}^{NE} \int_{V_e} {}^{t_1}P_{ij}\ \delta\Delta e_{ij} dV_e \tag{5.15}$$

where the summation is taken over NE elements and V_e is the volume of element i at time t_1

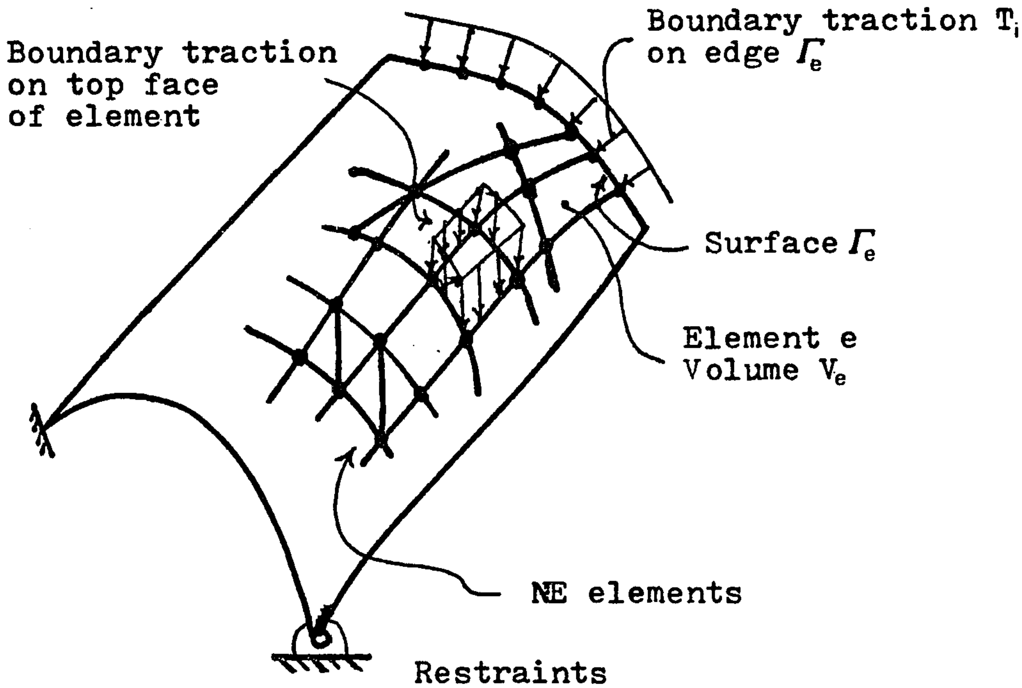

Figure 9 Discretization of a general shell.

and Γ_e is the surface area located on element i, on which forces T_i act The strains are related to displacements and the relations can be written in matrix form as

$$\underline{\Delta e} = \underline{\tilde{B}}_L \underline{\Delta u}$$

$$\underline{\Delta \eta} = \underline{\tilde{B}}_{NL} \underline{\Delta u}$$

The displacements at any point $\underline{\Delta u}$ are obtained from nodal point displacements $\underline{\Delta U}$ using interpolating functions N_i:

$$\Delta u = \underline{N}\underline{\Delta U} \tag{5.16}$$

where $\underline{N}$ = shape function matrix

$\underline{\Delta U}$ = nodal displacement vector

$$\underline{\Delta e} = \underline{\tilde{B}}_L \underline{N}\underline{\Delta U} \stackrel{\Delta}{=} \underline{B}_L \underline{\Delta U} \tag{5.17}$$

and

$$\underline{\Delta \eta} = \underline{\tilde{B}}_{NL} \underline{N}\underline{\Delta U} \stackrel{\Delta}{=} \underline{\hat{B}}_{NL} \underline{\Delta U} \tag{5.18}$$

where $\underline{B}_L$ and $\underline{B}_{NL}$ are the linear and nonlinear strain-displacement matrices

Also define

$$\hat{\underline{B}}_{NL} = \underline{B}_{NL}^{T}\,\underline{B}_{NL} \tag{5.19}$$

Similarly, shape functions can be used to relate the surface displacements on Γ_e.

$$\underline{\Delta U}^{s} = \underline{N}^{s}\,\underline{\Delta U} \tag{5.20}$$

Writing eq. 5.15 in discrete form and substituting (5.17), (5.19) and (5.20) we get

$$\left\{\sum_{i=1}^{NE} \int_{V_e} \underline{B}_L^{T}\,\underline{C}\,\underline{B}_L\,dV_e + \sum_{i=1}^{NE} \int_{V_e} \underline{B}_{NL}^{T}\,\underline{SM}\,\underline{B}_{NL}\,dV_e\right\}\underline{\Delta U} =$$

$$\sum_{i=1}^{NE} \int_{\Gamma_e} \underline{N}^{s}\,\underline{T}\,d\Gamma_e - \sum_{i=1}^{NE} \int_{V_e} \underline{B}_L^{T}\,\underline{SV}\,dV_e \tag{5.21}$$

where $\underline{SM}$ = stress matrix

$\underline{SV}$ = stress vector

and it is understood that all quantities are measured at time t_1 for element i (the superscripts for indicating this have been omitted for simplicity).

This equation can be written as

$$({}^{t_1}\underline{SK}_L + {}^{t_1}\underline{SK}_{NL})\underline{\Delta U} = {}^{t_2}\underline{R} - {}^{t_1}\underline{F} \tag{5.22}$$

where $$^{t_1}\underline{SK}_L = \sum_{i=1}^{NE} \int_{V_e} \underline{B}_L^T \, \underline{C} \, \underline{B}_L \, dV_e = \text{Linear System Stiffness Matrix}$$

$$^{t_1}\underline{SK}_{NL} = \sum_{i=1}^{NE} \int_{V_e} \underline{B}_{NL}^T \, \underline{SM} \, \underline{B}_{NL} \, dV_e = \text{Nonlinear System Stiffness Matrix}$$

$$^{t_2}R = \sum_{i=1}^{NE} \int_{\Gamma_e} \underline{N}^s \, \underline{T} \, d\Gamma_e = \text{Applied Load Vector}$$

$$^{t_1}F = \sum_{i=1}^{NE} \int_{V_e} \underline{B}_L^T \, \underline{SV} \, dV_e = \text{Internal Load Vector}$$

Finally, we write

$$^{t_1}\underline{SK} \; \underline{\Delta U} = {}^{t_2}\underline{XL} \tag{5.23}$$

where $^{t_1}\underline{SK}$ = System Stiffness Matrix at t_1
$^{t_2}\underline{XL}$ = Load vector at t_2

Selection of Elements

A wide variety of elements are available in the literature, consequently, there is no need to formulate a new element here. When looking at the requirements, we need an element that is suitable for large displacements, can undergo both translation and rotation, and can model cylindrical shells in the D/t range of interest.

Suitable elements can be divided into groups: continuum and structural. Continuum elements, such as one-dimensional cable two-dimensional (plane stress, plane strain, and axisymmetric elements), and three-dimensional elements can be formulated using isoparametric interpolation i.e. the displacements u,v,w (whichever applicable) are interpolated in terms of nodal point displacements, such that the interpolating function is the same for both displacements and position. However, for structural elements, such as beam, plate, or shell elements, the displacements u,v,w are interpolated in terms of the midsurface displacements and rotations. This can be interpreted as using a higher degree of interpolation on the geometry than on the displacements. Thus, these elements are referred to as superparametric elements, which amounts to isoparametric formulation with displacement constraints.

Whereas for continuum elements the equilibrium equation can be used directly to compute element stiffness matrices and the load vector, the stiffness matrix for structural elements is derived from the expression of total potential energy applicable to that type of structure. Formulations based on Kirchhoff's theory, which neglects shear deformations, cannot satisfy inter-element continuity on displacements because the shell rotations are calculated from the transverse displacements. However, if shear effects are included, the displacements and rotations of the midsurface normals are independent, and the interelement continuity can be satisfied easily [46].

Another difficulty with structural elements is that low order elements can grossly overestimate the structural stiffness for thin elements, so only high-order elements should be used [46]. However, it is possible to use some modified, low order, structural elements that eliminate this problem by the use of selective or reduced integration of the element matrices.

On the other hand, using 3-D continuum elements for thin structures leads to the following problems [77]:

1. Computational difficulties due to increase in stiffness corresponding to shell thickness
2. Errors caused by strain energy of the normal stresses in the thickness direction
3. Inefficiency because the interpolation order in the thickness direction is high and in the surface direction it is low

Degenerate shell elements alleviate this problem. In the study reported in this dissertation, both continuum and degenerated elements were used and a comparison made.

Formulation of Large Displacement Shell Elements

Large displacement shell elements have been developed by many researchers: Ramm and Stegmuller [106], Bergan and Clough [130], Ramm [77], Krakeland [64], Gallagher [63], Bathe and Bolourchi [71], to name a few. In this study, the Bathe and Bolourchi element is specialized to cylindrical shells, extended to elastic-plastic analysis, and degenerated, as shown in the following pages.

Curved boundaries must be defined accurately; this can be done by using a large number of linear elements or a fewer number of parabolic elements. For the same number of nodes, it is computationally more efficient to use parabolic elements.

For the D/t range being studied here, it is essential that thin as well as thick shells be modelled effectively. For this reason it is necessary to have rotational degrees of freedom in addition to the three translations of the shell midsurface. For points not lying on the midplane, the displacements can be interpolated in terms of the midsurface translational and rotational displacements. This provides a more accurate representation of thick shells subjected to bending loads in addition to membrane loads.

Figure 10 shows the deformation of an eight-noded, parabolic shell element which has five degrees of freedom per node: the translations u,v,w and rotations α and β . Thus, we have a 40 degrees-of-freedom element. The angles α and β are the rotations of a vector, V_3 defined as the unit normal to the shell midplane at the nodal point. The rotations are measured in an arbitrarely defined orthogonal Cartesian system.

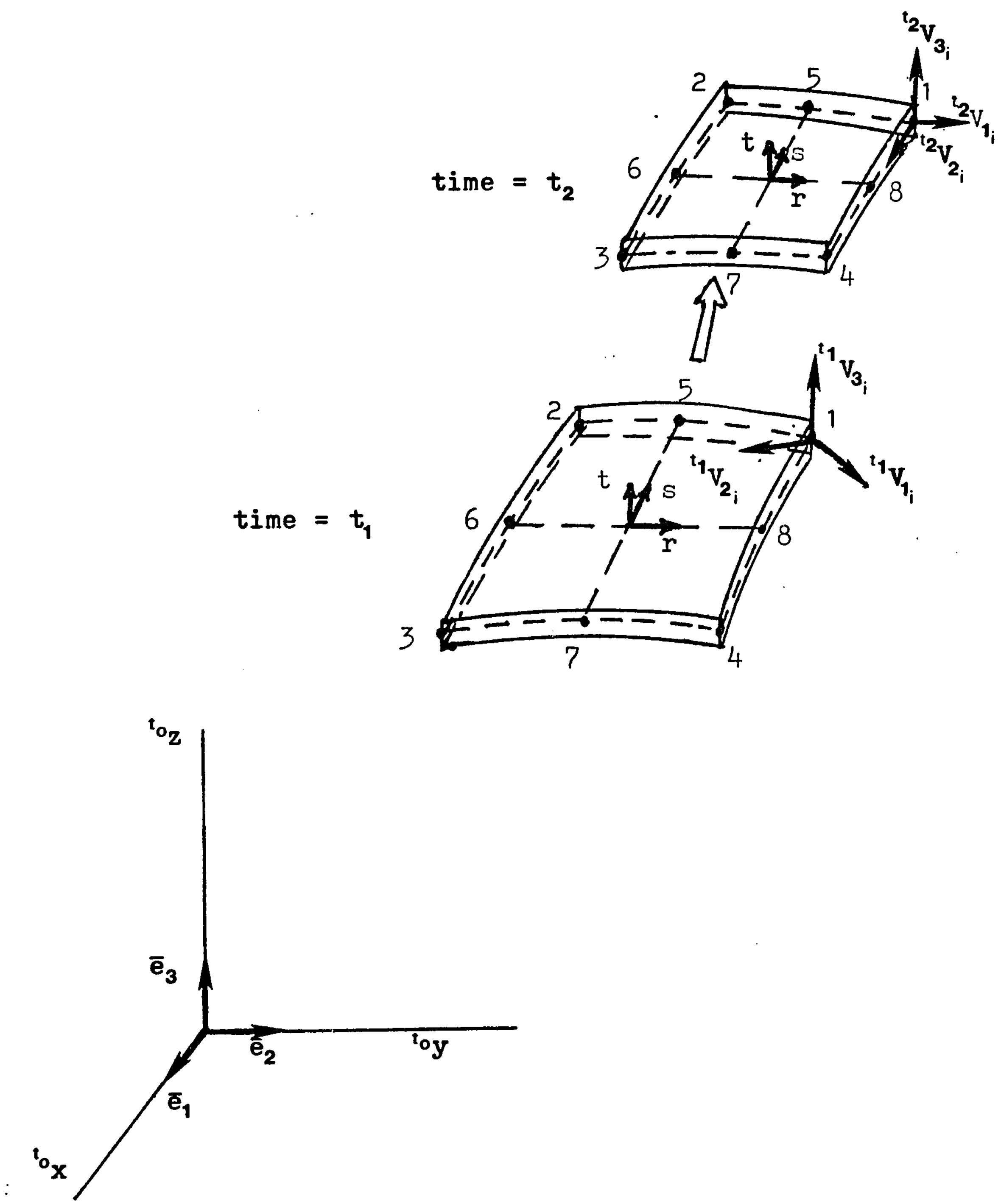

Figure 10 Deformation of shell elements.

As shown in Fig. 11, the normal vector $\vec{V}_3$ at any node i can be calculated from trignometric relations, provided the circular cylindrical shell is undeformed. Therefore, at time t_o the vector ${}^{\circ}\vec{V}_{3i}$ is

$$ {}^{\circ}\vec{V}_{3i} = \left(\frac{{}^{\circ}x_i}{\sqrt{{}^{\circ}x_i^2 + {}^{\circ}y_i^2}} \; , \; \frac{{}^{\circ}y_i}{\sqrt{{}^{\circ}x_i^2 + {}^{\circ}y_i^2}} \; , \; 0 \right) \tag{5.24} $$

At subsequent positions the vector ${}^{\circ}\vec{V}_{3i}$ is updated using the rotations α_i and β_i as shown in Fig. 12.

$$ {}^{t_2}\vec{V}_{3i} = {}^{t_1}\vec{V}_{3i} + \Delta\vec{V}_{3i} \tag{5.25} $$

where $\Delta\vec{V}_{3i}$ is the vector change in $\vec{V}_{3i}$ between times t_1 and t_2

$\Delta\vec{V}_{3i}$ is obtained from the rotations about $\vec{V}_{1i}$ and $\vec{V}_{2i}$

$$ \begin{Bmatrix} \Delta V_{3i}^{x} \\ \Delta V_{3i}^{y} \\ \Delta V_{3i}^{z} \end{Bmatrix} = -\alpha_i \begin{Bmatrix} {}^{t_1}V_{2i}^{x} \\ {}^{t_1}V_{2i}^{y} \\ {}^{t_1}V_{2i}^{z} \end{Bmatrix} + \beta_i \begin{Bmatrix} {}^{t_1}V_{1i}^{x} \\ {}^{t_1}V_{1i}^{y} \\ {}^{t_1}V_{1i}^{z} \end{Bmatrix} \tag{5.26} $$

Even though the orthogonal system, $\vec{V}_1$, $\vec{V}_2$, $\vec{V}_3$ is arbitrarily defined, the same definition must be used for all nodes. $\vec{V}_{1i}$ is

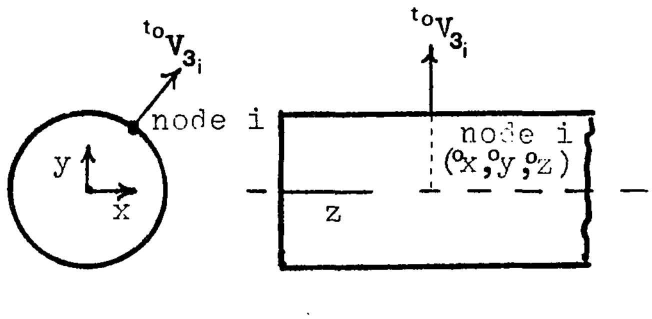

Figure 11 Vector normal to cylinderical shell

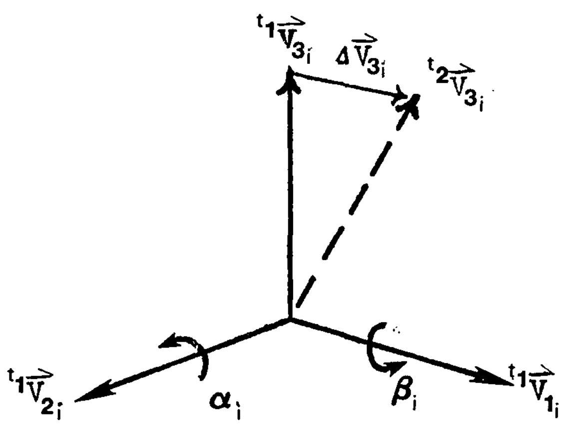

Figure 12 Measurement of shell rotations

obtained by taking the cross-product of $\vec{V}_{3i}$ and the global Cartesian vector in the direction y.

$$ {}^{t}\vec{V}_{1i} = \vec{e}_2 \times {}^{t}{}^{1}\vec{V}_{3i} \tag{5.27}$$

$$ = \begin{bmatrix} 0 \\ 1 \\ 0 \end{bmatrix} \times \begin{bmatrix} {}^{t}V_{3i}^{x} \\ {}^{t}V_{3i}^{y} \\ {}^{t}V_{3i}^{z} \end{bmatrix} = \begin{bmatrix} {}^{t}V_{3i}^{z} \\ 0 \\ {}^{t}V_{3i}^{x} \end{bmatrix} $$

and

$$ \frac{{}^{t}\vec{V}_{1i}}{||{}^{t}\vec{V}_{1i}||} = \begin{bmatrix} {}^{t}V_{3i}^{z} \Big/ \sqrt{({}^{t}V_{3i}^{x})^2 + ({}^{t}V_{3i}^{z})^2} \\ 0 \\ {}^{t}V_{3i}^{x} \Big/ \sqrt{({}^{t}V_{3i}^{x})^2 + ({}^{t}V_{3i}^{z})^2} \end{bmatrix} \tag{5.28}$$

Finally, $\vec{V}_{2i}$ is obtained by taking the vector product of $\vec{V}_{3i}$ and $\vec{V}_{1i}$:

$$ {}^{t}\vec{V}_{2i} = {}^{t}\vec{V}_{3i} \times {}^{t}\vec{V}_{1i} $$

or

$$
{}^{t}\vec{V}_{2i} = \begin{bmatrix} {}^{t}V_{3i}^{y} \cdot V_{1i}^{z} \\ -{}^{t}V_{3i}^{x} \; V_{1i}^{z} + V_{1i}^{x} \; V_{3i}^{z} \\ - V_{3i}^{y} \; V_{1i}^{x} \end{bmatrix} . \tag{5.29}
$$

${}^{t}\vec{V}_{2i}$ must then be normalized.

The vector equations are limited to shells that were of circular cross-section in the undeformed state.

The coordinates of any point on the shell is obtained from the nodal coordinates by means of interpolating functions, using the relation

$$
\begin{aligned}
{}^{t}x &= \sum_{i=1}^{8} N_i \, {}^{t}x_i + \frac{At}{2} \sum_{i=1}^{8} N_i \, {}^{t}V_{3i}^{x} \\
{}^{t}y &= \sum_{i=1}^{8} N_i \, {}^{t}y_i + \frac{At}{2} \sum_{i=1}^{8} N_i \, {}^{t}V_{3i}^{y} \\
{}^{t}z &= \sum_{i=1}^{8} N_i \, {}^{t}z_i + \frac{At}{2} \sum_{i=1}^{8} N_i \, {}^{t}V_{3i}^{z}
\end{aligned} \tag{5.30}
$$

where ^tx, ^ty, ^tz are the coordinates of a point on the element

$N_i = N_i(r,s)$ are the shape functions in terms of the local coordinates r and s

A = shell thickness (assumed constant)

$V_{3i}^{\ k}$ = components of normal vector at node i

In the above relations, a local curvilinear coordinate system r,s,t, is used. The coordinates are defined in the conventional manner i.e. node 1 is located at r = +1, s = +1; node 2 at r = −1, s = −1; node 3 at r = −1, s = −1; node 4 at r = +1, s = −1. The midnode coordinates are: node 5 at r = 0, s = +1; node 6 at r = −1, s = 0; node 7 at r = 0, s = −1 and node 8 at r = +1, s = 0. These are the node numbers in the local system and are thus the same for all elements. The origin is located at the point whose coordinates can be calculated from eq. (5.30) by using r = 0, s = 0, t = 0. For all nodes, the value of t = 0 since nodes are located in the midplane. $\vec{t}$ is defined as the normal vector to the shell surface at r = 0, s = 0.

It can be observed that in eq. (5.30) the second term vanishes for t = 0, i.e. at the midplane. Also, if the shell thickness A is small, the second term has little influence on the values of the coordinate being interpolated. This term, therefore, influences thick shell analysis, and its inclusion allows a better representation of thick shells undergoing bending. However, degeneration is not applicable to thick shells as discussed later.

For isoparametric elements, the same shape functions are used for interpolating the displacements as those used for the coordinates.

$$^{t}u = \sum_{i=1}^{8} N_i \, {}^{t}u_i + \frac{At}{2} \sum_{i=1}^{8} N_i \, {}^{t}V_{3i}^{x}$$

$$^{t}v = \sum_{i=1}^{8} N_i \, {}^{t}v_i + \frac{At}{2} \sum_{i=1}^{8} N_i \, {}^{t}V_{3i}^{y}$$

$$^{t}w = \sum_{i=1}^{8} N_i \, {}^{t}w_i + \frac{At}{2} \sum_{i=1}^{8} N_i \, {}^{t}V_{3i}^{z} \qquad (5.31)$$

The most popular isoparametric shape functions for quadratic elements, as presented by Irons and Ahmad [144] are

Corner nodes: $\frac{1}{4}(1 + \xi_i\xi)(1 + \eta_i\eta)(\xi_i\xi + \eta_i\eta - 1)$

Midnodes: $\xi_i = 0 \, ; N_i = \frac{1}{2}(1 - \xi^2)(1 + \eta_i\eta)$

$$\eta_i = 0 \, ; N_i = \frac{1}{2}(1 + \xi_i\xi)(1 - \eta^2) \qquad (5.32)$$

where ξ, η are the local coordinates (equivalent to r, s in present nomenclature). Substituting the local coordinates for each node one obtains

$$N_1 = 0.25(1 + r)(1 + s)(-1 + r + s)$$

$$N_2 = 0.25(1 - r)(1 + s)(-1 - r + s)$$

$$N_3 = 0.25(1 - r)(1 - s)(-1 - r - s)$$

$$N_4 = 0.25(1 + r)(1 - s)(-1 + r - s)$$

$$N_5 = 0.5(1 - r^2)(1 + s)$$
$$N_6 = 0.5(1 - r)(1 - s^2)$$
$$N_7 = 0.5(1 - r^2)(1 - s)$$
$$N_8 = 0.5(1 + r)(1 - s^2) \qquad (5.33)$$

Incremental Green-Lagrange Strains

As given previously, the incremental Green-Lagrange strains between steps t_1 and t_2 are

$$\Delta G_{ij} = {}^{t_2}G_{ij} - {}^{t_1}G_{ij} \qquad (5.34)$$

Substituting the definition of G_{ij} from eq. (5.6), one obtains

$$\Delta G_{ij} = \frac{1}{2}\left[\frac{\partial\,{}^{t_2}u_i}{\partial\,{}^{t}{}_{o}x_j} + \frac{\partial\,{}^{t_2}u_j}{\partial\,{}^{t}{}_{o}x_i} + \left(\frac{\partial\,{}^{t_2}u_k}{\partial\,{}^{t}{}_{o}x_i}\right)\left(\frac{\partial\,{}^{t_2}u_k}{\partial\,{}^{t}{}_{o}x_j}\right)\right]$$
$$- \frac{1}{2}\left[\frac{\partial\,{}^{t_1}u_i}{\partial\,{}^{t}{}_{o}x_j} + \frac{\partial\,{}^{t_1}u_j}{\partial\,{}^{t}{}_{o}x_i} + \left(\frac{\partial\,{}^{t_1}u_k}{\partial\,{}^{t}{}_{o}x_i}\right)\left(\frac{\partial\,{}^{t_1}u_k}{\partial\,{}^{t}{}_{o}x_j}\right)\right] \qquad (5.35)$$

But

$${}^{t_2}u_i = {}^{t_1}u_i + \Delta u_i$$
$$\therefore \quad \frac{\partial\,{}^{t_2}u_i}{\partial\,{}^{t}{}_{o}x_j} = \frac{\partial\,{}^{t_1}u_i}{\partial\,{}^{t}{}_{o}x_j} + \frac{\partial \Delta u_i}{\partial\,{}^{t}{}_{o}x_j} \qquad (5.36)$$

Substituting (5.36) in (5.35)

$$\Delta G_{ij} = \frac{1}{2}\left[\left(\frac{\partial\,{}^{t_2}u_i}{\partial\,{}^{t_o}x_j} - \frac{\partial\,{}^{t_1}u_i}{\partial\,{}^{t_o}x_j}\right) + \left(\frac{\partial\,{}^{t_2}u_j}{\partial\,{}^{t_o}x_i} - \frac{\partial\,{}^{t_1}u_j}{\partial\,{}^{t_o}x_i}\right)\right.$$

$$\left. + \frac{\partial\,{}^{t_2}u_k}{\partial\,{}^{t_o}x_i} \cdot \frac{\partial\,{}^{t_2}u_k}{\partial\,{}^{t_o}x_j} - \frac{\partial\,{}^{t_1}u_k}{\partial\,{}^{t_o}x_i}\;\frac{\partial\,{}^{t_1}u_k}{\partial\,{}^{t_o}x_j}\right]$$

$$= \frac{1}{2}\left[\frac{\partial \Delta u_i}{\partial\,{}^{t_o}x_j} + \frac{\partial \Delta u_j}{\partial\,{}^{t_o}x_i} + \left(\frac{\partial\,{}^{t_1}u_k}{\partial\,{}^{t_o}x_i} + \frac{\partial \Delta u_k}{\partial\,{}^{t_o}x_i}\right)\left(\frac{\partial\,{}^{t_1}u_k}{\partial\,{}^{t_o}x_j} + \frac{\partial \Delta u_k}{\partial\,{}^{t_o}x_j}\right)\right.$$

$$\left. - \frac{\partial\,{}^{t_1}u_k}{\partial\,{}^{t_o}x_i}\;\frac{\partial\,{}^{t_1}u_k}{\partial\,{}^{t_o}x_j}\right]$$

$$= \frac{1}{2}\left[\frac{\partial \Delta u_i}{\partial\,{}^{t_o}x_j} + \frac{\partial \Delta u_j}{\partial\,{}^{t_o}x_i} + \cancel{\frac{\partial\,{}^{t_1}u_k}{\partial\,{}^{t_o}x_i}\;\frac{\partial\,{}^{t_1}u_k}{\partial\,{}^{t_o}x_j}} + \frac{\partial \Delta\, u_k}{\partial\,{}^{t_o}x_i}\;\frac{\partial \Delta\, u_k}{\partial\,{}^{t_o}x_j}\right.$$

$$\left. + \frac{\partial\,{}^{t_1}u_k}{\partial\,{}^{t_o}x_i}\;\frac{\partial \Delta u_k}{\partial\,{}^{t_o}x_j} + \frac{\partial\,{}^{t_1}u_k}{\partial\,{}^{t_o}x_j}\;\frac{\partial \Delta u_k}{\partial\,{}^{t_o}x_i} - \cancel{\frac{\partial\,{}^{t_1}u_k}{\partial\,{}^{t_o}x_i}\;\frac{\partial\,{}^{t_1}u_k}{\partial\,{}^{t_o}x_j}}\right]$$

$$\Delta G_{ij} = \frac{1}{2}\left[\frac{\partial \Delta u_i}{\partial\,{}^{t_o}x_j} + \frac{\partial \Delta u_j}{\partial\,{}^{t_o}x_i} + \frac{\partial\,{}^{t_1}u_k}{\partial\,{}^{t_o}x_i}\;\frac{\partial \Delta u_k}{\partial\,{}^{t_o}x_j} + \frac{\partial\,{}^{t_1}u_k}{\partial\,{}^{t_o}x_j}\;\frac{\partial \Delta u_k}{\partial\,{}^{t_o}x_i} + \frac{\partial \Delta u_k}{\partial\,{}^{t_o}x_i}\;\frac{\partial \Delta u_k}{\partial\,{}^{t_o}x_j}\right] \tag{5.37}$$

We now split ΔG_{ij} into its linear and nonlinear components:

$$\Delta G_{ij} = \Delta e_{ij} + \Delta \eta_{ij}$$

$$\Delta e_{ij} = \frac{1}{2}\left[\frac{\partial \Delta u_i}{\partial\, {}^{t_o}x_j} + \frac{\partial \Delta u_j}{\partial\, {}^{t_o}x_i} + \frac{\partial\, {}^{t_1}u_k}{\partial\, {}^{t_o}x_i}\ \frac{\partial \Delta u_k}{\partial\, {}^{t_o}x_j} + \left(\frac{\partial\, {}^{t_1}u_k}{\partial\, {}^{t_o}x_j}\right)\left(\frac{\partial \Delta u_k}{\partial\, {}^{t_o}x_i}\right)\right] \tag{5.38}$$

$$\Delta \eta_{ij} = \left(\frac{\partial \Delta u_k}{\partial\, {}^{t_o}x_i}\right)\left(\frac{\partial \Delta u_k}{\partial\, {}^{t_o}x_j}\right) \tag{5.39}$$

All the terms in eq. (5.38) are linear in Δu_k. It should be noted that when calculating the incremental displacements Δu_k, the displacements in the previous iteration ${}^{t_1}u_k$ are known. Therefore, these are treated as constants in the above equation. Equation (5.39) is nonlinear (quadratic) in Δu_k.

Jacobian Matrix

The Jacobian matrix relates the derivatives in the local curvilinear coordinate system r,s,t to the global Cartesian system at time step t_o.

$$\begin{bmatrix} \frac{\partial}{\partial r} \\ \\ \frac{\partial}{\partial s} \\ \\ \frac{\partial}{\partial t} \end{bmatrix} = \underbrace{\begin{bmatrix} \frac{\partial\, {}^t_o x}{\partial r} & \frac{\partial\, {}^t_o y}{\partial r} & \frac{\partial\, {}^t_o z}{\partial r} \\ \\ \frac{\partial\, {}^t_o x}{\partial s} & \frac{\partial\, {}^t_o y}{\partial s} & \frac{\partial\, {}^t_o z}{\partial s} \\ \\ \frac{\partial\, {}^t_o x}{\partial t} & \frac{\partial\, {}^t_o y}{\partial t} & \frac{\partial\, {}^t_o z}{\partial t} \end{bmatrix}}_{[{}^t_o J]} \begin{bmatrix} \frac{\partial}{\partial\, {}^t_o x} \\ \\ \frac{\partial}{\partial\, {}^t_o y} \\ \\ \frac{\partial}{\partial\, {}^t_o z} \end{bmatrix} \tag{5.40}$$

$[{}^t_o J]$ is the Jacobian matrix in a Total Lagrangian system. The elements of this matrix can be calculated by differentiating equation (5.30), with respect to the local coodinates, as follows.

$$\frac{d\, {}^t_o x}{dr} = \left(\frac{\partial}{\partial r} \sum_{i=1}^{8} N_i \; {}^t_o x_i + \frac{At}{2} \sum_{i=1}^{8} N_i \; {}^t V_{3i}^{x} \right)$$

$$= \sum_{i=1}^{8} \frac{\partial N_i}{\partial r} \; {}^t_o x_i + \frac{At}{2} \sum_{i=1}^{8} \frac{\partial N_i}{\partial r} \; {}^t V_{3i}^{x}$$

$$\frac{d\, {}^t_o x}{ds} = \frac{\partial}{\partial r} \sum_{i=1}^{8} \frac{\partial N_i}{\partial s} \; {}^t_o x_i + \frac{At}{2} \sum_{i=1}^{8} \frac{\partial N_i}{\partial s} \; {}^t V_{3i}^{x}$$

$$\frac{\partial\, {}^t_o x}{dt} = \frac{A}{2} \sum_{i=1}^{8} N_i \left({}^t_o V_{3i}^{x} \right)$$

And similarly, the derivatives for ${}^t_o y$ and ${}^t_o z$ can be evaluated. It should be noted here that N_i is a function of r and s only.

$$
{}^t_oJ_{11} = \frac{\partial\, {}^t_o x}{\partial r} = \begin{bmatrix} \frac{\partial N_1}{\partial r} & \frac{\partial N_2}{\partial r} & \cdots & \frac{\partial N_8}{\partial r} \end{bmatrix} \begin{bmatrix} {}^t_o x_1 \\ {}^t_o x_2 \\ \cdot \\ \cdot \\ \cdot \\ {}^t_o x_8 \end{bmatrix} + \frac{At}{2} \begin{bmatrix} \frac{\partial N_1}{\partial r} & \frac{\partial N_2}{\partial r} & \cdots & \frac{\partial N_8}{\partial r} \end{bmatrix} \begin{bmatrix} {}^t_o V^x_{31} \\ {}^t_o V^x_{32} \\ \cdot \\ \cdot \\ \cdot \\ {}^t_o V^x_{38} \end{bmatrix} \tag{5.41}
$$

and

$$
{}^t_oJ_{23} = \frac{\partial\, {}^t_o z}{\partial s} = \begin{bmatrix} \frac{\partial N_1}{\partial s} & \cdots & \frac{\partial N_8}{\partial s} \end{bmatrix} \begin{bmatrix} {}^t_o z_1 \\ \cdot \\ \cdot \\ \cdot \\ {}^t_o z_8 \end{bmatrix} + \frac{At}{2} \begin{bmatrix} \frac{\partial N_1}{\partial s} & \cdots & \frac{\partial N_8}{\partial s} \end{bmatrix} \begin{bmatrix} {}^t_o V^z_{31} \\ \cdot \\ \cdot \\ \cdot \\ {}^t_o V^z_{38} \end{bmatrix} \tag{5.42}
$$

whereas the element of the last row are obtained as

$$
{}^{t}_{o}J_{32} = \frac{{}^{t}_{o}y}{t} = \frac{A}{2}\begin{bmatrix} N_1 N_2 , & \cdots & N_8 \end{bmatrix} \begin{bmatrix} {}^{t}_{o}V_{31}^{y} \\ {}^{t}_{o}V_{32}^{y} \\ \vdots \\ {}^{t}_{o}V_{38}^{y} \end{bmatrix} \tag{5.43}
$$

and so on.

The derivatives of the shape functions are obtained by differentiating equation (5.33).

$$
\begin{aligned}
\frac{\partial N_1}{\partial r} &= 0.25(1 + s)(2r + s) \\
\frac{\partial N_2}{\partial r} &= 0.25(1 + s)(2r - s) \\
\frac{\partial N_3}{\partial r} &= 0.25(1 - s)(2r + s) \\
\frac{\partial N_4}{\partial r} &= 0.25(1 - s)(2r - s) \\
\frac{\partial N_5}{\partial r} &= -r(1 + s) \\
\frac{\partial N_6}{\partial r} &= -0.5(1 - s^2) \\
\frac{\partial N_7}{\partial r} &= -r(1 - s) \\
\frac{\partial N_8}{\partial r} &= 0.5(1 - s^2)
\end{aligned} \tag{5.44}
$$

$$\frac{\partial N_1}{\partial s} = 0.25(1 + r)(r + 2s)$$

$$\frac{\partial N_2}{\partial s} = 0.25(1 - r)(-r + 2s)$$

$$\frac{\partial N_3}{\partial s} = 0.25(1 - r)(-r - 2s)$$

$$\frac{\partial N_4}{\partial s} = 0.25(1 + r)(r - 2s)$$

$$\frac{\partial N_5}{\partial s} = 0.5(1 - r^2)$$

$$\frac{\partial N_6}{\partial s} = -s(1 - r)$$

$$\frac{\partial N_7}{\partial s} = -0.5(1 - r^2)$$

$$\frac{\partial N_8}{\partial s} = -s(1 + r) \qquad (5.45)$$

Linear Strain-Displacement Matrices

The linear components of the incremental strains can be obtained from eq. (5.37) as

$$\begin{array}{l} \Delta e_{xx} = \\ \\ \Delta e_{yy} = \end{array} \left| \begin{array}{l} \left|\dfrac{\partial \Delta u}{\partial\, {}^{t}_{o}x}\right| + \left(\dfrac{\partial\, {}^{t}_{1}u}{\partial\, {}^{t}_{o}x} \cdot \dfrac{\partial \Delta u}{\partial\, {}^{t}_{o}x}\right) + \left(\dfrac{\partial\, {}^{t}_{1}v}{\partial\, {}^{t}_{o}x} \cdot \dfrac{\partial \Delta v}{\partial\, {}^{t}_{o}x}\right) + \left(\dfrac{\partial\, {}^{t}w}{\partial\, {}^{t}_{o}x}\, \dfrac{\partial \Delta w}{\partial\, {}^{t}_{o}x}\right) \\ \\ \left|\dfrac{\partial \Delta v}{\partial\, {}^{t}_{o}y}\right| + \left(\dfrac{\partial\, {}^{t}_{1}u}{\partial\, {}^{t}_{o}y} \cdot \dfrac{\partial \Delta u}{\partial\, {}^{t}_{o}y}\right) + \left(\dfrac{\partial\, {}^{t}_{1}v}{\partial\, {}^{t}_{o}y} \cdot \dfrac{\partial \Delta v}{\partial\, {}^{t}_{o}y}\right) + \left(\dfrac{\partial\, {}^{t}w}{\partial\, {}^{t}_{o}y} \cdot \dfrac{\partial \Delta w}{\partial\, {}^{t}_{o}y}\right) \end{array} \right|$$

$$
\begin{aligned}
\Delta e_{zz} &= \frac{\partial \Delta w}{\partial\,{}^{t_o}z} + \left(\frac{\partial\,{}^{t_1}u}{\partial\,{}^{t_o}z}\cdot\frac{\partial \Delta u}{\partial\,{}^{t_o}z}\right) + \left(\frac{\partial\,{}^{t_1}v}{\partial\,{}^{t_o}z}\,\frac{\partial \Delta v}{\partial\,{}^{t_o}z}\right) + \left(\frac{\partial\,{}^{t_1}w}{\partial\,{}^{t_o}z}\cdot\frac{\partial \Delta w}{\partial\,{}^{t_o}z}\right) \\
2\Delta e_{xy} &= \frac{\partial \Delta u}{\partial\,{}^{t_o}y} + \frac{\partial \Delta v}{\partial\,{}^{o}x} + \frac{\partial\,{}^{t_1}u}{\partial\,{}^{t_o}x}\cdot\frac{\partial \Delta u}{\partial\,{}^{t_o}y} + \frac{\partial\,{}^{t_1}v}{\partial\,{}^{t_o}x}\cdot\frac{\partial \Delta v}{\partial\,{}^{t_o}y} + \frac{\partial\,{}^{t_1}w}{\partial\,{}^{t_o}x}\cdot\frac{\partial \Delta w}{\partial\,{}^{t_o}y} \\
&\quad + \frac{\partial\,{}^{t_1}u}{\partial\,{}^{t_o}y}\cdot\frac{\partial \Delta u}{\partial\,{}^{t_o}x} + \frac{\partial\,{}^{t_1}v}{\partial\,{}^{t_o}y}\cdot\frac{\partial \Delta v}{\partial\,{}^{t_o}x} + \frac{\partial\,{}^{t_1}w}{\partial\,{}^{t_o}y}\cdot\frac{\partial \Delta w}{\partial\,{}^{t_o}x} \\
2\Delta e_{xz} &= \frac{\partial \Delta u}{\partial\,{}^{t_o}z} + \frac{\partial \Delta w}{\partial\,{}^{t_o}x} + \frac{\partial\,{}^{t_1}u}{\partial\,{}^{t_o}z}\,\frac{\partial \Delta u}{\partial\,{}^{t_o}x} + \frac{\partial\,{}^{t_1}v}{\partial\,{}^{t_o}z}\cdot\frac{\partial \Delta v}{\partial\,{}^{t_o}x} + \frac{\partial\,{}^{t_1}w}{\partial\,{}^{t_o}z}\cdot\frac{\partial \Delta w}{\partial\,{}^{t_o}x} \\
&\quad + \frac{\partial\,{}^{t_1}u}{\partial\,{}^{t_o}x}\cdot\frac{\partial \Delta u}{\partial\,{}^{t_o}z} + \frac{\partial\,{}^{t_1}v}{\partial\,{}^{t_o}x}\cdot\frac{\partial \Delta v}{\partial\,{}^{t_o}z} + \frac{\partial\,{}^{t_1}w}{\partial\,{}^{t_o}x}\cdot\frac{\partial \Delta w}{\partial\,{}^{t_o}z} \\
2\Delta e_{yz} &= \frac{\partial \Delta v}{\partial\,{}^{t_o}z} + \frac{\partial \Delta w}{\partial\,{}^{t_o}y} + \frac{\partial\,{}^{t_1}u}{\partial\,{}^{t_o}z}\cdot\frac{\partial \Delta u}{\partial\,{}^{t_o}y} + \frac{\partial\,{}^{t_1}v}{\partial\,{}^{t_o}z}\cdot\frac{\partial \Delta v}{\partial\,{}^{t_o}y} + \frac{\partial\,{}^{t_1}w}{\partial\,{}^{t_o}z}\cdot\frac{\partial \Delta w}{\partial\,{}^{t_o}y} \\
&\quad + \frac{\partial\,{}^{t_1}u}{\partial\,{}^{t_o}y}\cdot\frac{\partial \Delta u}{\partial\,{}^{t_o}z} + \frac{\partial\,{}^{t_1}v}{\partial\,{}^{t_o}y}\cdot\frac{\partial \Delta v}{\partial\,{}^{t_o}z} + \frac{\partial\,{}^{t_1}w}{\partial\,{}^{t_o}y}\cdot\frac{\partial \Delta w}{\partial\,{}^{t_o}z}
\end{aligned}
\tag{5.46}
$$

[BL1] [BL2]

The first term of the normal strain equations and the first two terms of the shear strains are dependent upon the displacement increments only. It is convenient to separate these terms from the rest for the purpose of writing the strain-displacement matrices. Thus, we write

$$[\Delta e] = [BL1][\Delta U] + [BL2][\Delta U] \tag{5.47}$$

where $[\Delta e]$ = incremental linear strain vector

$= [e_{xx}\ e_{yy}\ e_{zz}\ 2e_{xy}\ 2e_{yz}\ 2e_{xz}]^T$

$[BL1]$ = linear strain-displacement matrix no. 1, (6x40 size) at t_1

$[BL2]$ = linear strain-displacement matrix no. 2, (6x40 size) at t_1

$[\Delta U]$ = incremental nodal displacement vector (40x1 size)

$= [u_1\ v_1\ w_1\ u_2\ \ldots\ u_8\ v_8\ w_8]^T$

Define

$$[\Delta e]_1 \triangleq [BL1][\Delta U] \tag{5.48}$$

$$[\Delta e]_2 \triangleq [BL2][\Delta U] \tag{5.49}$$

Combining (5.46) and (5.48) yields

$$[\Delta e]_1 = \begin{bmatrix} \dfrac{\partial \Delta u}{\partial\, {}^{t}o_x} \\[2ex] \dfrac{\partial \Delta v}{\partial\, {}^{t}o_y} \\[2ex] \dfrac{\partial \Delta w}{\partial\, {}^{t}o_z} \\[2ex] \dfrac{\partial \Delta u}{\partial\, {}^{t}o_y} + \dfrac{\partial \Delta v}{\partial\, {}^{t}o_x} \\[2ex] \dfrac{\partial \Delta u}{\partial\, {}^{t}o_z} + \dfrac{\partial \Delta w}{\partial\, {}^{t}o_x} \\[2ex] \dfrac{\partial \Delta v}{\partial\, {}^{t}o_z} + \dfrac{\partial \Delta w}{\partial\, {}^{t}o_y} \end{bmatrix} \qquad (5.50)$$

The elements of this vector can be obtained by differentiating (5.21) with respect to the corresponding coordinates. For example,

$$\Delta u_i = {}^{t_2}u_i - {}^{t_1}u_i$$

$$= \sum_{i=1}^{8} N_i \; {}^{t_2}u_i + \frac{At}{2} \sum_{i=1}^{8} N_i \; {}^{t_2}V_{3i}^{x} - \sum_{i=1}^{8} N_i \; {}^{t_1}u_i$$

$$- \frac{At}{2} \sum_{i=1}^{8} N_i \; {}^{t_1}V_{3i}^{x}$$

$$= \sum_{i=1}^{8} N_i({}^{t_2}u_i - {}^{t_1}u_i) + \frac{At}{2} \sum_{i=1}^{8} N_i\ ({}^{t_2}V_{3i}^{x} - {}^{t_1}V_{3i}^{x})$$

$$= \sum_{i=1}^{8} N_i({}^{t_2}u_i - {}^{t_1}u_i) + \frac{At}{2} \sum_{i=1}^{8} N_i\ (-\alpha_i V_{2i}^{x} + \beta_i V_{1i}^{x})$$

$$\frac{\partial}{\partial\, {}^{t}o_x}(\Delta u) = \frac{\partial}{\partial\, {}^{t}o_x}\left[\sum_{i=1}^{8} N_i \Delta u_i + \frac{At}{2} \sum_{i=1}^{8} N_i(-\alpha_i V_{2i}^{x} + \beta_i V_{1i}^{x})\right]$$

$$= \sum_{i=1}^{8} \frac{\partial N_i}{\partial\, {}^{t}o_x} \Delta u_i + \frac{A}{2} \cdot \frac{\partial t}{\partial\, {}^{t}o_x} \sum_{i=1}^{8} N_i(-\alpha_i V_{2i}^{x} + \beta_i V_{1i}^{x})$$

$$+ \frac{At}{2} \sum_{i=1}^{8} \frac{\partial N_i}{\partial\, {}^{t}o_x} (-\alpha_i V_{2i}^{x} + \beta_i V_{1i}^{x}) \qquad (5.51)$$

Now $N_i = N_i(r,s)$

$$\therefore \quad \frac{\partial N_i}{\partial\, {}^{t}o_x} = \frac{\partial N_i}{\partial r} \cdot \frac{dr}{d\, {}^{t}o_x} + \frac{\partial N_i}{\partial s} \cdot \frac{ds}{d\, {}^{t}o_x}$$

$$= {}^{t}_{o}J^{-1}_{11} \frac{\partial N_i}{\partial r} + {}^{t}_{o}J^{-1}_{12} \frac{\partial N_i}{\partial s} \tag{5.52}$$

where ${}^{t}_{o}J_{ij}^{-1}$ are the elements of the inverse of the Jacobian matrix for the given element given by eq. (5.40)

and $\frac{\partial N_i}{\partial r_i}$ are the derivatives of the shape functions with respect to local coordinates, given by eq. (5.44) and (5.45).

Define three (8,3) arrays SH, SG1, SG2 as

$$SH(I,J) \stackrel{\Delta}{=} {}^{t}_{o}J^{-1}_{J1} \frac{\partial N_I}{\partial r} + {}^{t}_{o}J^{-1}_{J2} \frac{\partial N_I}{\partial s} \tag{5.53}$$

$$SG1(I,J) \stackrel{\Delta}{=} -0.5 \; AV^{J}_{2,I} \tag{5.54}$$

$$SG2(I,J) \stackrel{\Delta}{=} 0.5 \; AV^{J}_{1,I} \tag{5.55}$$

Equation (5.39) can be written as

$$\frac{\partial}{\partial\,{}^{t}o_{x}}(\Delta u) = \sum_{i=1}^{8}\left({}^{t}o J_{11}^{-1}\frac{\partial N_i}{\partial r} + {}^{t}o J_{12}^{-1}\frac{\partial N_i}{\partial s}\right)\Delta u_i$$

$$+ \sum_{i=1}^{8} -\frac{A}{2}\, V_{2i}^{x}\left(N_i\frac{\partial t}{\partial\,{}^{t}o_{x}} + t\frac{\partial N_i}{\partial\,{}^{t}o_{x}}\right)\alpha_i$$

$$+ \sum_{i=1}^{8} \frac{A}{2}\, V_{1i}^{x}\left(N_i\frac{\partial t}{\partial\,{}^{t}o_{x}} + t\frac{\partial N_i}{\partial\,{}^{t}o_{x}}\right)\beta_i$$

Define an (8,3) array GG as

$$GG(I,J) = N_I J_{J3}^{-1} + t(SH(I,J))$$

and note that

$$\frac{\partial t}{\partial\,{}^{t}o_{x}} = J_{13}^{-1}$$

$$\therefore\ \frac{\partial}{\partial\,{}^{t}o_{x}}(\Delta u) = \sum_{i=1}^{8} SH(i,1)\Delta u_i + \sum_{i=1}^{8} SG1(i,1)\; GG(i,1)\alpha_i + \sum_{i=1}^{8} SG2(i,1)GG(i,1)\beta_i \tag{5.56}$$

Similarly, the other elements $\frac{\partial v}{\partial^{t}o_{y}}$ and $\frac{\partial w}{\partial^{t}o_{z}}$ can be calculated in terms of SH, SG1, SG2, and GG. The shear terms involve mixed derivatives and these can also be written in terms of the four arrays defined. For example, the fourth term is

$$ {}^{t}u_{i} = \sum_{i=1}^{8} N_{i}\, {}^{t_1}u_{i} + \frac{At}{2} \sum_{i=1}^{8} N_{i} \left({}^{t_2}V_{3i}^{x} - {}^{t_o}V_{3i}^{x} \right) $$

$$ \frac{\partial\, {}^{t}u_{i}}{\partial\, {}^{t_o}x} = \sum_{i=1}^{8} \frac{\partial N_{i}}{\partial\, {}^{t_o}x}\, {}^{t_1}u_{i} + \sum_{i=1}^{8} \left(\frac{A}{2} \frac{dt}{d\, {}^{t_o}x} N_{i} + \frac{A}{2}\, t\, \frac{dN_{i}}{d\, {}^{t_o}x} \right) \left({}^{t_2}V_{3i}^{x} - {}^{t_o}V_{3i}^{x} \right) $$

$$ = \sum_{i=1}^{8} SH(i,1)\, {}^{t_1}u_{i} + \frac{A}{2} \sum_{i=1}^{8} \left({}^{t_o}J_{13}^{-1}\, N_{i} + t\, SH(i,1) \right) \left({}^{t_2}V_{3i}^{x} - {}^{t_o}V_{3i}^{x} \right) $$

$$ \triangleq SL(1,1) \tag{5.59} $$

The array SL is of size (3,3). Substitute (5.47) in (5.46) to obtain

$$ \Delta e_{2}(1) = SL(1,1) \frac{\partial \Delta u}{\partial\, {}^{t_o}x} + SL(2,1) \frac{\partial \Delta v}{\partial\, {}^{t_o}x} + SL(3,1) \frac{\partial \Delta w}{\partial\, {}^{t_o}x} $$

Substitute for the displacement derivatives from (5.44) to get

$$ \begin{aligned} \Delta e_{2}(1) = {} & SL(1,1) \Big[\sum_{i=1}^{8} SH(i,1) \Delta u_{i} + \sum_{i=1}^{8} SG1(i,1) GG(i,1) \alpha_{i} \\ & \qquad + \sum_{i=1}^{8} SG2(i,1) GG(i,1) \beta_{i} \Big] \\ & + SL(2,1) \Big[\sum_{i=1}^{8} SH(i,1) \Delta v_{i} + \sum_{i=1}^{8} SG1(i,2) GG(i,1) \alpha_{i} \\ & \qquad + \sum_{i=1}^{8} SG2(i,2) GG(i,1) \beta_{i} \Big] \end{aligned} $$

$$+ SL(3,1)\left[\sum_{i=1}^{8} SH(i,1)\Delta w_i + \sum_{i=1}^{8} SG1(i,3)GG(i,1)\alpha_i + \sum_{i=1}^{8} SG2(i,3)GG(i,1)\beta_i\right]$$

$$= SL(1,1)\sum_{i=1}^{8} SH(i,1)\Delta u_i + SL(2,1)\sum_{i=1}^{8} SH(i,1)\Delta v_i + SL(3,1)\sum_{i=1}^{8} SH(i,1)\Delta w_i$$

$$+ [SL(1,1)SG1(i,1) + SL(2,1)SG1(i,2) + SL(3,1)SG1(i,3)]GG(i,1)\alpha_i$$

$$+ [SL(1,1)SG2(i,1) + SL(2,1)SG2(i,2) + SL(3,1)SG2(i,3)]GG(i,1)\beta_i \tag{5.60}$$

Similarly, expressions for the other elements of $[\Delta e]_2$ may be calculated, and the matrix [BL2] obtained.

Nonlinear Strain Displacement Matrix

From eq. (5.39) the nonlinear strains are

$$\Delta\eta_{ij} = \frac{\partial \Delta u_k}{\partial\, {}^t_o x_i} \cdot \frac{\partial \Delta u_k}{\partial\, {}^t_o x_j} .$$

$$\begin{bmatrix} \eta_{xx} \\ \eta_{yy} \\ \eta_{zz} \\ \\ \eta_{xy} \\ \eta_{yz} \\ \eta_{xz} \end{bmatrix} = \begin{bmatrix} \left(\frac{\partial \Delta u}{\partial\, {}^t_o x}\right)^2 + \left(\frac{\partial \Delta v}{\partial\, {}^t_o x}\right)^2 + \left(\frac{\partial \Delta w}{\partial\, {}^t_o x}\right)^2 \\ \left(\frac{\partial \Delta u}{\partial\, {}^t_o y}\right)^2 + \left(\frac{\partial \Delta v}{\partial\, {}^t_o y}\right)^2 + \left(\frac{\partial \Delta w}{\partial\, {}^t_o y}\right)^2 \\ \left(\frac{\partial \Delta u}{\partial\, {}^t_o z}\right)^2 + \left(\frac{\partial \Delta v}{\partial\, {}^t_o z}\right)^2 + \left(\frac{\partial \Delta w}{\partial\, {}^t_o z}\right)^2 \\ \\ \frac{\partial \Delta u}{\partial\, {}^t_o x}\,\frac{\partial \Delta u}{\partial\, {}^t_o y} + \frac{\partial \Delta v}{\partial\, {}^t_o x}\,\frac{\partial \Delta v}{\partial\, {}^t_o y} + \frac{\partial \Delta w}{\partial\, {}^t_o x}\,\frac{\partial \Delta w}{\partial\, {}^t_o y} \\ \frac{\partial \Delta u}{\partial\, {}^t_o y}\,\frac{\partial \Delta u}{\partial\, {}^t_o z} + \frac{\partial \Delta v}{\partial\, {}^t_o y}\,\frac{\partial \Delta v}{\partial\, {}^t_o z} + \frac{\partial \Delta w}{\partial\, {}^t_o y}\,\frac{\partial \Delta w}{\partial\, {}^t_o z} \\ \frac{\partial \Delta u}{\partial\, {}^t_o x}\,\frac{\partial \Delta u}{\partial\, {}^t_o z} + \frac{\partial \Delta v}{\partial\, {}^t_o x}\,\frac{\partial \Delta v}{\partial\, {}^t_o z} + \frac{\partial \Delta w}{\partial\, {}^t_o x}\,\frac{\partial \Delta w}{\partial\, {}^t_o z} \end{bmatrix} = [ENL] \qquad (5.61)$$

Define

$$[BNL][\Delta U] = \left[\frac{\partial \Delta u}{\partial\, {}^t_o x} \quad \frac{\partial \Delta v}{\partial\, {}^t_o x} \quad \frac{\partial \Delta w}{\partial\, {}^t_o x} \;\vdots\; \frac{\partial \Delta u}{\partial\, {}^t_o y} \quad \frac{\partial \Delta v}{\partial\, {}^t_o y} \quad \frac{\partial \Delta w}{\partial\, {}^t_o y} \;\vdots\; \frac{\partial \Delta u}{\partial\, {}^t_o z} \quad \frac{\partial \Delta v}{\partial\, {}^t_o z} \quad \frac{\partial \Delta w}{\partial\, {}^t_o z} \right] \qquad (5.62)$$

The reason for this definition will become clear in the next section. The elements of matrix [BNL] can be calculated since expressions for the incremental displacement derivatives have already been obtained in the last section.

Element Stiffness Matrices

From eq. (5.22) the linear and nonlinear element stiffness matrices at t_1 are

$$[{}^{t_1}SKL]_e = \int_{V_e} [BL]^T [C] [BL] \, dV_e \tag{5.63}$$

$$[{}^{t_1}SKNL]_e = \int_{V_e} [BNL]^T [SM] [BNL] \, dV_e \tag{5.64}$$

Looking at eq. (5.47) it can be seen that

$$[BL] = [BL1] + [BL2] \tag{5.65}$$

Since the elements of [BL1] and [BL2] have been calculated, [BL] is obtained by adding the two matrices. Calculation of the constitutive matrix [C] is discussed later. It will be observed that $[\,{}^{t_1}SKL]_e$ is of size (40x40) since [BL] is (6x40) and [C] is (6x6).

From the definition of [BNL] it can be seen that it is of size (9x40). A (9x9) stress matrix is defined to obtain $[\,{}^{t_1}SKNL]_e$ as (40x40) so that the linear and nonlinear matrices can be added directly.

The stress matrix is defined as

$$[SM] = \begin{bmatrix} {}^{t_1}P_{xx} & 0 & 0 & {}^{t_1}P_{xy} & 0 & 0 & {}^{t_1}P_{xz} & 0 & 0 \\ & {}^{t_1}P_{xx} & 0 & 0 & {}^{t_1}P_{xy} & 0 & 0 & {}^{t_1}P_{xz} & 0 \\ & & {}^{t_1}P_{xx} & 0 & 0 & {}^{t_1}P_{xy} & 0 & 0 & {}^{t_1}P_{xz} \\ & & & {}^{t_1}P_{yy} & 0 & 0 & {}^{t_1}P_{yz} & 0 & 0 \\ & & & & {}^{t_1}P_{yy} & 0 & 0 & {}^{t_1}P_{yz} & 0 \\ & & & & & {}^{t_1}P_{yy} & 0 & 0 & {}^{t_1}P_{yz} \\ & & & & & & {}^{t_1}P_{zz} & 0 & 0 \\ & & \text{Symmetric} & & & & & {}^{t_1}P_{zz} & 0 \\ & & & & & & & & {}^{t_1}P_{zz} \end{bmatrix} \qquad (5.66)$$

where ${}^{t_1}P_{ij}$ are the elements of the Piola-Kirchhoff stress tensor at time t_1.

Numerical Integration

Equations (5.63) and (5.64) must be integrated numerically to obtain the element stiffness. Therefore, one must choose a numerical integration scheme and the order of integration. Gauss quadrature, which optimizes both the positions of the sampling points and the weighting functions, is used widely in finite element analysis. The basic equation is

$$\int_{-1}^{+1} F(x)\,dx = \sum_{i=1}^{n} \alpha_i F(x_i) \qquad (5.67)$$

where n = no. of sampling points (order of integration)

x_i = position of sampling point

α_i = weightage at sampling point i

Equations (5.63) and (5.64) involve volume integrals, which are evaluated from

$$\int_{-1}^{+1}\int_{-1}^{+1}\int_{-1}^{+1} F(a,b,c)\,da\,db\,dc = \sum_{i=1}^{n_1}\sum_{j=1}^{n_2}\sum_{k=1}^{n_3} \alpha_i\alpha_j\alpha_k\, F(a_i,\, b_j,\, c_k) \qquad (5.68)$$

where n_1 = order of integration in direction a

n_2 = order of integration in direction b

n_3 = order of integration in direction c

If the limits of integration are not ±1 then the above formulae are modified.

$$\text{Now } dV_e = dx\,dy\,dz$$

$$= \left(\frac{dx}{dr}\,dr\right)\left(\frac{dy}{ds}\,ds\right)\left(\frac{dz}{dt}\,dt\right)$$

$$= \left(\frac{dx}{dr}\cdot\frac{dy}{ds}\cdot\frac{dz}{dt}\right) drdsdt$$

$$dV_e = \det [{}^{t}_{o}J]\; dr\; ds\; dt \tag{5.69}$$

where det $\triangleq$ 'determinant of'

The limits of r, s, t are ±1 so these formulae may be used without any change.

$$[{}^{t_1}SKL]_e = \sum_{i=1}^{n_1}\sum_{j=1}^{n_2}\sum_{k=1}^{n_3} [BL(r_i,s_j,t_k)]^T[C][BL(r_i,s_j,t_k)]\det[{}^{t}_{o}J]\cdot\alpha_i\alpha_j\alpha_k \tag{5.70}$$

$[{}^{t_1}SKNL]_e$ is evaluated similarily.

Next, the order of integrations n_1, n_2, n_3 are determined. The terms in [BL] and [BNL] are of the general form

$$f\left(J^{-1}_{ij}\;\frac{\partial N_i}{\partial r_i}\right)$$

But

$$J_{ij}^{-1} = g(\frac{\partial N_i}{\partial r_i})$$

where g is some general function

$$\therefore \quad f(J_{ij}^{-1}\frac{\partial N_i}{\partial r_i}) = f'(\frac{\partial N_i}{\partial r_i} \cdot \frac{\partial N_j}{\partial r_j})$$

The derivatives of N_i can contain at the most quadratic powers of r and s.

$$\begin{aligned}\therefore \quad BL(i,j) &= f'(h_1(r^2,s^2),\ h_2(r^2,s^2)) \\ &= f''(r^4,\ s^4 \ \ldots) \\ \therefore \quad [BL]^T[BL] &= \tilde{f}\ (r^8,\ s^8 \ \ldots)\end{aligned}$$

The same applies to [BNL]. Also, upon inspection of the components of [BL] and [BNL], one finds the highest power of t is 1. Therefore, the stiffness matrix terms can contain, at most, quadratic powers of t.

Therefore, for exact integration, the order of Gauss quadrature must be 8 x 8 x 2. In linear analyses, reduced integration is used commonly. Shells can be integrated in 3 x 3 x 2 quadrature reliably and in 2 x 2 x 2 in some cases. The only way to determine a reliable order of reduced integration is to experiment with different values and compare the results. In linear analyses, a great deal of experience has been gained and standard practices established. No such norms exist in nonlinear analysis because of lack of experience. Therefore, in the present study, the order of integration in the shell plane has been made a user input variable, and different orders were tested. The order of integration in the thickness plane can be safely taken as 2, but it has also been incorporated as a variable.

Assembly

The system stiffness matrix, in the unreduced form, is of size (ND x ND) where ND is the product of the total number of nodes and the number of degrees of freedom per node, which is 5 in this case. The system matrix [SKL] is obtained by adding the components of $[BL]^T[C][BL]$ in the corresponding position. The elements of [SKNL] are obtained from $[BNL]^T[SM][BNL]$. In turn, [BL] and [BNL] are sums of the weighted values of the integrals at the Gauss sampling points. In this study, the conventional assembly by elements is used. The matrices $[BL]^T[C][BL]$ and $[BNL]^T[SM][BNL]$ are of size (40x40), correponding to the 40 degrees of freedom per element. Each component of this is placed directly into the system matrix at the end of Gauss point calculations for each element, using the relation

SK(NR1 + M, NR2 + L) = BTCB(5(I - 1) + M, 5(J - 1) + L)

where NR1 = (ICON(NELM, I) - 1)x5

NR2 = (ICON(NELM, J) - 1)x5.

I and J are the local node numbers (1 thru 8) of the nodes being assembled and ICON is the connectivity of the element being assembled. BTCB can be taken to mean either $[BL]^T[C][BL]$ or $[BNL]^T[SM][BNL]$.

Constitutive Relations

The constitutive matrix was defined earlier as

$$[\Delta P] = [{}^{t}_{1}C][\Delta e]$$

It relates the incremental Piola-Kirchhoff stresses to the linear component of the linear Green-Lagrange strains. It can be approximately taken as the relation between Cauchy stresses and strains.

The merits and demerits of continuum elements vis-a-vis structural elements were discussed in an earlier section. The kinematic relations used in formulating the stiffnesses were for a general three-dimensional continuum. Therefore, if the general three-dimensional constitutive relations are used, the result would be a continuum element. However, if shell theory assumptions are forced on the constitutive matrix, a degenerated shell element is obtained.

In this problem, the focus is on linear elastic and elastic-plastic materials. Therefore, two sets of constitutive relations must be specified and a criterion defined for yielding.

<u>Elasticity Matrix</u>

The relation between Cauchy stresses and strains in three dimensions are:

$$
\begin{aligned}
e_{xx} &= \frac{1}{E}\,[\sigma_{xx} - \nu(\sigma_{yy} + \sigma_{zz})] \\
e_{yy} &= \frac{1}{E}\,[\sigma_{yy} - \nu(\sigma_{xx} + \sigma_{zz})] \\
e_{zz} &= \frac{1}{E}\,[\sigma_{zz} - \nu(\sigma_{xx} + \sigma_{yy})] \\
2e_{xy} &= \frac{\tau_{xy}}{G} = \frac{\tau_{xy}}{E/2(1+\nu)} \\
2e_{yz} &= \frac{\tau_{yz}}{E/2(1+\nu)} \\
2e_{xz} &= \frac{\tau_{xz}}{E/2(1+\nu)}
\end{aligned}
\tag{5.71}
$$

where E = Young's Modulus, G = shear Modulus, and ν = Poisson's Ratio

Inverting these relations, the elasticity matrix [CE] is obtained as

$$
[CE] = \frac{E}{1-\nu-2\nu^2}
\begin{bmatrix}
1-\nu & \nu & \nu & 0 & 0 & 0 \\
 & 1-\nu & \nu & 0 & 0 & 0 \\
 & & 1-\nu & 0 & 0 & 0 \\
 & & & \frac{1-2\nu}{2} & 0 & 0 \\
 & \text{Symmetric} & & & \frac{1-2\nu}{2} & 0 \\
 & & & & & \frac{1-2\nu}{2}
\end{bmatrix}
\tag{5.72}
$$

Plasticity Constitutive Relations

Complete specification of plasticity relations involve the specification of the following:

1. a yield criterion
2. a flow rule
3. a hardening rule

It is the aim of the study to focus primarily on steel pipelines, which may be considered as materially isotropic and ductile. Therefore, the yield criterion chosen is the Von Mises or Distortion Energy Theory. In terms of the six stress components, this criterion can be expressed as

$$\{\tfrac{1}{2}[(\sigma_{xx}-\sigma_{yy})^2 + (\sigma_{yy}-\sigma_{zz})^2 + (\sigma_{zz}-\sigma_{xx})^2] + 3\tau_{xy} + 3\tau_{yz}^{\,2} + 3\tau_{zx}^{\,2}\}^{\frac{1}{2}} \geq S_y \tag{5.73}$$

where S_y = uniaxial yield strength

It should be noted here that the stress components in eq. (5.73) are the elements of the conventional engineering stress tensor. Therefore, the Piola-Kirchhoff stresses must be transformed to Cauchy stresses to test for yielding.

Plastic stress-strain relations are of two kinds: incremental and deformation. Incremental theories relate the deviatoric stresses in the material to the corresponding plastic strain increments. This equation must be integrated over the load interval to get the total stresses and strains. On the other hand, deformation theories relate the total stresses and strains directly.

The Prandtl-Reuss flow rule is an incremental theory in its simplest form, and can be written as

$$de^{p}_{ij} = S_{ij}\ d\lambda \tag{5.74}$$

where $d\lambda = \frac{3}{2}\ \frac{de_e}{\sigma_e}$

e^{p}_{ij} = plastic component of strain

S_{ij} = deviatoric stresses

σ_e and de_e are the effective stress and effective strain increment given as

$$\sigma_e = \frac{1}{\sqrt{2}}\left[(\sigma_{xx} - \sigma_{yy})^2 + (\sigma_{yy} - \sigma_{zz})^2 + (\sigma_{zz} - \sigma_{xx})^2 + 6(\tau_{xy}{}^2 + \tau_{yz}{}^2 + \tau_{zx}{}^2)\right]^{1/2} \tag{5.75}$$

$$de_e = \frac{\sqrt{2}}{3}\left[(de^{p}_{xx} - de^{p}_{yy})^2 + (de^{p}_{yy} - de^{p}_{zz})^2 + (de^{p}_{zz} - de^{p}_{xx})^2 + 6(de^{p}_{xy})^2 + 6(de^{p}_{yz})^2 + 6(de^{p}_{xz})^2\right]^{1/2} \tag{5.76}$$

The equivalent deformation theory as proposed by Hencky [67] is

$$e^p_{ij} = \frac{3}{2} \frac{e_e}{\sigma_e} S_{ij} \tag{5.77}$$

According to eq. (5.77) the plastic strains are functions of the current state of stress and are independent of the loading history. At first sight, deformation theories appear to be inferior to incremental theories because the loading path is assumed to influence strains. However, inspite of this discrepancy, many researchers have shown that results obtained from this theory are in better agreement with experimental results than the analytically sound incremental theories. Batterman [27] proved this for proportional loads and Budiansky [69] experimented with nonproportional loads. The latter found that for lower hardening rates the results for nonproportional loading were good. This support of deformation theories has been disputed by other researchers, such as Drucker [97].

In this study, the basic equations of motion were written in incremental form, which makes it easier to incorporate incremental theories. Since nonproportional loads must be studied also and since the hardening indices for steel are moderate, it seems better to use an incremental theory.

The next step is to calculate the hardening in the material and incorporate it in the Prandtl-Reuss equations. For perfectly plastic materials (no hardening), the flow rule is written as [67]

$$de^p_{ij} = \frac{3}{2} \frac{d\dot{e}_e}{S_y} S_{ij} \tag{5.78}$$

Mendelson [67] has defined two measures of hardening. The first one, known as work hardening, depends only upon the plastic work and is independent of the strain path. The second measure, known as strain hardening, depends upon the slope of the effective stress-strain curve.

The Prandtl-Reuss equations now take the form

$$de^p_{ij} = \frac{3}{2} \frac{d\sigma_e}{{}^tH\sigma_e} S_{ij} \tag{5.79}$$

where ${}^tH$ = hardening measure

$${}^tH = \frac{2}{3}\, {}^t\sigma \frac{d\sigma}{dW_p} \tag{5.80}$$

${}^tH$ for the three material models studied is computed in a later section.

After yielding, the strain is composed of two parts, elastic and plastic.

$$de = de^e + de^p \tag{5.81}$$

or

$$de^p = de - de^e \tag{5.82}$$

where de = total strain

de^e = elastic component

de^p = plastic component

Also, $[d\sigma] \triangleq [CE][de^e] = [CE][de - de^p]$ (5.83)

and $[d\sigma] \triangleq [CEP][de]$ (5.84)

where [CE] = elasticity matrix

[CEP] = elastic-plastic matrix

Reference [46] has derived the plasticity matrix for a Bilinear material model. Generalizing this result here and writing it in a more compact form, one gets

$$[CP] = {}^t\beta[{}^tS]^T[{}^tS] \qquad (5.85)$$

where $$[{}^tS]^T = [{}^tS_{11}\ {}^tS_{22}\ {}^tS_{33}\ {}^tS_{12}\ {}^tS_{23}\ {}^tS_{13}] \qquad (5.86)$$

$$\begin{aligned} {}^tS_{ij} &= \text{deviatoric stresses} \\ &= {}^t\sigma_{ij} - \frac{\sigma_1 + \sigma_2 + \sigma_3}{3} \end{aligned} \qquad (5.87)$$

${}^t\sigma_{ij}$ = Cauchy stresses

and $${}^t\beta = \frac{3E}{2(1+\nu)} \cdot \frac{1}{{}^t\sigma_e^{\,2}} \left(\frac{1}{1 + \frac{2}{3}\,{}^tH\,\frac{1+\nu}{E}}\right) \qquad (5.88)$$

The elastic-plastic constitutive matrix is obtained from

$$[CEP] = [CE] - [CP] \tag{5.89}$$

The only remaining unknown is ${}^{t}H$ which is computed in a later section for the three material models used here. The constitutive matrix must be computed in each iteration from the stresses found in the previous iteration. The matrix is calculated at each Gauss point separately allowing for both elastic and plastic deformations to occur at different points in the cylinder, giving a more realistic model than those based on average material stresses.

Material Models

The hardening index in eq. (5.78) was defined in terms of the incremental work under the effective stress-strain curve. It is standard practice to use the uniaxial stress-strain curve, obtained from a tension test, instead of the effective stress-strain curve. For this purpose, material models must be defined and compared to experimentally obtained data. Figure 13 shows the three models used in this study.

The simplest model is the bilinear model, defined by the equations

$$\sigma = Ee \qquad S \leq S_y \tag{5.90}$$

$$(\sigma - S_y) = E_T(e - e_y) \qquad S > S_y \tag{5.91}$$

where E = Young's Modulus

E_T = Tangent Modulus

S_y, e_y = yield stress, strain

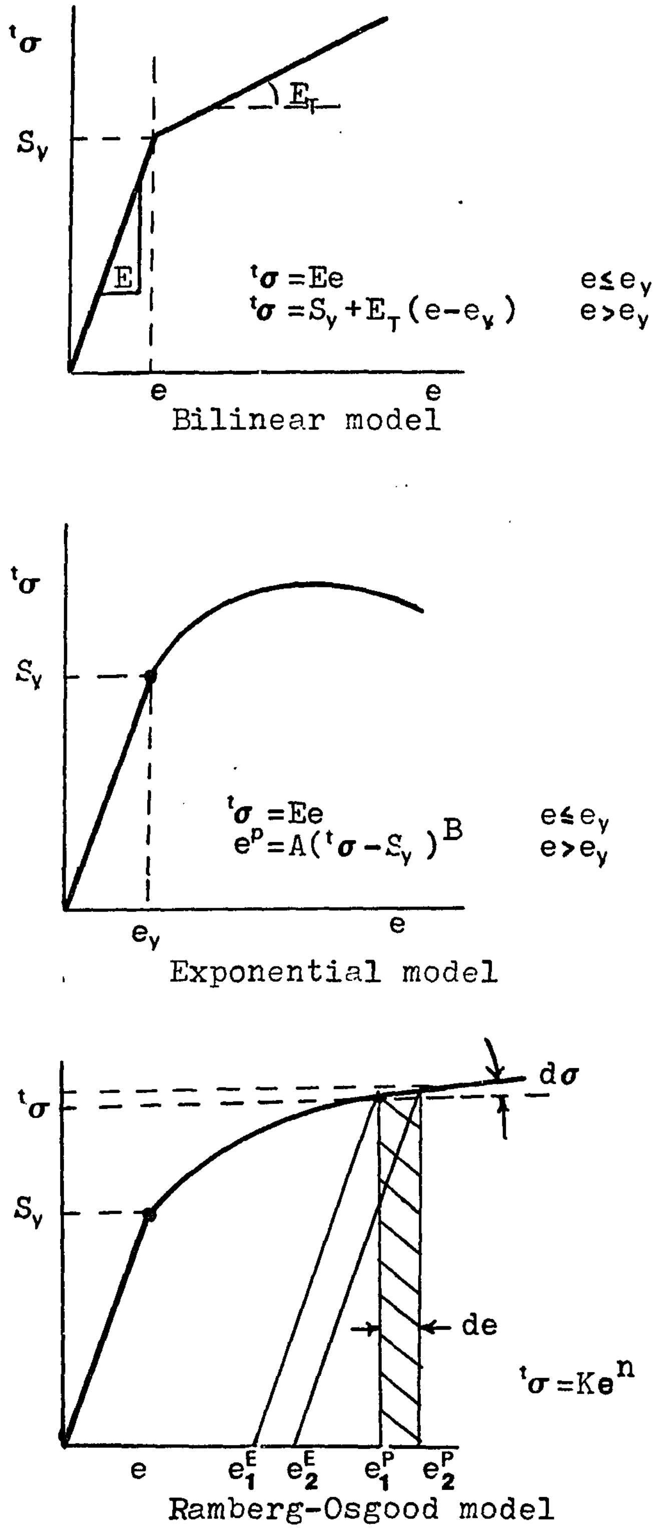

Figure 13 Material models.

Now $e_y = S_y/E$

$$\sigma = S_y + E_T(e - \frac{S_y}{E})$$

$$\sigma = (S_y - \frac{E_T S_y}{E}) + E_T e$$

$$\sigma = K_1 + K_2 e \tag{5.92}$$

where K_1 and K_2 are constants

In order to determine E_T from experimental data, eq. (5.91) is written as

$$y = b_1 x$$

where $y = \sigma - K_1$

$x = e - e_y$

Using least square fit

$$\Delta y = b_1 x_i - y_i$$

where x_i, y_i are experimentally measured values

$$(\Delta y)^2 = b_1{}^2 (x_i)^2 + (y_i)^2 - 2b_1 (x_i)(y_i)$$

$$\therefore \sum_{i=1}^{n} (\Delta y)^2 = b_1{}^2 \sum_{i=1}^{n} x_i{}^2 + \sum_{i=1}^{n} y_i - 2b_1 \sum_{i=1}^{n} x_i y_i$$

$$\therefore \frac{\partial \Sigma (\Delta y)^2}{\partial b_1} = 2b_1 \Sigma x_i{}^2 - 2 \Sigma x_i y_i = 0$$

$$b_1 = \frac{\Sigma x_i y_i}{\Sigma x_i{}^2}$$

or

$$E_T = \frac{\sum_{i=1}^{N} (e_i - e_y)(\sigma_i - S_y)}{\sum_{i=1}^{N} (e_i - e_y)^2} \tag{5.93}$$

The exponential model, defined by Barnard and Sherman [104] as

$$\begin{aligned} e^p &= A(\sigma - S_y)^B & \sigma &> S_y \\ e^p &= 0 & \sigma &\leq S_y \end{aligned} \qquad (5.94)$$

where A = hardening coefficient

B = hardening exponent

To determine A and B from experimental data, a least square fit is used as follows

$$y \triangleq Ax^B \qquad (5.95)$$

where

$$y = e^p = e - e_y$$

$$x = \sigma - S_y$$

then $\log y = \log A + B \log x$

or $\tilde{y} = \tilde{A} + B\tilde{x}$

where

$$\tilde{y} = \log y,$$

$$\tilde{A} = \log A,$$

$$\tilde{x} = \log x$$

$$\Delta\tilde{y} = \tilde{A} + B\tilde{x} - \tilde{y}_i$$

and

$$\sum_{i=1}^{N} (\Delta\tilde{y})^2 = N\tilde{A}^2 + B^2 \Sigma\tilde{x}_i^{\,2} + \Sigma\,\tilde{y}_i^{\,2} + 2\tilde{A}B\,\Sigma\,\tilde{x}_i - 2\tilde{B}\,\Sigma\,\tilde{x}_i\tilde{y}_i - 2\tilde{A}\,\Sigma\tilde{y}_i$$

$$\frac{\partial \Sigma (\Delta \tilde{y})^2}{\partial \tilde{A}} = 2N\tilde{A} + 2B\,\Sigma\,\tilde{x}_i - 2\,\Sigma\,\tilde{y}_i = 0$$

and

$$\frac{\partial \Sigma\,(\Delta \tilde{y})^2}{\partial \tilde{B}} = 2B\,\Sigma\,\tilde{x}_i^{\,2} + 2\tilde{A}\,\Sigma\,\tilde{x}_i - 2\,\Sigma\,\tilde{x}_i\tilde{y}_i = 0$$

Solving the above simultaneous equations, one gets

$$B = \frac{\Sigma\tilde{x}_i\,\Sigma\tilde{y}_i - N\,\Sigma\,\tilde{x}_i\tilde{y}_i}{(\Sigma\tilde{x}_i)^2 - N\,\Sigma\,\tilde{x}_i^{\,2}}$$

$$\tilde{A} = \frac{\Sigma\,\tilde{y}_i - B\,\Sigma\,\tilde{x}_i}{N}$$

$$A = \text{alog}\left[\frac{\Sigma\log(e_i - e_y) - B\,\Sigma\log(\sigma_i - S_y)}{N}\right]$$

$$\text{and } B = \frac{\Sigma\log(\sigma_i - S_y)\;\Sigma\log(e_i - e_y) - N\,\Sigma\log(\sigma_i - S_y)\log(e_i - e_y)}{(\Sigma\log(\sigma_i - S_y))^2 - N\,\Sigma\,(\log(\sigma_i - S_y))^2} \tag{5.96}$$

The Ramberg-Osgood model is of the form

$$\sigma = Ke^{n} \tag{5.97}$$

where K = strain hardening coefficient

n = strain hardening exponent

To obtain the values of K and n, take logs of both sides

$$\log \sigma = \log K + n \log e$$

or

$$\tilde{y} = K_3 + n\tilde{x}$$

where $\tilde{y} = \log \sigma$

$K_3 = \log K$

$\tilde{x} = \log e$

This is similar to the equation of the exponential model, so K and n can be evaluated as

$$K = \text{alog}\left[\frac{\Sigma \log \sigma_i - n\,\Sigma \log e_i}{N}\right]$$

where

$$n = \frac{\Sigma \log e_i \,\Sigma \log \sigma_i - N\,\Sigma \log e_i \log \sigma_i}{(\Sigma \log e_i)^2 - N\,\Sigma(\log e_i)^2} \tag{5.98}$$

<u>Hardening Variable ^{t}H</u>

The hardening variable ^{t}H, at time t_1, was defined in eq. (5.63) as

$$^{t}H = {}^{t}\sigma \frac{d\sigma}{dW_p}$$

where $dW_p = \sigma_{ij}\, de_{ij}$

The hardening variable is evaluated below for each of the material models.

In Fig. 13, the definitions of stress/strain components are shown on the Ramberg-Osgood model. These definitions are valid for all models. The shaded area is the change in the total strain energy dW.

$$dW_p = dW - dW_e$$

$$= {}^{t}\sigma de - {}^{t}\sigma de^{E}$$

Now

$$de^{E} = e_2^{E} - e_1^{E}$$

$$= \frac{^{t}\sigma_2}{E} - \frac{^{t}\sigma_1}{E}$$

$$= \frac{d\sigma}{E}$$

$$\therefore \quad dW_p = {}^{t}\sigma\left(de - \frac{d\sigma}{E}\right) \qquad (5.99)$$

Eq. (5.99) is valid for all elastic-plastic models. For the Bilinear model

$$\frac{d\sigma}{de} = E_T$$

$$\therefore \quad dW_p = {}^t\sigma\left(\frac{d\sigma}{E_T} - \frac{d\sigma}{E} \right)$$

$$\therefore \quad \frac{dW_p}{d\sigma} = {}^t\sigma\left(\frac{1}{E_T} - \frac{1}{E} \right)$$

$$= {}^t\sigma\left(\frac{E - E_T}{E_T E}\right) \tag{5.100}$$

Substituting eq. (5.100) in (5.80)

$$t_H = \frac{\cancel{{}^t\sigma}}{\cancel{{}^t\sigma}} \frac{E_T E}{E - E_T}$$

$$= \frac{E_T E}{E - E_T} \tag{5.101}$$

For the exponential model

$$e^P = A({}^t\sigma - S_y)^B$$

$$de^P = AB({}^t\sigma - S_y)^{B-1} d\sigma$$

Also, $$dW_p = {}^t\sigma de^p$$

$$= {}^t\sigma \; AB({}^t\sigma - S_y)^{B-1} d\sigma \qquad (5.102)$$

$$\frac{dW_p}{d\sigma} = AB^t \; ({}^t\sigma - S_y)^{B-1} \qquad (5.103)$$

Substituting (5.103) in (5.80)

$${}^tH = {}^t\sigma \; \frac{d\sigma}{dW_p}$$

$$= {}^t\sigma \cdot \frac{1}{AB^t\sigma({}^t\sigma - \sigma_y)^{B-1}}$$

$$\therefore \; {}^tH = \frac{1}{AB({}^t\sigma - \sigma_y)^{B-1}} \qquad (5.104)$$

For the Ramberg-Osgood model

$${}^t\sigma = Ke^n$$

$$\therefore \; d\sigma = nKe^{n-1}de$$

Also $$e = (\frac{{}^t\sigma}{K})^{\frac{1}{n}}$$

$$d\sigma = nK \; (\frac{{}^t\sigma}{K})^{\frac{n-1}{n}}$$

$$= n \cdot {}^t\sigma^{(\frac{n-1}{-n})} \; \frac{1}{K^n} \; de \qquad (5.105)$$

Now $dW_p = {}^t\sigma(de - \frac{d\sigma}{E})$

$$= \frac{{}^t\sigma d\sigma}{n\ {}^t\sigma^{(\frac{n-1}{n})} (\frac{1}{K^n})} - \frac{{}^t\sigma d\sigma}{E}$$

$$\frac{dW_p}{d\sigma} = {}^t\sigma \left[\frac{1}{n\ {}^t\sigma^{\frac{1-n}{n}} K^{\frac{1}{n}}} - \frac{1}{E} \right]$$

$$= {}^t\sigma \left[\frac{E - n\ {}^t\sigma^{\frac{n-1}{n}} K^{\frac{1}{n}}}{n\ E \cdot K^{\frac{1}{n}}\ {}^t\sigma^{\frac{n-1}{n}}} \right] \tag{5.106}$$

Substituting (5.106) in (5.80)

$${}^tH = {}^t\sigma \frac{d\sigma}{dW_p}$$

$$= \frac{\cancel{{}^t\sigma}}{\cancel{{}^t\sigma}} \left[\frac{nE\ K^{\frac{1}{n}}\ {}^t\sigma^{\frac{n-1}{n}}}{E - n\,{}^t\sigma^{\frac{n-1}{n}} K^{\frac{1}{n}}} \right] \tag{5.107}$$

$$\therefore\ {}^tH = \left[\frac{nEK^{\frac{1}{n}}\ \sigma^{\frac{n-1}{n}}}{E - n\,{}^t\sigma^{\frac{n-1}{n}} K^{\frac{1}{n}}} \right]$$

Degeneration

So far all kinematic and constitutive relations used are valid for the general three-dimensional continuum. However, if Kirchhoff's shell assumption that the stress normal to the shell surface is zero is now introduced via the constitutive matrix, one would have the formulation of a shell element. This is done by first writing the constitutive matrix in the element local coordinate system. The direction t is normal to the shell surface, so the components of stress in that direction are forced to zero. Thus,

$$
\begin{aligned}
e_{rr} &= \frac{1}{E}(\sigma_{rr} - \sigma_{ss}) \\
e_{ss} &= \frac{1}{E}(\sigma_{ss} - \sigma_{rr}) \\
e_{tt} &= \frac{-\nu}{E}(\sigma_{rr} - \sigma_{ss}) \\
2e_{ij} &= \frac{2(1+\nu)}{E}\,\tau_{ij} \qquad \text{for } i \neq j
\end{aligned}
\qquad (5.108)
$$

From the first two equations, one gets

$$
\begin{aligned}
\sigma_{rr} &= \frac{E}{1-\nu^2}(e_{rr} - \nu e_{ss}) \\
\sigma_{ss} &= \frac{E}{1-\nu^2}(e_{ss} - \nu e_{rr})
\end{aligned}
\qquad (5.109)
$$

Therefore, in the shell element coordinate system the constitutive matrix [CSE] is written as

$$
[CSE] = \frac{E}{1-\nu^2}\begin{bmatrix}
1 & -\nu & 0 & 0 & 0 & 0 \\
-\nu & 1 & 0 & 0 & 0 & 0 \\
0 & 0 & 0 & 0 & 0 & 0 \\
0 & 0 & 0 & \frac{1-\nu}{2} & 0 & 0 \\
0 & 0 & 0 & 0 & \frac{1-\nu}{2} & 0 \\
0 & 0 & 0 & 0 & 0 & \frac{1-\nu}{2}
\end{bmatrix}
\qquad (5.10)
$$

This tensor must be transformed to the global coordinate system by orthogonal rotation matrix, which is determined from the direction cosines of the local axes (see Fig. 14). For this purpose, vectors in directions r and s should be evaluated at the point $r = 0$, $s = 0$, $t = 0$. Since this point is on the midplane the coordinates can be interpolated as (from eq. (5.30) for $t = 0$)

$$^{t}x_{i} = \sum_{i=1}^{8} N_{i}\,^{t}x_{i}$$

$$^{t}y_{i} = \sum_{i=1}^{8} N_{i}\,^{t}y_{i}$$

$$^{t}z_{i} = \sum_{i=1}^{8} N_{i}\,^{t}z_{i}$$

For $r = 0$, $s = 0$

$$N_{i} = -0.25, \; i = 1,4$$
$$N_{i} = 0.5, \; i = 5,8$$

Using these values of N_i and the nodal coordinates, the global coordinates of point 0 are obtained as (x_o, y_o, z_o). The vectors $\vec{r}$ and $\vec{s}$ may be obtained by writing the equation of straight lines joining

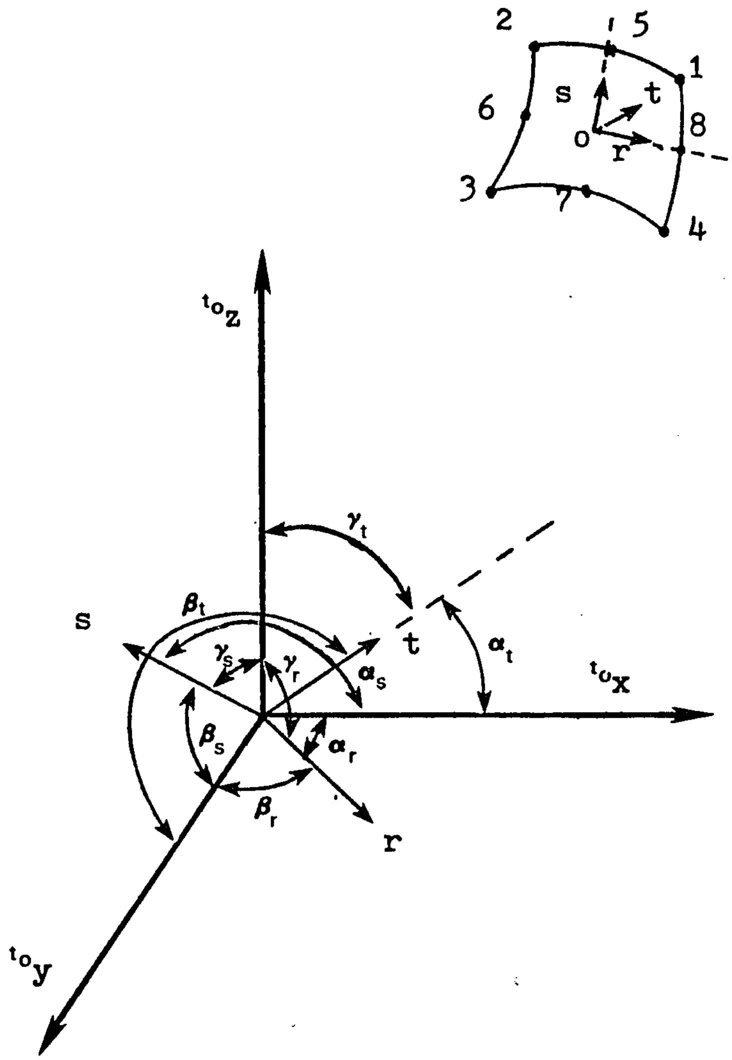

Figure 14 Transformation from local to global coordinate system.

points 0 and 8 and 0 and 5, respectively (see Fig. 14). For cylinders, whose s direction is alligned with the length direction of the cylinder, this will give the exact vector for $\vec{s}$ but the value for $\vec{r}$ will only be approximate. However, as the number of elements along the circumference is increased, this error in $\vec{r}$ is reduced. Thus

$$\vec{r} = (x_8-x_0)\hat{i} + (y_8-y_o)\hat{j} + (z_8-z_0)\hat{k} \tag{5.111}$$

$$\vec{s} = (x_5-x_0)\hat{i} + (y_8-y_0)\hat{j} + (z_8-z_0)\hat{k} \tag{5.112}$$

$$\vec{t} = \vec{r} \times \vec{s} \tag{5.113}$$

The angles between $\vec{r}$, $\vec{s}$, $\vec{t}$ and $\vec{x}$, $\vec{y}$, $\vec{z}$ as defined in Fig. 14 can be calculated from the scalar products

$$\vec{A} \cdot \vec{B} = \|A\| \cdot \|B\| \cos\theta$$

$$= A_xB_x + A_yB_y + A_zB_z$$

$$\cos\theta = \frac{A_xB_x + A_yB_y + A_zB_z}{\sqrt{(A_x{}^2 + A_y{}^2 + A_z{}^2)(B_x{}^2 + B_y{}^2 + B_z{}^2)}} \tag{5.114}$$

Since the global unit vectors are (1,0,0), (0,1,0), and (0,0,1), the angles α, β, γ are given by

$$\begin{aligned} \alpha_i &= \cos^{-1}(e_x, B_i) = \cos^{-1}\frac{B_x}{\|B\|} \\ \beta_i &= \cos^{-1}(e_y, B_i) = \cos^{-1}\frac{B_y}{\|B\|} \\ \gamma_i &= \cos^{-1}(e_z, B_i) = \cos^{-1}\frac{B_z}{\|B\|} \end{aligned} \tag{5.115}$$

The stresses in the local system can be transformed to the stresses in the global system using the tensor transformation given in books on Elasticity. From Ref. [147]

$$P_{xx} = \ell_1^2 P_{rr}+m_1^2P_{ss}+n_1^2P_{tt}+2\ell_1m_1P_{rs}+2m_1n_1P_{st}+2n_1\ell_1P_{rt}$$

$$P_{yy} = \ell_2^2 P_{rr}+m_2^2P_{ss}+n_2^2P_{tt}+2\ell_2m_2P_{rs}+2m_2n_2P_{st}+2n_2\ell_2P_{rt}$$

$$P_{zz} = \ell_3^2 P_{rr}+m_3^2P_{ss}+n_3^2P_{tt}+2\ell_3m_3P_{rs}+2m_3n_3P_{st}+2n_3\ell_3P_{rt}$$

$$P_{xy} = \ell_1\ell_2P_{rr}+m_1m_2P_{ss}+n_1n_2P_{tt}+(\ell_1m_2+m_1\ell_2)P_{rs}$$

$$+(m_1n_2+n_1m_2)P_{st}+(n_1\ell_2+\ell_1n_2)P_{rt}$$

$$P_{yz} = \ell_2\ell_3P_{rr}+m_2m_3P_{ss}+n_2n_3P_{tt}+(\ell_2m_3+m_2\ell_3)P_{rs}$$

$$+(m_2n_3+n_2m_3)P_{st}+(n_2\ell_3+\ell_2n_3)P_{rt}$$

$$P_{xz} = \ell_3\ell_1P_{rr}+m_3m_1P_{ss}+n_3n_1P_{tt}+(\ell_3m_1+m_3\ell_1)P_{rs}$$

$$+(m_3n_1+n_3m_1)P_{st}+(n_3\ell_1+\ell_3n_1)P_{rt} \qquad (5.116)$$

where $\ell_i = \cos \alpha_i$

$m_i = \cos \beta_i$

$n_i = \cos \gamma_i$

Thus, we can write eq. (5.109) in matrix form for incremental stresses

$$[\Delta P]_{xyz} = [\hat{T}][\Delta P]_{rst} \tag{5.117}$$

Similarly, for strains we can write

$$[\Delta e]_{xyz} = [\hat{T}][\Delta e]_{rst}$$

Also

$$[\Delta P]_{rst} = [{}^{t}_{1}CE][\Delta e]_{rst}$$

$$\therefore \quad [\hat{T}][\Delta P]_{xyz} = [{}^{t}_{1}CE][\hat{T}][\Delta e]$$

$$\therefore \quad [\Delta P]_{xyz} = [\hat{T}]^T[{}^{t}_{1}CE][\hat{T}][\Delta e]_{xyz} \tag{5.118}$$

(Since $[\hat{T}]$ is an orthogonal matrix)

Therefore, the degenerated elasticity matrix is

$$[{}^{t}_{1}DE] = [\hat{T}]^T[{}^{t}_{1}CE][\hat{T}] \tag{5.119}$$

where $[\Delta P]_{xyz} = [{}^{t}_{1}DE][\Delta e]_{xyz}$

Degeneration of Plasticity Matrix

In the plasticity matrix [CP], the Kirchhoff assumption is substituted ($P_{tt} = 0$), giving

$$[{}^{t_1}CP] = \frac{\beta E}{1+\nu}\begin{bmatrix} S_{rr} & S_{ss} & 0 & S_{rs} & S_{st} & S_{rt} \end{bmatrix} \begin{bmatrix} S_{rr} \\ S_{ss} \\ 0 \\ S_{rs} \\ S_{st} \\ S_{rt} \end{bmatrix} \tag{5.120}$$

where S_{ij} are the deviatoric stresses

The degenerated matrix is obtained from

$$[{}^{t_1}DEP] = [\hat{T}]^T([{}^{t_1}CE] - [{}^{t_1}CP])[\hat{T}] \tag{5.121}$$

When the strain displacement matrices derived before are used in conjunction with (5.121), one obtains the large displacement, degenerated, elastic-plastic shell element.

Calculation of Piola-Kirchhoff Stresses

The Piola-Kirchhoff stresses at the end of step t_2 are calculated from the linearized relation

$${}^{t_2}P_{ij} = {}^{t_1}P_{ij} + {}^{t_1}C_{ijrs}\ \Delta e_{rs} \tag{5.122}$$

The linear component of the Green-Lagrange strains Δe_{rs} are obtained from

$$[\Delta e] = [{}^{t_1}_{1}BL][{}^{t_1}_{1}\Delta U]$$

As seen from (5.90), the nonlinear strains are not required for computing ${}^{t_2}_{2}P_{ij}$. However, if need be, the nonlinear strains can be calculated from

$$\Delta\eta\ (I,J) = \frac{1}{2} \sum_{K=1}^{3} DD(K,I) \cdot DD(K,J) \qquad (5.123)$$

where DD(I,J) = derivative of displacement I with respect to coordinate J

$$= \frac{\partial u_I}{\partial x_J}$$

The elements of [DG] can be found from the nonlinear strain-displacement matrix, using the following relations from eq. (5.50)

$$DD(i,1) = \sum_{J=1}^{40} BNL(i,J)\cdot U(J) \qquad \text{for } i = 1,3$$

$$DD(j,2) = \sum_{J=1}^{40} BNL(j+3,J)\cdot U(J) \qquad \text{for } j = 1,3$$

$$DD(k,3) = \sum_{J=1}^{40} BNL(k+6,J)\cdot U(J) \qquad \text{for } k = 1,3 \qquad (5.124)$$

Transformation of Piola-Kirchhoff Tensor to Cauchy Tensor

The Piola-Kirchhoff tensor was defined by eq. (5.5). Inverting this relation, the Cauchy stresses are obtained as

$$ {}^{t_1}\sigma_{kl} = \frac{{}^{t_1}\rho}{{}^{t_o}\rho} \frac{\partial\, {}^{t_1}x_k}{\partial\, {}^{t_o}x_i} \, {}^{t_1}P_{ij} \, \frac{\partial\, {}^{t_o}x_l}{\partial\, {}^{t_o}x_j} \tag{5.125} $$

Define the deformation gradient matrix as a (3x3) matrix containing the derivatives of the coordinates at time t_1 with respect to the coordinates at t_o

$$ [DG] = \begin{bmatrix} \dfrac{\partial\, {}^{t_1}x}{\partial\, {}^{t_o}x} & \dfrac{\partial\, {}^{t_1}x}{\partial\, {}^{t_o}y} & \dfrac{\partial\, {}^{t_1}x}{\partial\, {}^{t_o}z} \\[2ex] \dfrac{\partial\, {}^{t_1}y}{\partial\, {}^{t_o}x} & \dfrac{\partial\, {}^{t_1}y}{\partial\, {}^{t_o}y} & \dfrac{\partial\, {}^{t_1}y}{\partial\, {}^{t_o}z} \\[2ex] \dfrac{\partial\, {}^{t_1}z}{\partial\, {}^{t_o}x} & \dfrac{\partial\, {}^{t_1}z}{\partial\, {}^{t_o}y} & \dfrac{\partial\, {}^{t_1}z}{\partial\, {}^{t_o}z} \end{bmatrix} $$

Also, from constancy of mass

$$ {}^{t_1}\rho \; {}^{t_1}dV = {}^{t_o}\rho \; {}^{t_o}dV $$

$$ \frac{{}^{t_1}\rho}{{}^{t_o}\rho} = \frac{{}^{t_o}dV}{{}^{t_1}dV} = \frac{d\,{}^{t_o}x \;\; d\,{}^{t_o}y \;\; d\,{}^{t_o}z}{d\,{}^{t_1}x \;\; d\,{}^{t_1}y \;\; d\,{}^{t_1}z} $$

$$ = \frac{1}{\det\,[DG]} \tag{5.127} $$

Therefore, eq. (5.125) can be written as

$$ [{}^{t_1}\sigma] = \frac{1}{\det[DG]} \; [DG][PP][DG]^T \tag{5.128} $$

where $$ [PP] = \begin{bmatrix} P_1 & P_4 & P_6 \\ P_4 & P_2 & P_5 \\ P_6 & P_5 & P_3 \end{bmatrix} $$

and P_i are the elements of the stress vector. The only thing remaining in the transformation is to calculate the elements of [DG], which is done as follows:

$$ \frac{\partial\, {}^{t_1}x_i}{\partial\, {}^{t_o}x_j} = \sum_{k=1}^{40} \frac{\partial N_k}{\partial\, {}^{t_o}x_j} \; {}^{t_1}x_{ik} + \frac{A}{2} \sum_{k=1}^{40} \frac{\partial}{\partial\, {}^{t_o}x_j} (N_k t) \, {}^{t_1}V_{3i}{}^k $$

where $x_i = x, y, z$

Define $[DG] = [DG1] + \frac{A}{2} \cdot [DG2]$

where $$DG1(i,j) = \sum_{k=1}^{40} \frac{\partial N_k}{\partial\, {}^{t_o}x_j}\, {}^{t_1}x_{ik}$$

and $$DG2(i,j) = \sum_{k=1}^{40} \frac{\partial}{\partial\, {}^{t_o}x_j} (N_k t)\, {}^{t_1}V_{3i}{}^{k}$$

$$= \sum_{k=1}^{40} \left(\frac{\partial N_k}{\partial r} \cdot \frac{dr}{\partial\, {}^{t_o}x_j} + \frac{\partial N_k}{\partial s} \cdot \frac{ds}{\partial\, {}^{t_o}x_j}\right) {}^{t_1}x_{ik}$$

or

$$DG2(i,j) = \sum_{k=1}^{40} \left(N_k \frac{\partial t}{\partial\, {}^{t_o}x_j} + t \frac{\partial N_k}{\partial\, {}^{t_o}x_j}\right) {}^{t_1}V_{3i}{}^{k}$$

$$= \sum_{k=1}^{40} ((N_k)({}^{t_o}J^{-1}_{j,3}))V_{3i}{}^{k} + t \sum_{k=1}^{40} \left(\frac{\partial N_k}{\partial r} \cdot {}^{t_o}J^{-1}_{j,1} + \frac{\partial N_k}{\partial s}\, {}^{t_o}J^{-1}_{j,2}\right) {}^{t_1}V_{3i}{}^{x} \qquad (5.130)$$

Load Vector

The right hand side of eq. (5.22) is termed the 'load vector', XL.

$$[{}^{t_2}XL] = [{}^{t_2}R] - [{}^{t_1}F] \qquad (5.131)$$

Since an incremental scheme is used, the applied loads [R] are updated at the beginning of each load step and subtracted from the internal loads [F]. The calculation of these vectors is discussed below.

It is the objective of this study to examine not only buckling under proportional loads but also nonproportional nonlinear loads which have not been studied by any previous researcher using finite elements. Incorporating of nonproportional loads also permits the study of the influence of the order of loading and loading history on the buckling modes and critical loads. Any combination of axial loads, lateral loads, bending moments, and internal/external pressure can be incorporated in the following formulation.

Figure 15 shows pressure p, bending moment M, and axial load P, increasing linearly from zero to p_{max}, M_{max}, and P_{max}, respectively. If equal size steps are taken then the loads in any step are p_{max}/N, M_{max}/N, and P_{max}/N, where N is the total number of load steps. The load vector, therefore, is an exact multiple of the load vector at the maximum loads

$$[{}^{t_1}R] = (i)[{}^{t_N}R]/N \tag{5.132}$$

Figure 16 shows an example of nonlinear nonproportional loads. All loads increase or decrease independent of each other. Incorporating this type of loading via equivalent nodal loads does not present a problem. However, major changes are required in the solution phase during displacement control, and in the use of linearity indices and stability criteria, as discussed in later sections.

These nonproportional loads may be incorporated as follows. A certain reference value for each type of load should be specified along

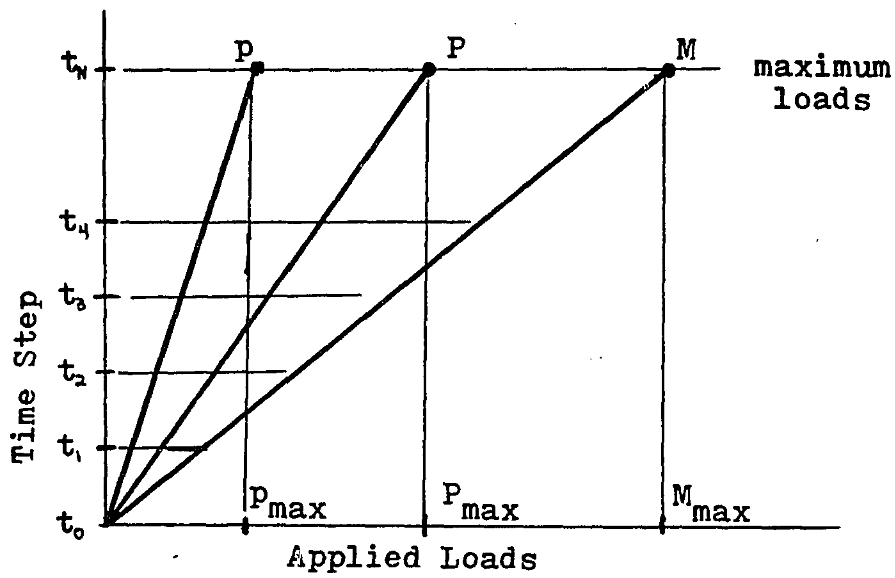

Figure 15 Proportional loads.

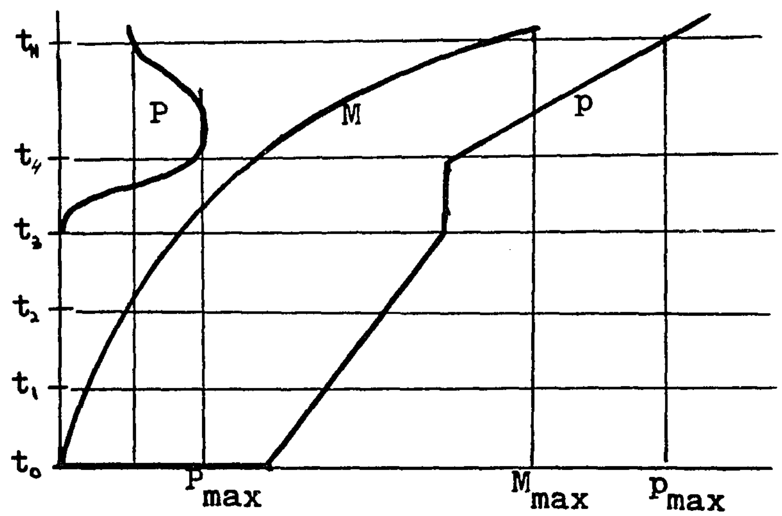

Figure 16 Nonproportional, nonlinear loads.

with the number of load steps. The ratio of each type of load to the reference value in each load must then be specified so that the loads may be calculated from

$$^{t_i}P = \text{Ratio}(P,i) \cdot P_{ref}, \quad \text{etc.} \tag{5.133}$$

where Ratio(P,i) is the ratio of the load type P in step i to the reference value of P

In the example shown in Fig. 16, one can see that the moment M and pressure p are applied first, but P is zero until step 3. Thus the Ratio(p,i) for i = 1 to 3 will be zero. Also, if the maximum values are used as the reference values, then Ratio(P,N) will be less than one. By using this scheme, any type of load variation and order of loading may be specified. It must be noted, however, that the load vectors in different steps are different, and this causes some problems in searching for limit points.

Figure 17 shows an example of a situation where nonproportional loads are encountered. In the laying of subsea pipelines, the pipe undergoes combined bending, axial tension, and external pressure loading.

The equivalent nodal loads have to be calculated for each type of loading. Four types of load encountered in pipeline problems are: uniformly distributed axial compression/tension, uniformly distributed lateral loads, pure bending moment, and external/internal pressure.

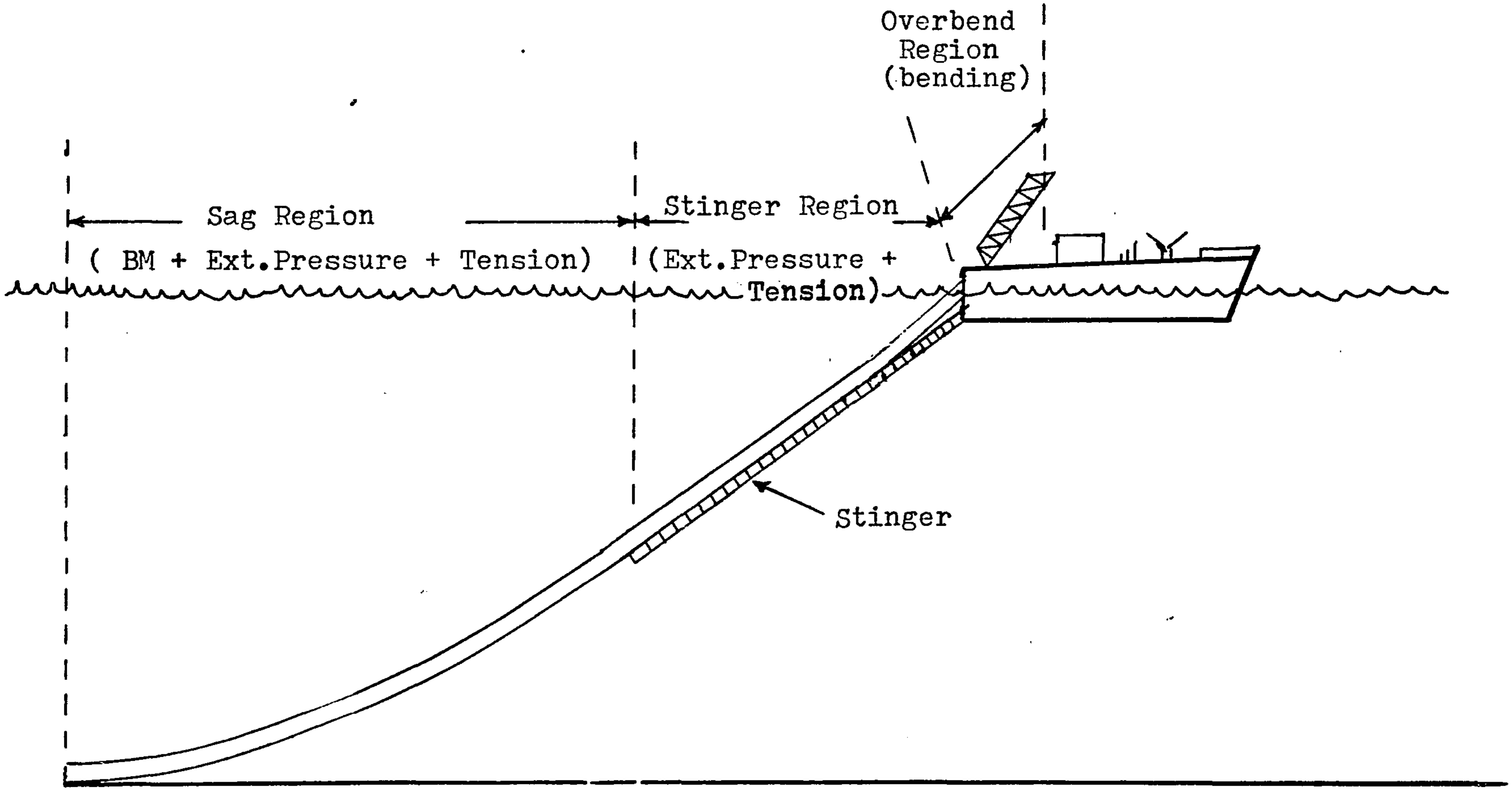

Figure 17 Laying of sub-sea pipelines.

For uniformly distributed axial loads, the equivalent nodal loads can be calculated from the total axial load as given below.

The load per unit length of circumference is $\frac{F_T}{\pi D}$

and load per element is $w_e = \frac{F_T}{\pi D(NC)}$ (5.134)

where F_T = total axial load

D = midplane diameter of cylinder

NC = number of elements along circumference

(assuming elements are equal along circumference)

From eq. (5.13)

$$[R]_e = \int_{\Gamma_e} [N^s]^T [T^s] d\Gamma_e \tag{5.135}$$

Figure 18 shows a parabolic element subjected to uniform pressure on face 1-5-2. The shape functions $[H^s]$ on the surface are evaluated by setting $s = 1$, which is for face 1-5-2.

Then

$$N_1 = 0.5r(1 + r)$$

$$N_2 = -0.5r(1 - r)$$

$$N_5 = (1 - r^2)$$

$$N_3 = N_4 = N_6 = N_7 = N_8 = 0$$

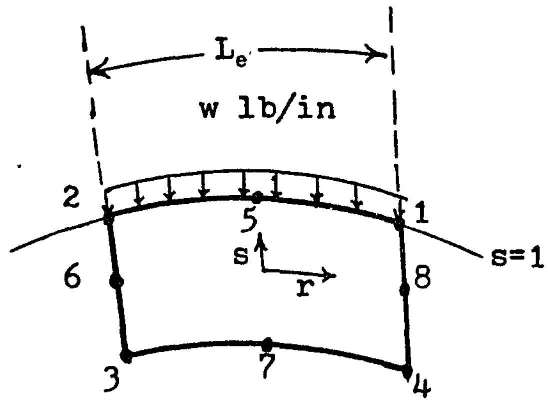

Figure 18 Uniform edge pressure on parabolic element.

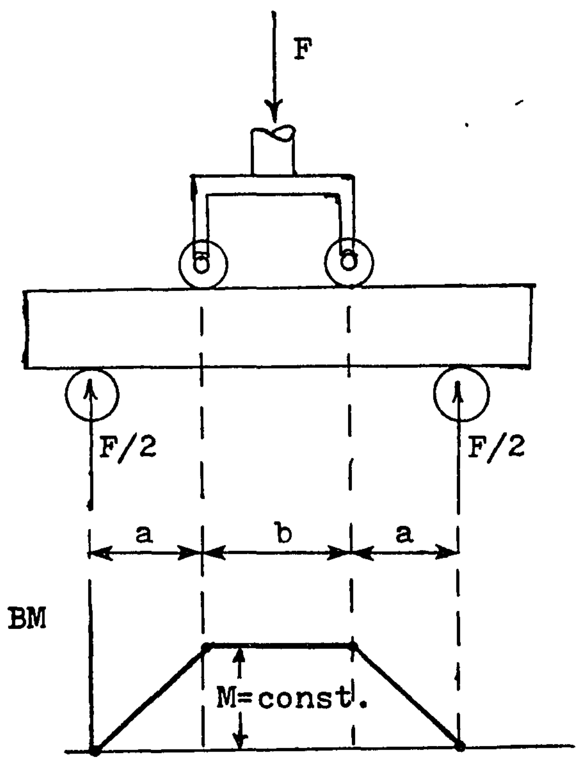

Figure 19 Four point bend test.

$$\therefore\ [N^s]^T[u^s] = \begin{bmatrix} 0.5r(1+r) & 0 \\ 0 & 0.5r(1+r) \\ -0.5r(1-r) & 0 \\ 0 & -0.5r(1-r) \\ (1-r^2) & 0 \\ 0 & (1-r^2) \end{bmatrix} \begin{bmatrix} u_1 & v_1 & u_2 & v_2 & u_5 & v_5 \end{bmatrix}$$

$$[T^s] = \begin{bmatrix} T_r^{\,s} \\ T_s^{\,s} \end{bmatrix} = \begin{bmatrix} 0 \\ w_e \end{bmatrix}$$

$$\therefore\ [R]_e = \int_{-1}^{+1} \begin{bmatrix} 0.5r(1+r) & 0 \\ 0 & 0.5r(1+r) \\ -0.5r(1-r) & 0 \\ 0 & -0.5r(1-r) \\ (1-r^2) & 0 \\ 0 & (1-r^2) \end{bmatrix} \begin{bmatrix} 0 \\ w_e \end{bmatrix}$$

$$= \int_{-1}^{+1} \begin{bmatrix} 0 \\ 0.5r(1+r)w_e \\ 0 \\ -0.5r(1-r)w_e \\ 0 \\ (1-r^2)w_e \end{bmatrix} dr = \begin{bmatrix} 0 \\ 1/3w_e \\ 0 \\ 1/3w_e \\ 0 \\ 4/3w_e \end{bmatrix} \qquad (5.136)$$

Since the global direction Z is aligned with the local direction s for elements on the cylinder if curvilinear rectangles are used, transformation to the global system was not used. It is also assumed that the midnode is located at the midpoint of 1-2.

The ratio of the equivalent load on corner nodes to that on the midnode is 1:4, for each element. However, the corner nodes get load contributions from two adjacent elements, so the ratio is reduced to 1:2. Therefore,

$$NC \cdot F_C + NC \cdot 2F_C = W_e \cdot \pi D$$

where F_C = equivalent load on corner nodes

and $$F_C = \frac{\pi W_e D}{3NC} \tag{5.137}$$

and $$F_M = \frac{2\pi W_e D}{3NC} \tag{5.138}$$

where F_M = equivalent load on midnodes

Uniformly distributed lateral loads can be calculated in a similar manner.

$$F_T = W_e L$$

where F_T = total lateral load

W_e = load per unit length

L = length of cylinder

No. of elements along length = NL , thus

$$F_C + 2F_C\,(NL-1) + 4F_C(NL) = W_eL$$

and

$$F_C = \frac{W_eL}{(6\ NL - 1)} \tag{5.139}$$

where $F_C = F_1$ = equivalent load on unrestrained extreme corner node

Thus, the load on all corner nodes, except the extremes is $2F_C$ and the load on midnodes is $4F_C$.

Since Battelle's study involved tests using four-point bending, which imparts a constant bending moment between the inner points (Fig. 19), several schemes for modelling constant bending moments were devised. The results of the most successful of such schemes are given in the last chapter. The nodal loads shown in Fig. 20, produce theoretical deflections equivalent to

$$M = F \times D/2 \tag{5.140}$$

Finally, equivalent loads must be calculated for uniform external/internal element pressures. As with distributed loads, the equivalent nodal loads must be consistent with the assumed shape functions. However, if the elements are small, the error in using equal nodal loads (on an element basis) is negligible.

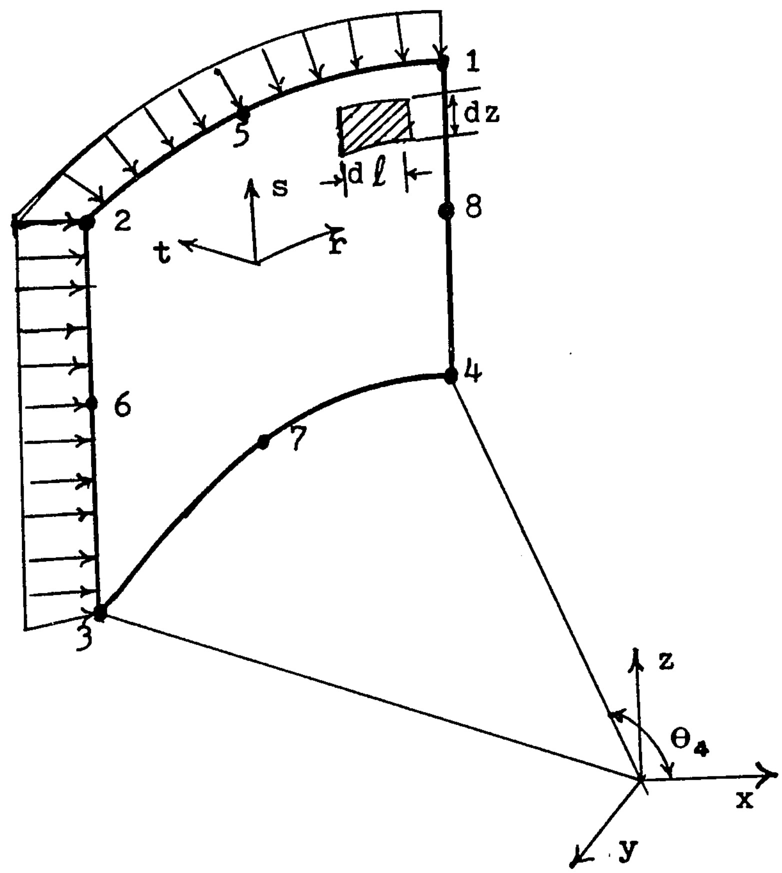

Figure 20 Uniform pressure on a general shell element.

Figure 20 shows uniform pressure on a shell element of general shape. The pressure is always normal to the shell surface; therefore, the components in x and y-directions would depend upon the position of the point. Since the local axis direction t is normal to the shell surface, the pressure can be said to always act in direction t, regardless of position. Pressure calculations can be simplified if it is observed that in the case of a right circular cylinder whose axis is aligned with the z direction and the origin of the global system lies somewhere along the cylinder axis. These assumptions are true if the model has been generated using the special purpose preprocessor PREP.

Equivalent nodal loads are calculated from eq. (5.141)

$$[R]_e = \int_{\Gamma_e} [H^s]^T [T^s] d\Gamma_e \tag{5.141}$$

Now
$$\begin{aligned} d\Gamma_e &= d\ell dz \\ &= (\sqrt{dx^2 + dy^2})dz \end{aligned} \tag{5.142}$$

Also
$$\begin{aligned} drds \det [J^s] &= d\Gamma_e \\ \therefore \det [J^s] &= \frac{(\sqrt{dx^2 + dy^2})dz}{drds} \end{aligned}$$

$$= (\sqrt{(\frac{dx}{dr})^2 + (\frac{dy}{dr})^2})(\frac{dz}{ds}) \tag{5.143}$$

$$= J^s_{23}\sqrt{(J^{s\,2}_{11} + J^{s\,2}_{12})}$$

$$d\Gamma_e = \left[J^s_{23}\sqrt{J^{s\,2}_{11} + J^{s\,2}_{12}} \right] drds \tag{5.144}$$

$[T^s]$ is calculated by breaking p into its components in the x,y,z directions

$$[T^s] = \begin{Bmatrix} p \cos\theta \\ p \sin\theta \\ 0 \end{Bmatrix} \tag{5.145}$$

Substituting (5.144) and (5.145) into (5.141) and using Gauss quadrature for numerical integration, one obtains

$$[R]_e = \sum_{i=1}^{n_1} \sum_{j=1}^{n_2} \alpha_i \alpha_j [H^s(r_i,s_j)]^T \begin{bmatrix} p \cos\theta \\ p \sin\theta \\ 0 \end{bmatrix}_m J^s_{23}(r_i,s_j) \sqrt{J^{s\,2}_{11}(r_i,s_j) + J^{s\,2}_{12}(r_i,s_j)} \tag{5.146}$$

where i,j = Legendre sampling points

n_1,n_2 = order of integration

α_i, α_j = weighting functions

m = node

It is seen that, in this case, a closed form solution cannot be obtained, and the equivalent loads must be calculated for each node by evaluating the shape functions, Jacobian matrix, the coordinates, and the current element pressures and numerically integrating over the entire element. If this procedure is repeated in every load step, the deformation of the cylinder will be taken into account in calculating the loads, i.e. the direction of the pressure is taken normal to the deformed shell not the original shell.

Finally, to obtain the incremental load vector, the internal load vector from the previous iteration is subtracted from the applied load vector. The internal loads are obtained for each element from eq. (5.15) as

$$[{}^{t}_{1}F]_e = \sum_{i=1}^{40} \sum_{j=1}^{40} \sum_{k=1}^{40} [BL(r_i, s_j, t_k)]^T [SV] \det J \alpha_i \alpha_j \alpha_k \qquad (5.147)$$

where $[SV] = [P_{11}\ P_{22}\ P_{33}\ P_{12}\ P_{22}\ P_{31}]^T$

Solution of Nonlinear Equations

Various solution schemes were discussed in Chapter IV. The incremental formulation used is equivalent to a Newton-Raphson scheme. Bathe [46] has shown that the stiffness matrix in an incremental analysis is equivalent to the gradient in the Newton-Raphson equation. The equation to be solved is

$$[{}^{t_1}SK][\Delta u] = [{}^{t_2}R] - [{}^{t_2}F] \tag{5.148}$$

An incremental-iterative scheme is used here i.e. the load is incremented in steps and convergence in each step is obtained by iterating. In step t_2 and iteration (i), the equation to be solved is

$$[{}^{t_1}SK]^{(i)}[\Delta u]^{(i)} = [{}^{t_2}R] - [{}^{t_2}F]^{(i-1)} \tag{5.149}$$

In eq. (5.149) the stiffness matrix must be recalculated in each iteration. This is too time consuming. Therefore, a quasi-Newton scheme is used in this study, which uses the equation

$$[{}^{t_1}SK]^{(1)}\ [\Delta u]^{(i)} = [{}^{t_2}R] - [{}^{t_2}F]^{(i-1)} \tag{5.150}$$

The stiffness matrix is calculated in the first iteration of each loadstep. In subsequent iterations only the internal loads $[{}^{t_2}F]$ are updated and the equation solved.

Convergence is checked by computing the ratio of the displacement norm to the root mean square of the displacements in that load step

$$\text{ERROR} = \frac{\|\Delta u^{(i)}\|}{\sqrt{\sum_{j=1}^{i} \|\Delta u^{j}\|^2}} \leq \text{CONV} \tag{5.151}$$

where CONV = convergence criterion

In each iteration, the linear matrix equation $\underline{K}\,\underline{U} = \underline{R}$ is solved. The linear solution technique used in this study is the LDL^T decomposition in the form of skyline reduction method. This is a standard procedure and is described in finite element text books, such as Zienkiewicz [47] and is briefly described here. The stiffness matrix is decomposed to a lower triangular matrix [L] and a diagonal matrix [D]

$$[SK] = [L][D][L]^T$$

Also

$$[R] = [L][V]$$

$$\therefore\ [L][D][L]^T[U] = [L][V]$$

$$[L]^T[U] = [D]^{-1}[V] \tag{5.152}$$

[U] may thus be calculated, starting from the last equation and back-substituting.

The stiffness matrix is symmetric and banded as shown in Fig. 21; the elements outside the band are zero. The skyline reduction method, operates on the stiffness matrix by columns, starting at the skyline i.e. the first nonzero element in the column. The last element reduced is the diagonal element in each column. Therefore, this method is computationally efficient because it takes advantage of the symmetric and banded nature of the matrix.

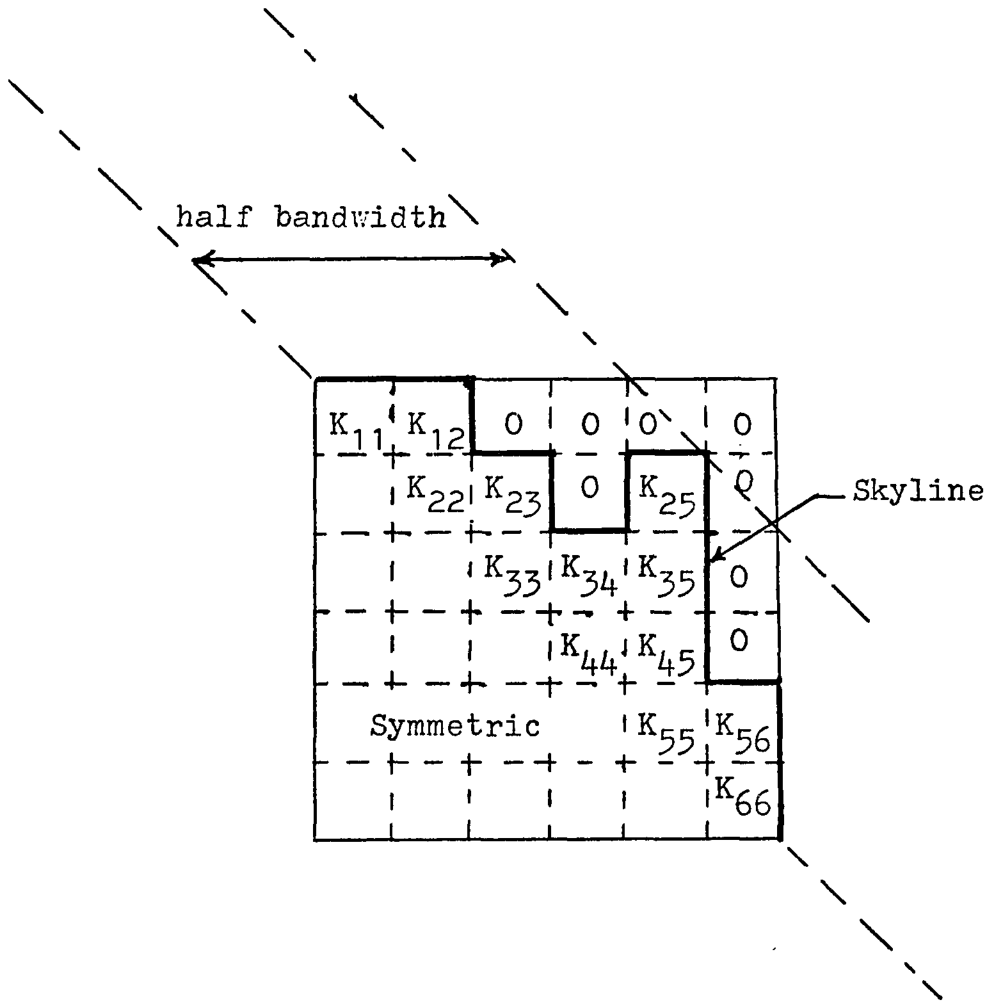

Figure 21 Nature of stiffness matrix.

Stability Analysis

It was pointed out in Chapter IV that when cylinders buckle (ovalization or gross column buckling, elastic or plastic) a limit point is encountered on the load-displacement curve. Therefore, in order to predict buckling loads, the position of the first limit point must be found. From a simple one dimensional representation in Fig. 22 it can be seen that the stiffness value $\tan\theta$ is reduced as the limit point is approached. Also, at the limit point $\theta = 0$. In multi-dimensional problems this is equivalent to saying that the stiffness matrix becomes singular. Since a quasi-Newton scheme is being used for solving the nonlinear equations, the solution will become unstable at or near the limit point. The reason is that one of the pivot elements will approach zero leading to division by zero in the reduction scheme.

To prevent numerical instability near limit points, the solution strategy must be altered. Newton-Raphson or quasi-Newton schemes cannot be used. It is, therefore, essential that the approach of a limit point be detected before it is actually reached. This can be done in the following ways.

Since the diagonal elements are used as pivots, the magnitude of these elements can give an indication of the approach of limit point. Thus, we define a stiffness index ST1

$$\mathrm{ST1} = \frac{(\mathrm{SK}(1,1)/D) \ldots (\mathrm{SK}(N,N)/D)i}{(\mathrm{SK}(1,1)/D) \ldots (\mathrm{SK}(N,N)/D)1} \tag{5.153}$$

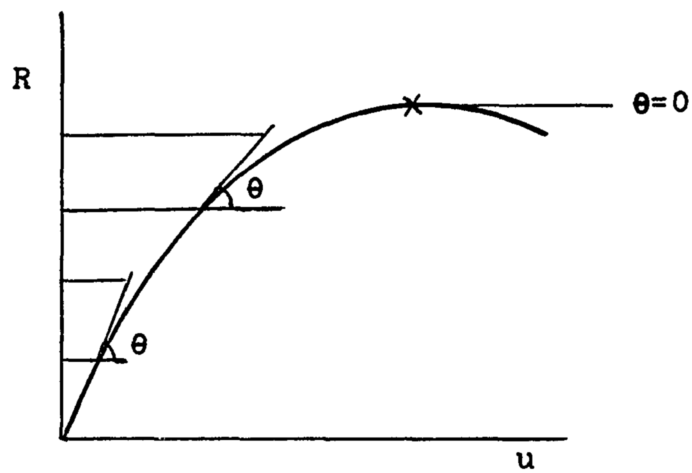

Figure 22 Structural softening.

where D = divider to prevent magnitude overflow

$/i$ = step i

$/1$ = step 1

Since the selection of D is difficult 'a priori' an alternative measure is defined as

$$ST1 = \frac{\sum_{k=1}^{N} \log SK(k,k)/i}{\sum_{k=1}^{N} \log SK(k,k)/1} \tag{5.154}$$

From these definitions, it would be expected that ST1 would be a number between 0 and 1. When the value of ST1 reaches a certain value (call it stability criterion STAB2) the solution strategy can be altered. The advantage of ST1 over other measures described below is that it is independent of the load vector and thus suitable for both proportional and nonproportional loads. A disadvantage is that it does not give a good measure in case of highly coupled equations and also numerical difficulties are involved with the exponent magnitude.

Bergan, et al [72] proposed the following parameter:

$$ST2 = \frac{\dfrac{[\Delta u]^T}{\Delta p_1} [R_{ref}]}{\dfrac{[\Delta u]_i^T}{\Delta p_i} [R_{ref}]} \qquad (5.155)$$

where $[\Delta R]_i = \Delta p_i [R_{ref}]$ for proportional loads

$$\therefore \ ST2 = \left(\frac{\Delta p_i}{\Delta p_1}\right)^2 \frac{[\Delta u]_1^T [\Delta R]_1}{[\Delta u]_i^T [\Delta R]_i} \qquad (5.156)$$

But $[SK][\Delta u] = [\Delta R]$

$$ST2 = \left(\frac{\Delta p_i}{\Delta p_1}\right)^2 \frac{[\Delta u]_1^T \ [SK]_1 [\Delta u]_1}{[\Delta u]_i^T \ [SK]_i [\Delta u]_i} \qquad (5.157)$$

The above is valid for proportional loads only. This is being extended here to nonproportional loads by using the actual $[{}^{t_2}R]$ in each iteration. Thus

$$ST2 = \frac{[\Delta u]_1^T \ [\Delta R]_1}{[\Delta u]_i^T \ [\Delta R]_i} \qquad (5.158)$$

A third measure is being proposed here on the basis of the slope of the norm [R] - norm [u] curve. From Fig. 22, the slope in step 1 is

$$\tan \theta_1 = \frac{||\Delta R||_1}{||\Delta u||_1}$$

$$\text{and} \quad \tan \theta_i = \frac{||\Delta R||_i}{||\Delta u||_i}$$

Define

$$ST3 = \frac{||\Delta R||_i / ||\Delta u||_i}{||\Delta R||_1 / ||\Delta u||_1}$$

$$= \frac{||\Delta R||_i \cdot ||\Delta u||_1}{||\Delta R||_1 \cdot ||\Delta u||_i} \tag{5.159}$$

For proportional loads

$$||\Delta R||_i = ||\Delta R||_1$$

and

$$ST3 = \frac{||\Delta u||_1}{||\Delta u||_i} \tag{5.160}$$

The value of ST3 will lie between 0 and 1 and will be an indication of 'softening' of the structure. This requires less computation than the Bergan criterion, and its performance will be compared to the Bergan criterion.

The stiffness parameters ST2 and ST3 have the same disadvantage. They measure an average change in the stiffness of the structure. Also, they provide no clue as to how the structure will buckle. It is proposed here to gear the stiffness parameter or index to the deformation mode. Two such modes are bending (column buckling) and ovalization.

In bending, if the global axis z is aligned with the cylinder axis, the displacements u_i and v_i measure the deflection. The resultant deflection of any point k is

$$\delta_k = \sqrt{u_k^2 + v_k^2}$$

$$\text{Define STBND} = \frac{||R||_i / ||\delta||_i}{||R||_1 / ||\delta||_1}$$

$$\text{where } ||\delta|| = \text{Norm of } \delta = \sqrt{\Sigma \delta_k^2}$$

For proportional loads

$$\text{STBND} = \frac{||\delta||_1}{||\delta||_i} \tag{5.162}$$

If the order of loading is such that there is no bending in the first iteration, the index STBND will be misleading. Therefore, there is need for a magnitude measure to be used in conjunction with STBND. The center deflection in Battelle's experiment of D/t = 16 is calculated below.

$$M_{cr} = 12{,}500 \text{ in-lb}$$

$$I = 0.0839 \text{ in}^4$$

$$\ell = 15 \text{ in}$$

$$\delta_{max} = \frac{M}{EI}\left(\frac{\ell^2}{2}\right) = 0.56 \text{ in}$$

Looking at equations for deflection of beams we see that the general form is

$$\delta_{max} \propto \left(\frac{\ell^3}{EI}\right)$$

$$\frac{\delta EI}{\ell^3} = \text{constant}$$

or $\frac{\delta I}{\ell^3}$ = constant for same material

Define

$$\text{STBNDA} = \frac{(\delta_{max}\ I/\ell^3)}{0.002} \qquad (5.163)$$

as $\frac{\delta_{max}\ I}{\ell^3}$ = .002 for Battelle's model

where all parameters are measured in inches.

The ovalization is calculated from Fig. 23 as

$$R' = \sqrt{t_{x_i}^{\,2} + t_{y_i}^{\,2}}$$

$$d = R' - R$$

$$= \sqrt{t_{x_i}^{\,2} + t_{y_i}^{\,2}} - R \qquad (5.164)$$

Ovalization = $d_{max} - d_{min}$ (on each plane)

To make this dimensionless, divide by the radius

$$\text{OVAL}_m \triangleq \frac{d_{max} - d_{min}}{R}$$

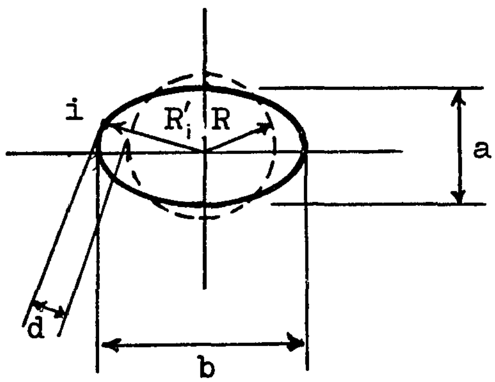

$$\text{ovalization} = \frac{(b-a)}{2R}$$

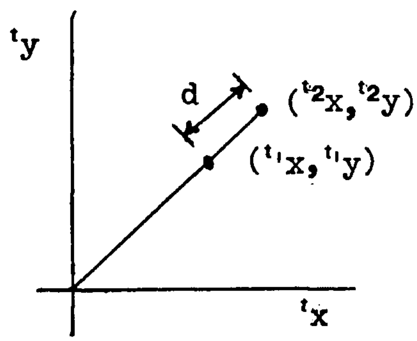

Figure 23 Measurement of ovalization.

where $OVAL_m$ is the ovalization on plane m

Define ovalization index as

$$STOVL = \frac{\| R \|_i / \| XO \|_i}{\| R \|_1 / \| XO \|_1} \tag{5.165}$$

where $$\| XO \|_i = \sqrt{\sum_{m=1}^{NL} \left(OVAL_m^2\right) / NL}$$

Since the ovalization may not be significant in the first step for certain types of loads, an absolute measure is used in conjunction with STOVL. This is based on the maximum ovalization calculated by Brazier [8] as

$$\frac{R_{max} - R_{min}}{R} = \frac{2}{9} \tag{5.166}$$

Therefore define

$$STBRAZ = \frac{MAX(OVAL_m)}{(2/9)}$$

The stiffness indices give an early warning of the approach of limit points. Once the value of the selected index falls below a certain level, quasi-Newton scheme must be abandoned. Instead, a displacement control scheme must be followed i.e. instead of incrementing the loads and solving for displacements, the displacements are increased and internal loads calculated. Bergan et al [72] have followed this scheme for proportional loads.

In displacement control the assumed displacement increment influences the solution significantly and, in fact, can give completely erroneous results. For proportional loads, Bergan used a fraction of the last displacement increment as the assumed displacement. However, in nonproportional loads this may not give displacement modes that are physically possible or load vectors corresponding to actual loads. If an iterative solution is used, there is no mathematical basis that guarantees convergence.

VI. COMPUTER PROGRAM

In order to validate the formulation presented in Chapter V, a series of computer programs were written, under the name "BUCKS". When this study was proposed, it was hoped that one of the existing nonlinear programs, such as AGGIE or ADINA could be used with appropriate changes to the element, material property, and loading subroutines and using the solution presented in this study. AGGIE was found to be inadequate for this purpose and a bit out of date. The lack of documentation in ADINA made it difficult to make any changes in it. Therefore, every subroutine in BUCKS had to be written from scratch.

Version 8.1 of BUCKS has been written in FORTRAN ANSI-77, suitable for batch processing on IBM mainframes as well as DEC minicomputers. The program is about 5600 lines of code consisting of 54 subroutines and functions. The organization of such a large program is a major task; the algorithms and computational procedures are discussed briefly in the following sections.

Analysis Procedure

Figure 24 shows the analysis procedure used. The finite element mesh is generated using the special purpose program PREP and checked graphically using DSPLAY. A brief write-up on these programs is given in the Appendix. The program SSCURV is used to curve-fit experimental

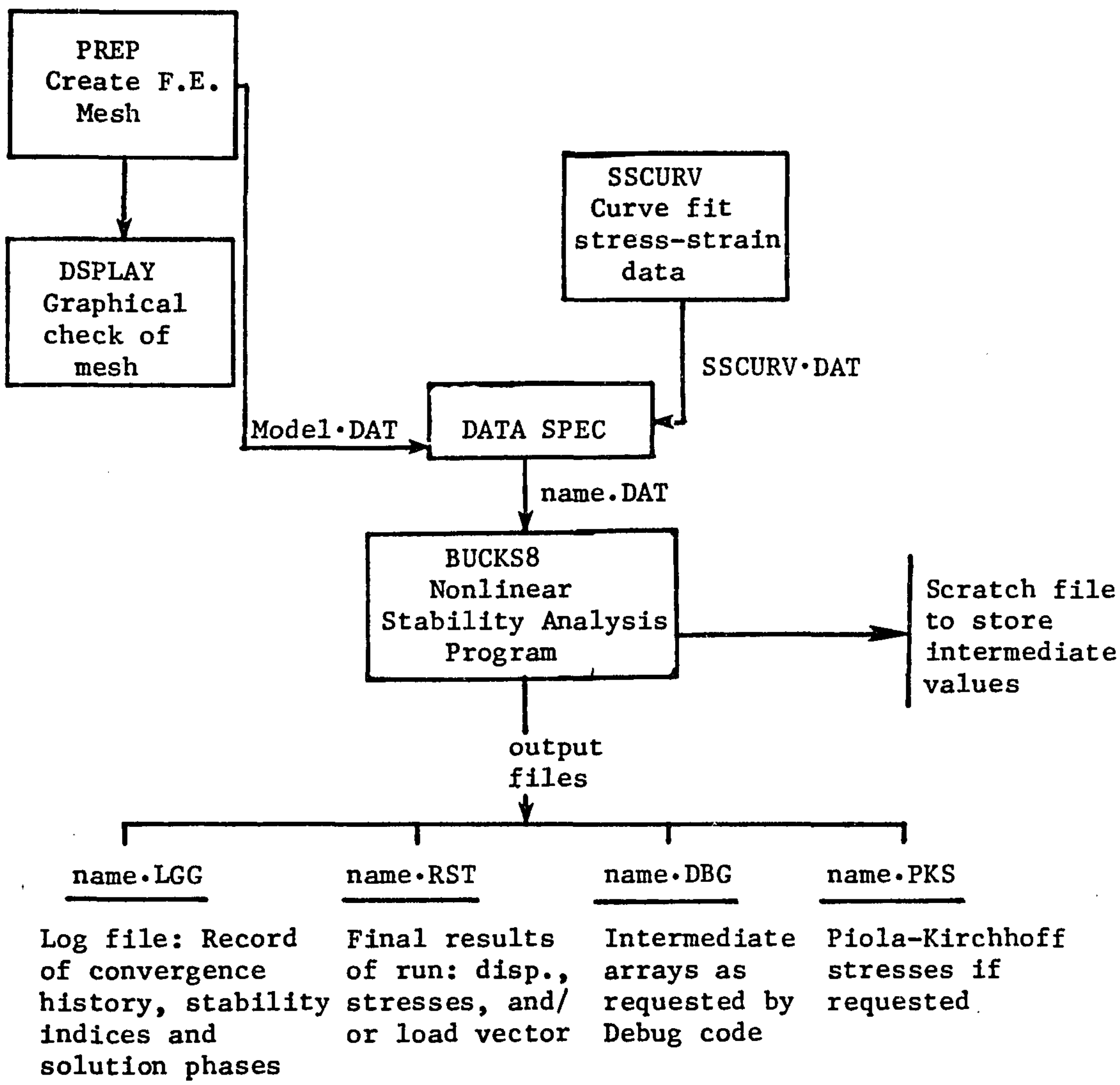

Figure 24. Analysis Procedure

stress-strain data to give the material constants for the three material models presented in the last chapter. Using the output from PREP and SSCURV a data file is prepared in the format given in the Appendix.

Algorithms

Figure 25 shows the main features of the program BUCKS8. A short description of each subroutine is given in the Appendix. Dynamic dimensioning is used to optimize storage. The main program serves the purpose of reading the parameters required in variable dimensioning. Control is then passed on the subroutine DRIVER which acts as the main program. Data is read from the formatted file by subroutines INPUT and LOADIN. The index IOL specifies whether the load is proportional and linear or nonproportional and even nonlinear.

For proportional loads, the maximum loads are calculated in the first step and the equivalent nodal loads from all types of loading are added. In each load step the load vector is calculated from

$$[\Delta R]_i = \left(\frac{ISTEP}{NSTEP}\right) [R]_{max} \qquad (6.1)$$

where ISTEP, i = load step no.

NSTEP = total no. of steps

To save memory, $[R]_{max}$ is not stored, so $[\Delta R]$ is calculated from

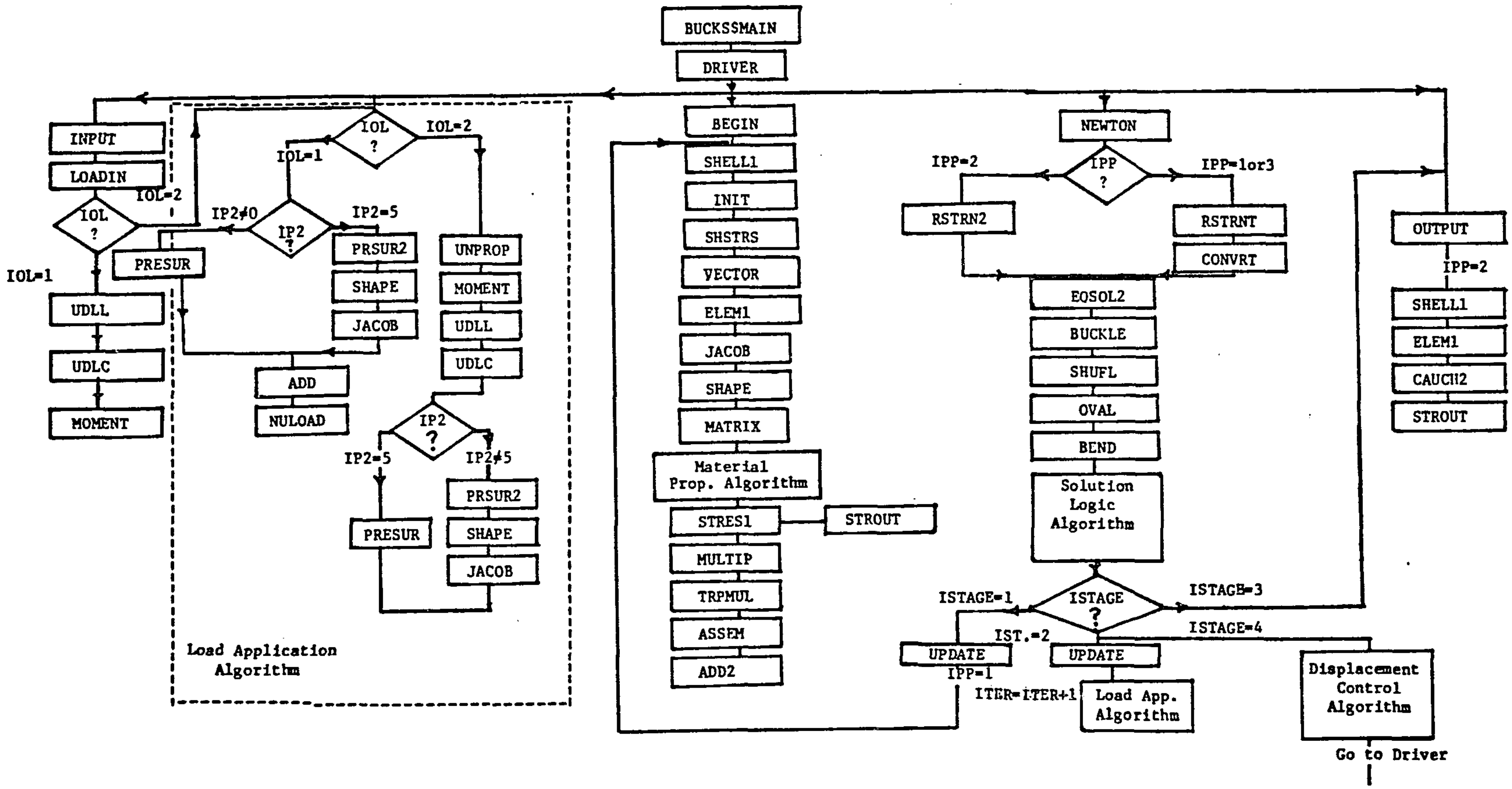

Figure 25 Structure of program BUCKS

$$[\Delta R]_i = \left(\frac{ISTEP}{ISTEP-1}\right) [\Delta R]_{i-1} \qquad (6.2)$$

Thus $[\Delta R]_1$ is calculated from (6.1) but all subsequent steps use (6.2).

Nonproportional loads are calculated from eq. (6.3).

$$[\Delta R]_i = PINP(i) \; [R]_p^{ref} + PINM(i) \cdot [R]_M^{ref} + PINUL(i) \cdot [R]_{UL} + PINUC(i) \cdot [R]_{UC}^{ref} \qquad (6.3)$$

where PINP(i) = ratio of external/internal pressures in step i to reference load vector $[R]_p^{ref}$

PINM(i) = ratio of bending moment to reference loads $[R]_M^{ref}$ in step i

PINUL(i) = ratio of uniformly distributed loads in step i to $[R]_{UL}^{ref}$

PINUC(i) = ratio of uniformly distributed axial loads in step i to $[R]_{UC}^{ref}$

This calculation is managed by subroutine UNPROP.

The element stiffness matrices are calculated and numerically integrated in SHELL1. In the first loadstep, vectors V_{1i}, V_{2i}, V_{3i} are calculated in VECTOR which also updates these vectors in subsequent steps. The strain-displacement matrices are calculated in ELEM1. All element subroutines are called once in each Gauss point cycle for each element. A maximum size of 4 x 4 x 4 quadrature can be used but this is a user input variable.

Calculation of the appropriate constitutive matrix is rather involved. The algorithm is shown separately in Fig. 26. In order to save computation time, the user specifies an integer-NCRIT which lies between 1 and NSTEP. NCRIT is the approximate time step in which the stresses are estimated to go into the plastic range. Thus, before NCRIT is reached no check is made on yielding of the material, and the elasticity matrices are used. Another user input parameter is IANY, which specifies the analysis type. If IANY = 1 the full elasticity matrix calculated in ELAST is used without degeneration. If IANY = 2, the modified elasticity matrix in ELAST2 is degenerated by DEGEN.

For ISTEP $\geq$ NCRIT the P/K stresses are transformed to Cauchy stresses in CAUCH2 and the Von Mises stresses calculated in VMISES. This is done individually for each Gauss point. If the material has yielded, the elastic-plastic stress-strain relations are calculated from ELAST and PLAST for IANY = 1 or degenerated matrices from ELAST2, PLAST2, and DEGEN. If the material is still in the elastic range, the procedure is the same as that before NCRIT. In case of yielding, the new yield stress is set equal to the Von Mises stress for use in PLAST and PLAST2 only. Plasticity relations are based on three material models specified by IH.

IH = 1 for Bilinear model

IH = 2 for Exponential model

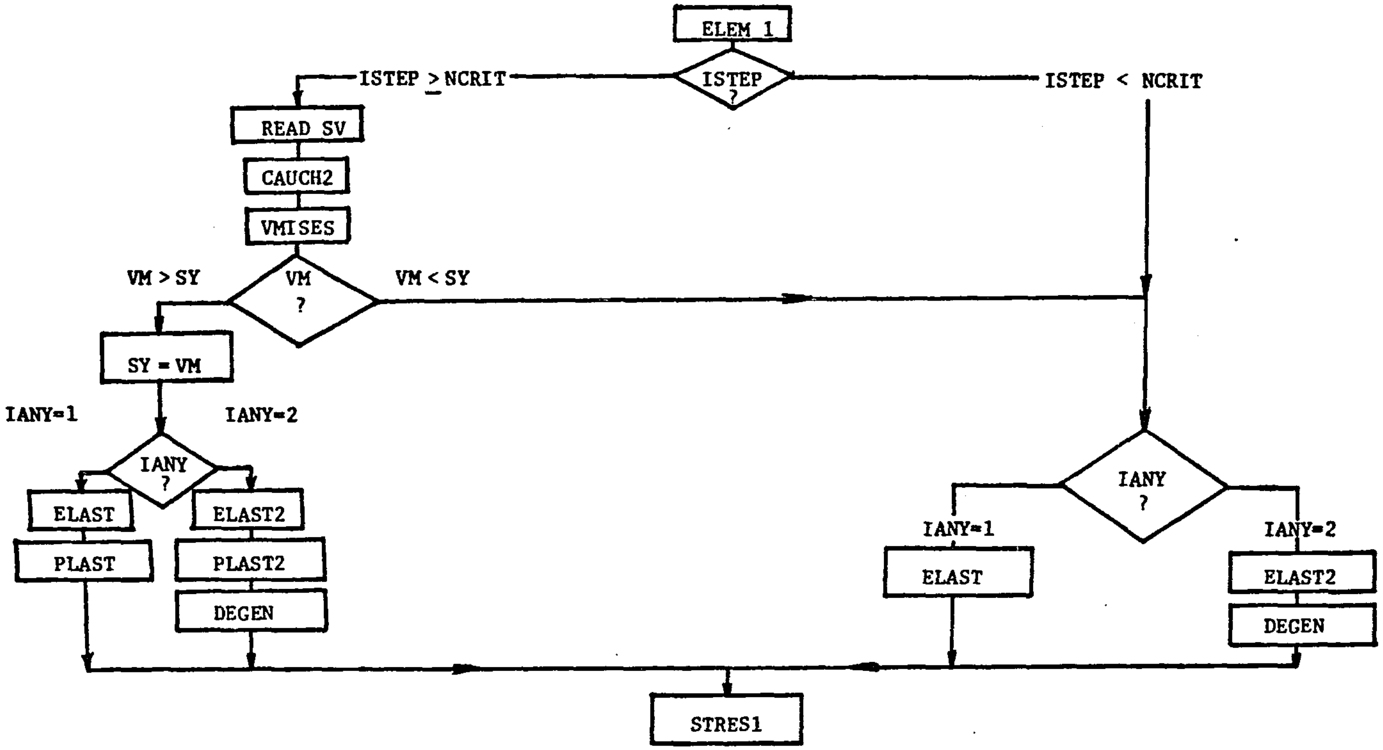

Figure 26. Material Properties Algorithm

IH = 3 for Ramberg-Osgood model

To save memory the total P/K stresses at each Gauss point are not stored in an array but instead are written to a binary scratch file. After calculating the incremental stresses in each iteration, the old stresses are read from the scratch file and the new stresses calculated using

$$^{t_2}P_{ij} = {}^{t_1}P_{ij} + \Delta P_{ij}$$

The updated stresses $^{t_2}P_{ij}$ overwrite the previous stresses in the scratch file. Since the scratch file used is binary and direct access, the I/O time is not a serious hinderance.

Assembly of integrated element matrices is done by elements. The contribution from each Gauss point is placed directly into the system matrix in subroutine ASSEM. By using the same memory space for the linear, nonlinear, and total system matrices considerable saving in storage is achieved. Load vectors are also assembled directly from the calculated internal loads in each step.

The solution scheme is very complex so the solution phase is tracked by a parameter ISTAGE. The are four phases.

ISTAGE = 1 Convergence not achieved in load step

ISTAGE = 2 Convergence achieved in load steps other than NSTEP

ISTAGE = 3 Convergence achieved in load step NSTEP; the structure carries the full load specified without buckling (if ISTAGE was 1 prior to ISTAGE 3)

ISTAGE = 4 Limit point is approached, solution strategy is changed to displacement control.

In the quasi-Newton scheme being used here, the stiffness matrix is updated only once per loadstep. Convergence is achieved in each step by iterating. Equations corresponding to restrained degress of freedom are removed before the solution is carried out. This is done by RSTRNT and CONVRT. If the stiffness matrix is not to be updated, as in ISTAGE = 1, no such rearrangement is needed. Only the load vector must have elements corresponding to restrained degrees of freedom removed. This is done by RSTRN2. Thus; IPP = 2 when iterating within a load step and IPP = 1 when updating the stiffness matrix.

The linear set of equations are solved in EQSOL2 by the skyline reduction method. If IPP = 2 [SK] is not factorized, using the old values. EQSOL2 has optimized storage since the matrices [L] and [D] use the same space as [SK] and [V] uses the same space as [R]. (All symbols have the same meaning as in Chapter V).

Several softening criteria were defined in Chapter V. These are calculated in subroutines BUCKLE, OVAL, and BEND. The subroutine SHUFL inserts zero displacements for restrained degrees of freedom so that the changes in the displacement vector are transparent to the user.

Figure 27 shows the logic used in determining solution strategy. It is recognized here that no single stiffness parameter or stability index can be used reliably for all cases. Therefore, the program first picks the critical index in each iteration, in accordance with user specifications via ICRIT. Suppose the chosen index is STCRIT. Then

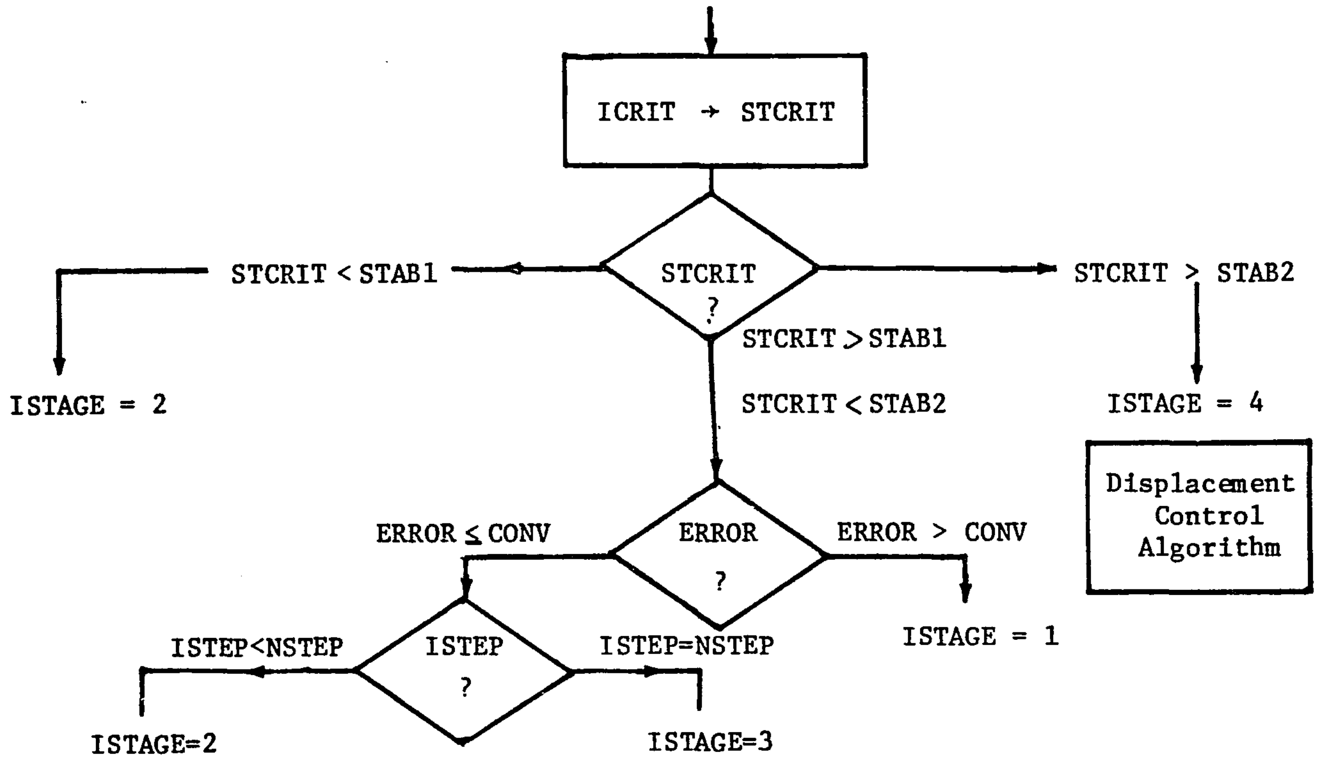

Figure 27. Solution Logic Algorithm

STCRIT is compared to the linearity criterion STAB1 and the stability criterion STAB2. The objective of the first one is to reduce computation time during the initial stages of the loading. Suppose STAB1 = 0.02: this implies that as long as the current stiffness is 98% of the original stiffness the load path is considered linear. Therefore, ISTAGE is set to 2 and one goes on to the next load step, saving an otherwise useless iteration. This is a new technique for speeding solutions by distinguishing between linear and nonlinear parts of the curve. STAB1 must be chosen with care and should not exceed 0.05.

On the other extreme, STAB2 heralds the approach of a limit point. If the stiffness reduces to, say, 20 - 30% of the original stiffness the limit point could not be far. When this happens, ISTAGE is set to 4 and the quasi-Newton scheme abandoned. Instead, displacement control is used. When STCRIT lies between the values STAB1 and STAB2, the norm of the displacement increment is compared to the displacements in that step. The ratio must be below CONV the specified convergence criterion.

When all the loads have been applied and buckling does not occur or when a limit point is found, the solution is complete. The results are output through the various files mentioned before. The element subroutines are called once again but this time with the objective of calculating stresses only. Thus, a different and shorter path is traversed.

VII. RESULTS AND CONCLUSIONS

To validate the formulation, several runs of the program BUCKS were made, and the results of some of the runs* are presented in this chapter. The results have been divided into the following groups.

1. Linear analysis
2. Stability analysis for single loads
3. Stability analysis for combined loads

Linear Analysis

The purpose of linear analysis was to compare the performance of the continuum and degenerated elements and to determine a reliable order of numerical integration. Also, the displacement mode shapes were compared to those predicted by analytical methods. Some modelling issues were resolved by using linear analysis: these include, mesh size, equivalent nodal loads and restraints for simulating certain types of loading. Once these issues were resolved and confidence in the program gained, the analysis was extended into the nonlinear regime where analytical solutions were available for only a few special cases.

---

* Throughout this chapter reference is made to certain model numbers and run numbers. These are not in any particular order. Many more runs were made than those presented here, but in order to provide a quick reference to the computer printouts, the original model numbers and run numbers are used.

Linear analysis was carried out with the help of several models of various dimensions and mesh sizes. The general trends are demonstrated here with the help of the model shown in Figure 28.

<u>Model No. 10</u>

Diameter, D	=	1.0 in
Length, L	=	3.0 in
Thickness, t	=	0.1 in
Cross-sectional area, A	$\cong$	$\pi Dt = 0.314\ in^2$
Moment of inertia, I	$\cong$	$\pi D^3 t/8 = 0.0397\ in^4$

The cylinder is divided into 4 elements along the circumference and 4 along the length; the model, therefore, consists of 16 elements and 56 nodes. The aspect ratio is

$$\frac{a_1}{a_2} = \frac{\pi D/NC}{L/NL}$$

where NC = Number of elements along circumference

NL = Number of elements along length

$$\frac{a_1}{a_2} = \frac{\pi D}{L} \text{ (since NC = NL = 4)}$$
$$\approx 1.05$$

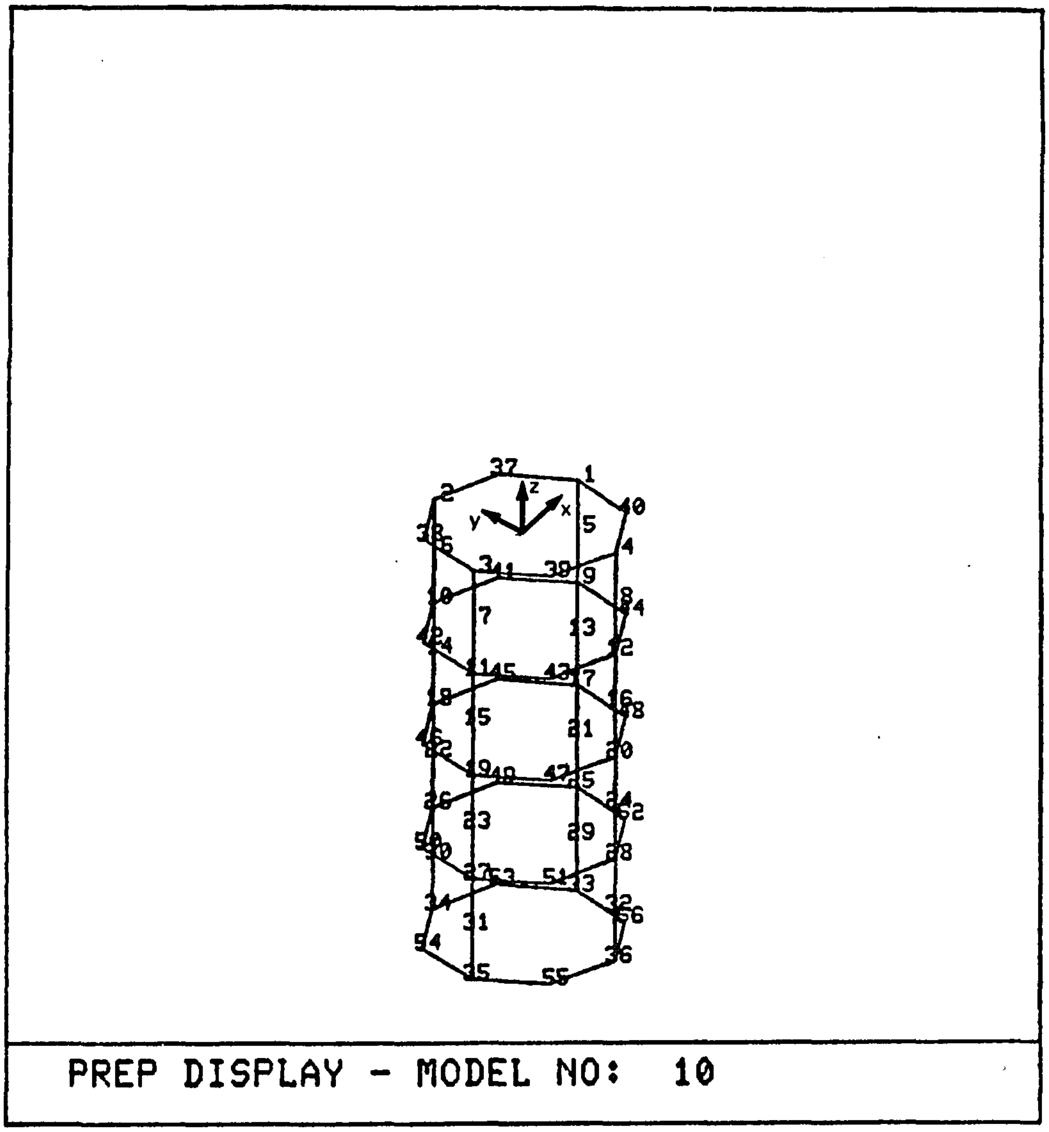

Figure 28 Model used in linear analysis.
(rotated by 45° toward the viewer)

Aspect ratios below 6:1 are generally considered acceptable. The selection of the cylinder dimensions were based on achieving aspect ratios in this range.

Uniformly Distributed Axial Loads in Model 10

Figure 29 shows Model 10 fixed at one end and under a uniformly distributed compressive load at the other end. The displacements for a load of W = 50 lb/in are calculated as follows:

The total axial load P is

$$P = \pi DW = \pi(1)(50) = 157 \text{ lb}_f$$

The axial stress is

$$\sigma_z = \frac{-P}{A} = \frac{-157}{0.314} = -500 \text{ psi}$$

The axial strain is

$$e_z = \frac{\sigma_z}{E} = \frac{-500}{30\text{x}10^6}$$

Thus, the change in length at a point whose z-coordinate is Z is given by

$$\Delta L = e_z Z$$

The maximum value occurs at the end (z = L)

$$\Delta L_{max} = e_z L = \frac{-3 \text{ x } 500}{30 \text{ x } 10^6}$$

$$= 0.5 \text{ x } 10^{-4} \text{ in}$$

The hoop strain e_θ is

$$e_\theta = -\nu e_z$$

$$= \frac{0.3 \text{ x } 500}{30 \text{ x } 10^6}$$

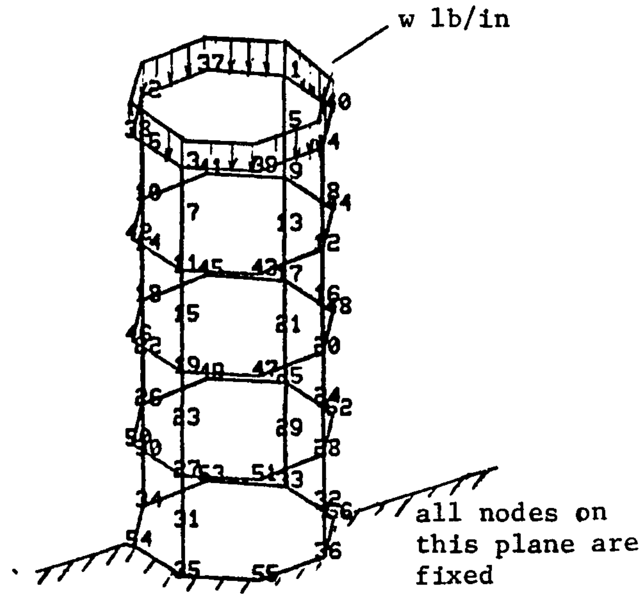

Figure 29 Uniformly distributed axial load.

Also $e_\theta = \frac{2\pi(R + \Delta R) - 2\pi R}{2\pi R}$

$$= \frac{\Delta R}{R}$$

where

R = radius of the cylinder

ΔR = dilation

$$\Delta R = Re_\theta$$

$$= \frac{0.5 \times 0.3 \times 500}{30 \times 10^6}$$

$$= 0.25 \times 10^{-5} \text{ in}$$

Table 1 compares the results obtained from BUCKS8 to the above analytical values. In obtaining the ΔR values, the boundary elements displacements were disregarded. RUN83A* is for degenerated elements and RUN83B for continuum elements. The order of integration in both cases was 3 x 3 x 2. It is concluded from the above results that degenerated elements give better results than continuum elements for axial compression.

---

* Data file names are of the form 'RUN_ _ _'

Table 1 Comparison of Displacements for Axial Loads

	Theoretical	RUN83A	RUN83B
ΔL_{max}	0.50×10^{-4}	0.499×10^{-4}	0.45×10^{-4}
ΔR	0.25×10^{-5}	0.25×10^{-5}	0.32×10^{-5}

The influence of the order of integration was investigated by performing an analysis with 2 x 2 x 2 quadrature and 4 x 4 x 3 quadrature. The results from the latter are completely erroneous and are not presented here. Table 2 shows the results for 2 x 2 x 2 quadrature.

RUN83C uses degenerated elements, RUN83D uses continuum elements. In both cases 2 x 2 x 2 quadrature is used. It is seen that the results of degenerated elements are not affected much, but the continuum elements give poorer results than before.

Table 2. Comparison of Numerical Integration Order

	Theoretical (in)	RUN83C (in)	RUN83D (in)
ΔL_{max}	0.50×10^{-4}	0.50×10^{-4}	0.46×10^{-4}
ΔR	0.25×10^{-5}	0.27×10^{-5}	0.36×10^{-5}

Model 10 has a D/t ratio of 10. To investigate the influence of the D/t ratio on the solution, the thickness was reduced to half the original value i.e. 0.05 in to give D/t = 20. The load on the D/t = 10 model is doubled to compare it to the D/t = 20 model. This is done in Table 3.

Table 3. Influence of D/t Ratio

	Theoretical (in) D/t=10, w= 100	RUN83A (in) D/t=10, w=100	RUN83E (in) D/t=20, w=50
ΔL_{max}	1.0×10^{-4}	0.99×10^{-4}	0.99×10^{-4}
ΔR	0.50×10^{-5}	0.50×10^{-5}	0.50×10^{-5}

As is evident from Table 3, there is no change in the displacement solution.

External Pressure Applied to Model 10

Equivalent nodal loads for external/internal pressure can be calculated in two ways: application of equal loads (on an element basis) on all nodes or loads consistent with the shape functions. Both options are available in all versions after BUCKS9. The former method is used in subroutine PRESUR, the latter in PRSUR2. In general, good results will be obtained from equal loads only if the mesh was very fine. The advantage of this method lies in lesser computation as opposed to consistent loading which requires numerical integration, as discussed in Chapter V.

The objective here is to obtain constant dilation for constant external/internal pressure. The dilation can be measured at three key points: corner nodes, lengthwise midnodes, and circumferential midnodes. This is shown in Fig. 30. A comparison of various loading options is made in Table 4.

Table 4. Comparison of Dilation

NODE	RUN46	RUN43L	RUN43E
Corner node, u_c	0.154×10^{-4}	0.98×10^{-4}	0.69×10^{-4}
Lengthwise midnode, u_L	0.152×10^{-4}	0.19×10^{-4}	0.06×10^{-4}
* Circumferential midnode, u_M	0.151×10^{-4}	0.65×10^{-4}	0.56×10^{-4}

* the value of u_M was divided by cos 45° for the circumferential midnodes to get the dilation.

RUN46 is with consistent loading, RUN43L with equal loads, and RUN43E with the standard load ratio of 1:-4:-4 for rectangular flat parabolic elements. Continuum elements and 3 x 3 x 2 quadrature was used for

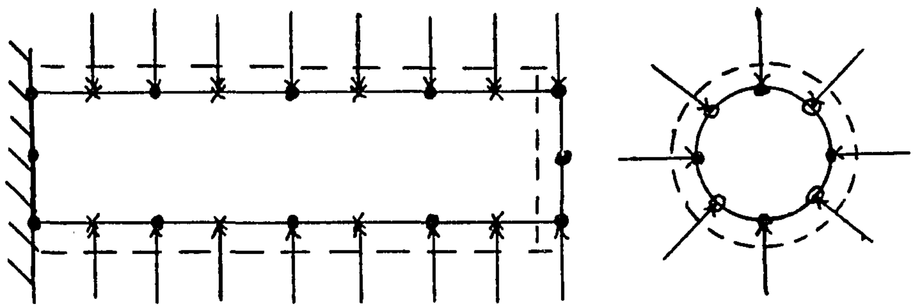

- corner nodes
- x lengthwise midnodes
- o circumferential midnodes
- ——— undeformed shell
- - - - deformed shell

Figure 30 Measurement of dilation.

all runs. It was to be expected that for such a coarse mesh only consistent loads will give good results. Since nonlinear analysis involves very high computation time, it would not be possible to use very fine meshes. Therefore, it was decided that only consistent loads can be used in all analyses involving uniform element pressures.

Next, the two elements were compared to each other and to analytical results. Suppose an external pressure of 25 psi is applied to Model 10. Since D/t = 10, this is just on the border line between thick and thin cylinders. Using membrane equations, the hoop stress σ_θ is

$$\sigma_\theta = \frac{pR}{t}$$

and

$$\sigma_r = 0 \text{ (for thin shells)}$$

The axial stress is

$$\sigma_z = 0 \text{ (one end fixed, other free; not capped)}$$

The hoop strain e_θ is

$$e_\theta = \frac{pR}{Et}$$

$$\therefore \frac{\Delta R}{R} = \frac{pR}{Et}$$

Thus, the dilation ΔR is

$$\Delta R = \frac{pR^2}{Et} \tag{7.2}$$

Substituting for the variables one gets

$$\Delta R = \frac{25(0.5)^2}{(30\text{x}10^6)(0.1)}$$

$$= 0.208 \times 10^{-5} \text{ in}$$

If thick cylinder formula is used, ΔR is found as (ref. [149])

$$\Delta R = \frac{b^2 p r}{E(b^2 - a^2)}[(1 - \nu) + (1 + \nu)\frac{a^2}{r^2}]$$

$$\Delta R_{max} = \frac{p b^3}{E(b^2 - a^2)}[(1 - \nu) + (1 + \nu)\frac{a^2}{b^2}] \qquad (7.3)$$

where $a = R - t/2$

$b = R + t/2$

$$\Delta R_{max} = \frac{25 \times 0.55^3}{30 \times 10^6(0.1)}[0.7 + 1.3(\frac{0.45}{0.55})^2]$$

$$= 0.217 \times 10^{-5} \text{ in}$$

Comparison is made (in Table 5) between the results obtained using degenerated elements (RUN86A) and continuum elements (RUN86B). Unless otherwise stated, the order of integration is 3 x 3 x 2.

Table 5. Comparison of Degenerated and Continuum Elements Under External Pressure

	Theoretical (in)	RUN86A (in)	RUN86B (in)
R	-0.208×10^{-5}	-0.207×10^{-5}	-0.188×10^{-5}
L_{max}	0.37×10^{-5}	0.35×10^{-5}	0.45×10^{-5}

Once again, degenerated elements give better results when compared to the membrane theory for radial displacements. It should be noted that L_{max} is measured at the boundary elements and good agreement is not expected because of end effects. Also, one can observe that continuum elements are stiffer in the radial direction

Constant Bending Moment

It was pointed out in Chapter V that the four point bend test produces constant bending moment between the inner points. In order to simulate this condition, several schemes of equivalent loads were tried. The method that gave the best results for deflections is shown in Fig. 31. It was found that this method gives the same theoretical displacements as those obtained from a constant bending moment of magnitude $F_z \times R$. The bending takes place in the x-z plane; hence all restrained nodes are restrained in direction x. This does not affect

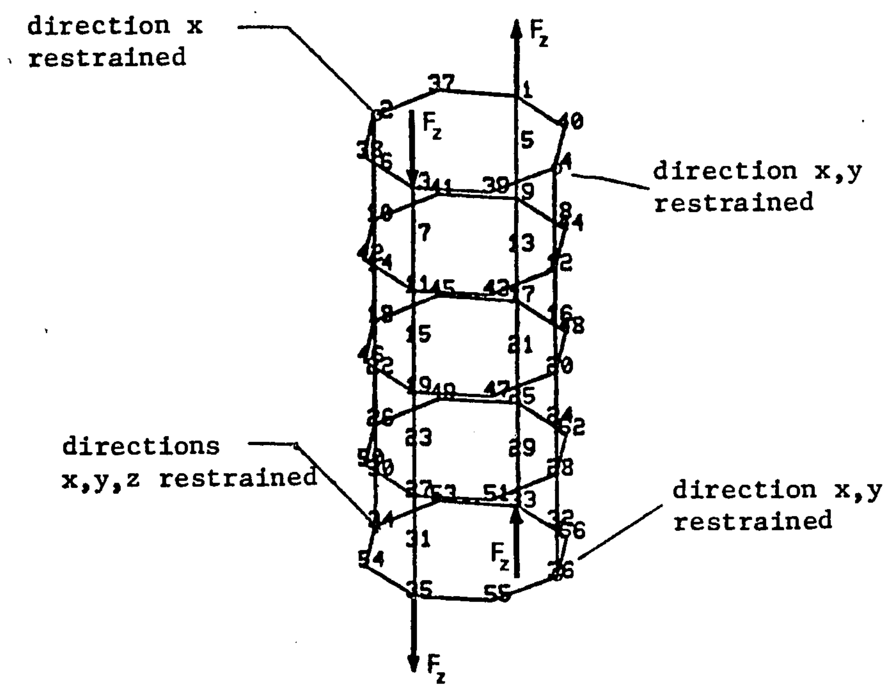

Figure 31 Modelling constant bending moment.

ovalization because of the way the nodes are chosen; direction x is tangential to the shell at the restrained nodes. The equivalent loads are calculated in the subroutine MOMENT.

The theoretical displacements are calculated as follows:
The differential equation for deflections u is

$$\frac{d^2u}{dz^2} = \frac{M}{EI}$$

$$\therefore \quad u = \frac{M}{EI} z^2 + C_1 z + C_2$$

At $z = 0$, $u = 0$

$$\therefore \quad C_2 = 0$$

at $z = L$, $u = 0$

$$\therefore \quad C_1 = \frac{-ML}{EI}$$

$$\therefore \quad u = \frac{M}{EI} (z^2 - Lz)$$

Table 6 compares the u deflections predicted by eq. (7.4) with the results obtained from BUCKS. Figure 32 shows the deflections graphically. RUN85C used degenerated elements; RUN85D used continuum elements. Barring slight deviations at the ends, degenerated elements prove to be better.

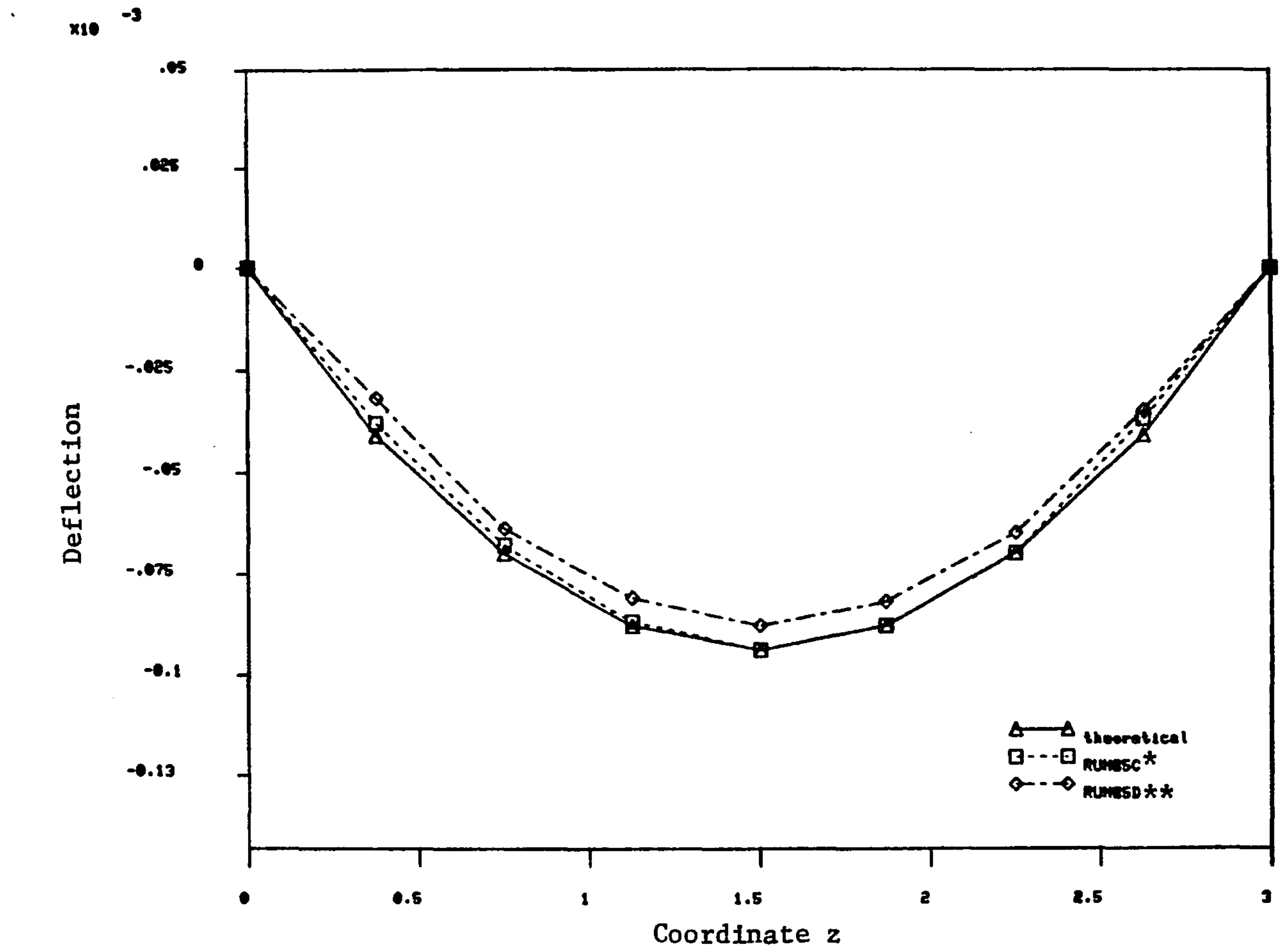

Figure 32 Comparison of deflections under constant bending moment.

* degenerated elements
** continuum elements

Table 6. Comparison of Deflections for Constant Bending Moment

Node	34	30	26	22	18	14	10	6	2
z(in)	0	.375	.75	1.125	1.5	1.875	2.25	2.625	3.0
				($u \times 10^4$)					
Theoretical	0	.41	.70	.88	.94	.88	.70	.41	0
RUN85C *	0	.38	.68	.87	.94	.88	.70	.37	0
RUN85D **	0	.32	.64	.81	.88	.82	.65	.35	0

*degenerated elements

**continuum elements

Uniformly Distributed Lateral Load

Figure 33 shows a cylinder being used as a cantilever beam. If the distributed lateral load is w = 10 lb/in, the deflections from beam theory can be calculated from

$$u = \frac{wz^2}{24EI}(z^2 - 4zL + 6L^2)$$

$$= .003498 \times 10^{-4} z^2 (z^2 - 12z + 54) \qquad (7.5)$$

The equivalent nodal loads for uniform lateral pressure are calculated in subroutine UDLL. The deflections of the neutral plane, represented

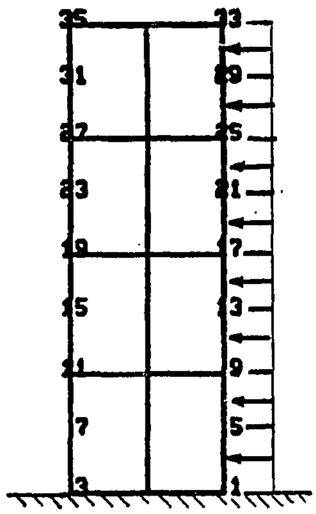

Figure 33   Uniform lateral load.

by the line joining nodes 2 to 34 and 3 to 35 are compared in Table 7. It was observed that the deflections on the line 2-34 were the same as those along 3 to 35, as expected.

Table 7. Deflections Caused by Uniform Lateral Load

Node	34	30	26	22	18	14	10	6	2
Z(in)	0	0.375	0.75	1.125	1.5	1.87	2.25	2.625	3.0
				($u \times 10^4$ in)					
Theoretical	0	0.024	.089	.228	.300	.428	.568	.708	.850
RUN84A*	0	.07	.19	.33	.48	.65	.82	.98	1.16
RUN84B**	0	.07	.19	.31	.45	.60	.76	.91	1.06

* degenerated
** continuum

Looking at the maximum deflections in Table 7, one finds that degenerated elements overestimate the deflection by 36% (RUN84A) and continuum elements by 25% (RUN84B). These results are not satisfactory and the reason will become clear in the following paragraphs.

The L/D ratio for Model 10 is 3; in this range shear effects are appreciable. The deflection due to shear can be calculated from (Ref. [148])

$$\frac{d^2u_s}{dz^2} = \frac{kw}{AG}$$

where u_s = shear deflection

G = shear modulus

k = $\tau_o/(V/A)$

τ_o = shear stress at the neutral plane

V = shear force

For thin tubes k = 2

$$\therefore \frac{d^2u_s}{dz^2} = \frac{-2w}{AG}$$

$$\therefore u_s = \frac{2w}{AG}\frac{z^2}{2} + K_1 z + K_2$$

For a cantilever beam

at $z = 0$, $u_s = 0$

$\therefore K_2 = 0$

at $z = L$, $\frac{du_s}{dz} = 0$

$\therefore K_1 = 0$

$$\therefore u_s = \frac{wz^2}{AG} \tag{7.6}$$

Adding eqs. (7.5) and (7.6), the total deflections are found as

$$u = \frac{wz^2}{24EI}(z^2 - 4zL - 6L^2) + \frac{wz^2}{AG} \tag{7.7}$$

If now the theoretical deflections are compared as in Table 8, the agreement is good for the continuum elements (excluding end effects).

Table 8. Deflections Corrected for Shear

Node	34	30	26	22	18	14	10	6	2
z(in)	0	0.375	0.75	1.125	1.5	1.875	2.25	2.625	3.0
				(u x 10 in)					
Theoretical	0	.03	.11	.22	.36	.52	.71	.89	1.09
RUN84A	0	.07	.19	.33	.48	.65	.82	.98	1.16
RUN84B	0	.07	.19	.31	.45	.60	.76	.91	1.06

The results are shown graphically in Fig. 34.

Concentrated Load

Finally, some runs were made with concentrated loads. As an example, an end load was applied laterally and the cylinder fixed at the other end. The deflections for this case can be calculated from

$$U = \frac{P}{6EI}(3Lz^2 - z^3) + u_s \tag{7.8}$$

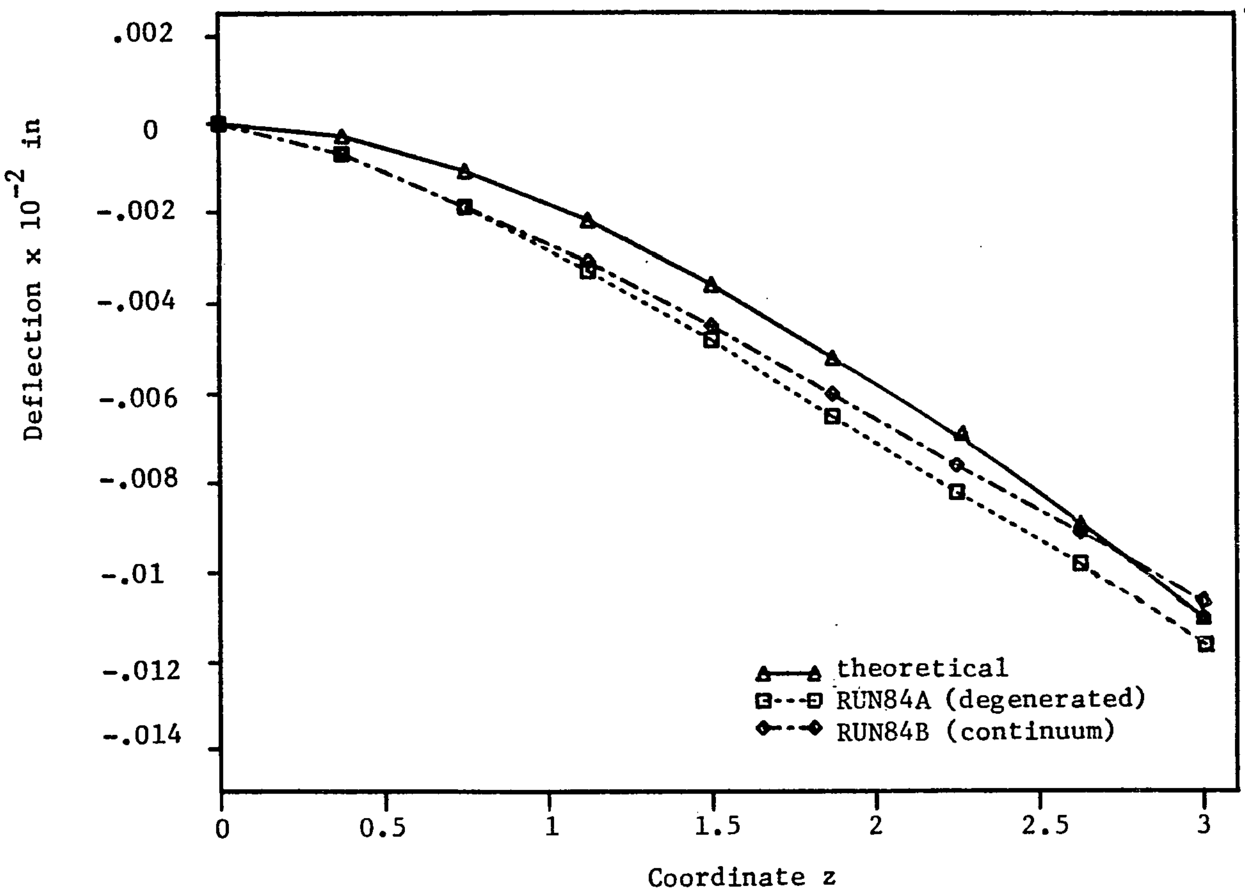

Figure 34 Total deflections under distributed lateral loads.

From Ref. [48], u_s is found from

$$\frac{du_s}{dz} = \frac{kV}{AG}$$

$$\therefore \quad u_s = \frac{kV}{AG} z + C_1$$

At $z = 0$, $V_s = 0$

$$\therefore \quad u_s = \frac{kV}{AG} z$$

$$= \frac{2V}{AG} z \quad \text{for thin tubes} \tag{7.9}$$

$$\therefore \quad u = \frac{P}{EI} (3\, Lz^2 - z^3) + \frac{2V}{AG} z \tag{7.10}$$

The deflections obtained from degenerated elements (RUN82A) and continuum elements (RUN82B) are compared to the values obtained from eq. (7.10) in Table 9 and Fig. 35. Degenerated element deflections give excellent agreement with those calculated from (7.10).

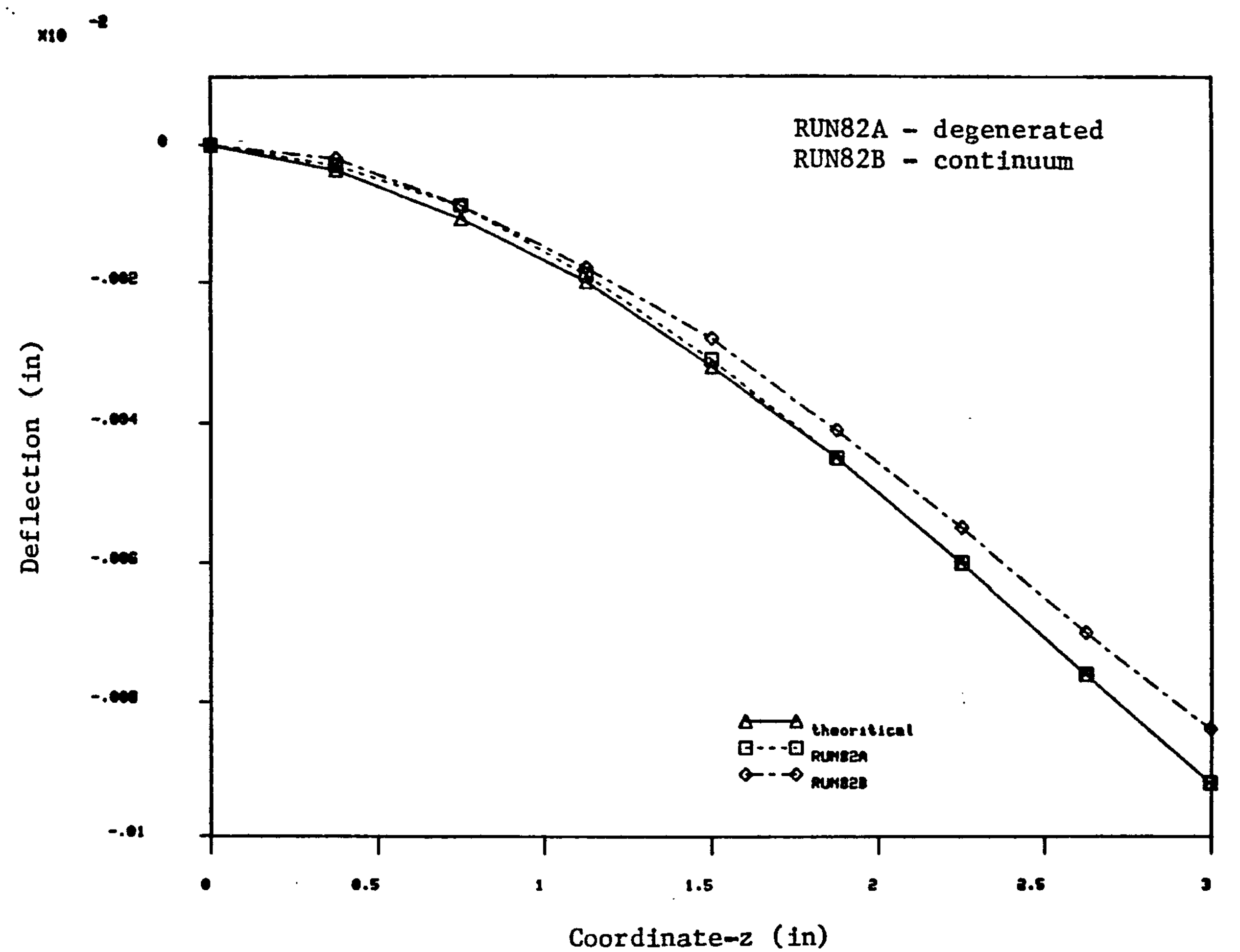

Figure 35 Deflection under concentrated end load.

Table 9. Deflections for Concentrated End Load

Node	34	30	26	22	18	14	10	6	2
z(in)	0	.375	.75	1.125	1.5	1.875	2.25	2.625	3.0
$u \times 10^4$									
Theoretical	0	.037	.11	.20	.32	.45	.60	.76	.92
RUN82A*	0	.03	.09	.19	.31	.45	.60	.76	.92
RUN82B**	0	.02	.09	.18	.28	.41	.55	.70	.84

* degenerated
** continuum

Conclusions from Linear Analysis

Only a few examples were included in this write-up. From these examples, as well as other runs, it was concluded that

1. The overall performance of degenerated elements is superior to that of continuum elements for all types of loading.
2. Degenerated elements are less sensitive to the order of integration.
3. Reduced integration of order 3 in the shell plane and exact integration of order 2 in the thickness plane gives reliable results.
4. The degenerated elements can model thin shells as well as thick shells for D/t greater than 10.
5. Consistent loading must be used when applying external/ internal pressure.

The Piola-Kirchhoff (P/K) stresses were compared to Cauchy stresses and theoretical values. Good agreement was found between the Cauchy stresses and analytical values. Since displacements were small, the P/K stresses were almost equal to Cauchy stresses, as expected.

Patch Test

This test is designed to determine whether or not the solution obtained by using a certain type of element will converge as the mesh is refined. Irons and Ahmad have described this test in detail in Ref. [144].

The test can be done in three ways: (a) impose deflections to give constant stress (b) calculate the nodal loads caused by the tractions along the boundaries (c) impose deflections at every node.

In this study, the test was done in two steps. First, displacements were calculated at the nodes by applying a constant axial load of 40 lb_f to Model 10.

$$\Delta L_{max} = \frac{PL}{AE} = \frac{40 \times 3}{0.314 \times 30 \times 10^6}$$

$$= 0.25 \times 10^{-4} \text{ in}$$

$$\sigma_z = \frac{P}{A} = \frac{40}{.314} = 255 \text{ psi}$$

The displacement w is plotted for nodes 1 through 33 in Fig. 36 as a straight line varying from zero to ΔL_{max}. The radial displacement is constant at $0.3 \times \frac{PR}{AE} = 0.125 \times 10^{-5}$ in. The theoretical displacements are compared to those obtained from RUN23B for continuum elements and RUN24A for degenerated elements. The displacements, representing a constant stress state, are substituted back to obtain the stresses.

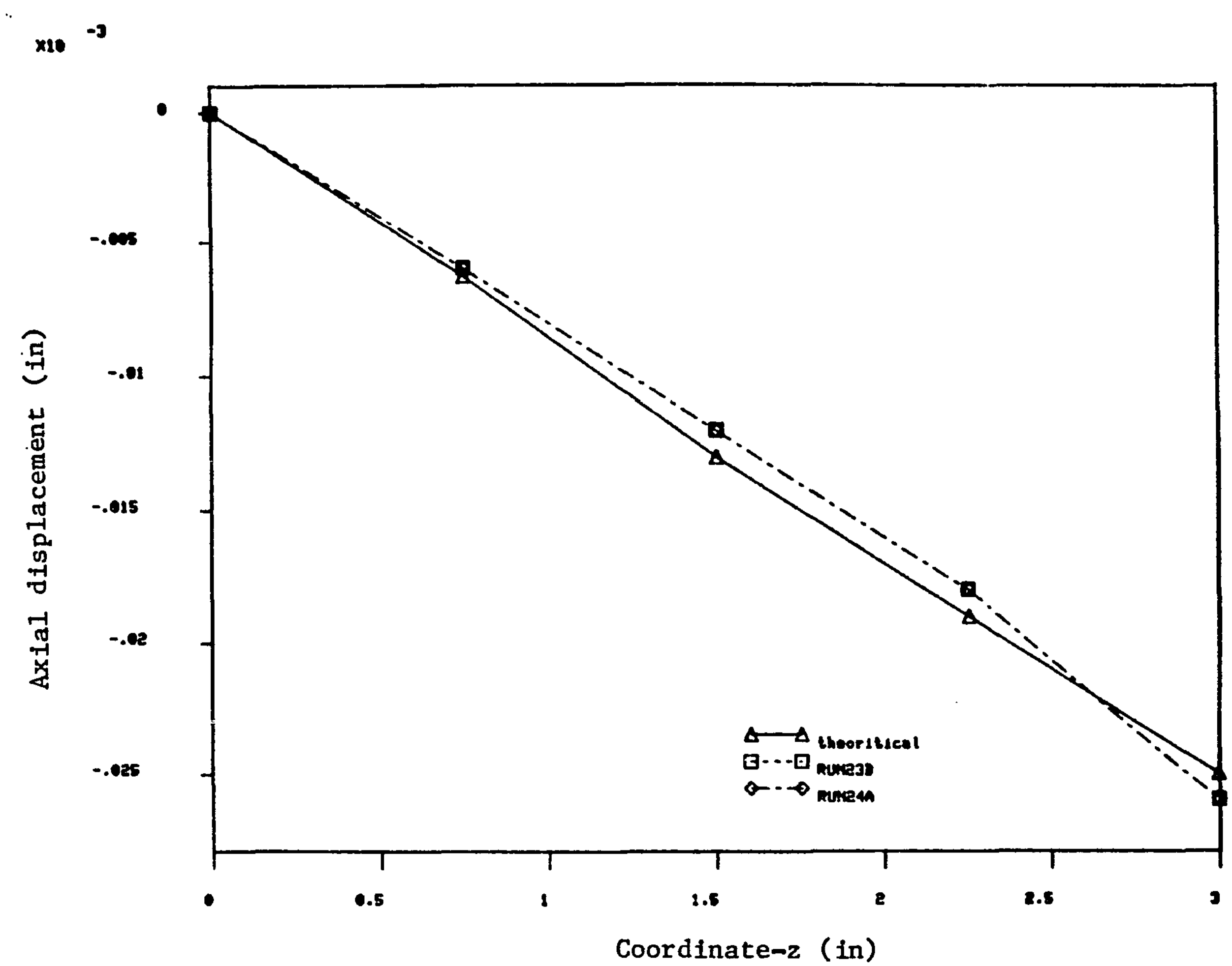

Figure 36 Displacements for patch test.

The results are shown in Table 10. It can be stated that both elements pass the patch test.

Table 10. Comparison of Axial Stresses for Patch Test+

Element No.	1	5	9	13
RUN24A (degenerated)	-261*	-257	-257	-264*
RUN23B (continuum)	-257*	-262	-262	-259*

* boundary elements

+ stresses in the other direction are approximately zero

Evaluation of Material Properties for Elastic-Plastic Analysis

Since it is desired to compare the results of this study to Battelle's experiments, it is assumed that all models are made of the same material that was used in Battelle's study, i.e. 1020 steel. The stress-strain curve for this material was obtained experimentally and has been plotted in Ref. [43]. The eight data points given in Table 11 were read off this curve.

The stress-strain data points were fed into the program SSCURV, which converts these engineering stress-strain values to true stress-strains and obtains the curve-fitting constants, as described in Chapter V. The results are shown in Table 12 and plotted in Fig. 37.

Table 11. Stress-Strain Data for 1020 Steel

Stress, ksi	0.	51.65*	55.0	60.5	66	71.5	77	82.5
Strain x 10^{-2}	0.	0.172	0.225	0.285	0.345	0.48	0.735	1.53

* yield point

From Fig. 37, it can be seen that both the Ramberg-Osgood and exponential models provide a good fit, but the bilinear model is not suitable for 1020 steel.

Table 12. Elastic-Plastic Material Constants

```
*****   RESULTS OF PROGRAM SSCURV   *****

  CURVE FITTING OF STRESS-STRAIN DATA


MATERIAL:              1020 STEEL
YOUNGS MODULUS, E:     0.29942029E+08
YIELD STRENGTH:        0.51650000E+05


BILINEAR MODEL -

TANGENT MODULUS, ET:    0.29870260E+07


EXPONENTIAL MODEL -

COEFFICIENT A :          0.66279609E-08
EXPONENT B :             0.13436849E+01


RAMBERG-OSGOOD MODEL -

COEFFICIENT K:           0.23240541E+06
EXPONENT N:              0.22979479E+00
```

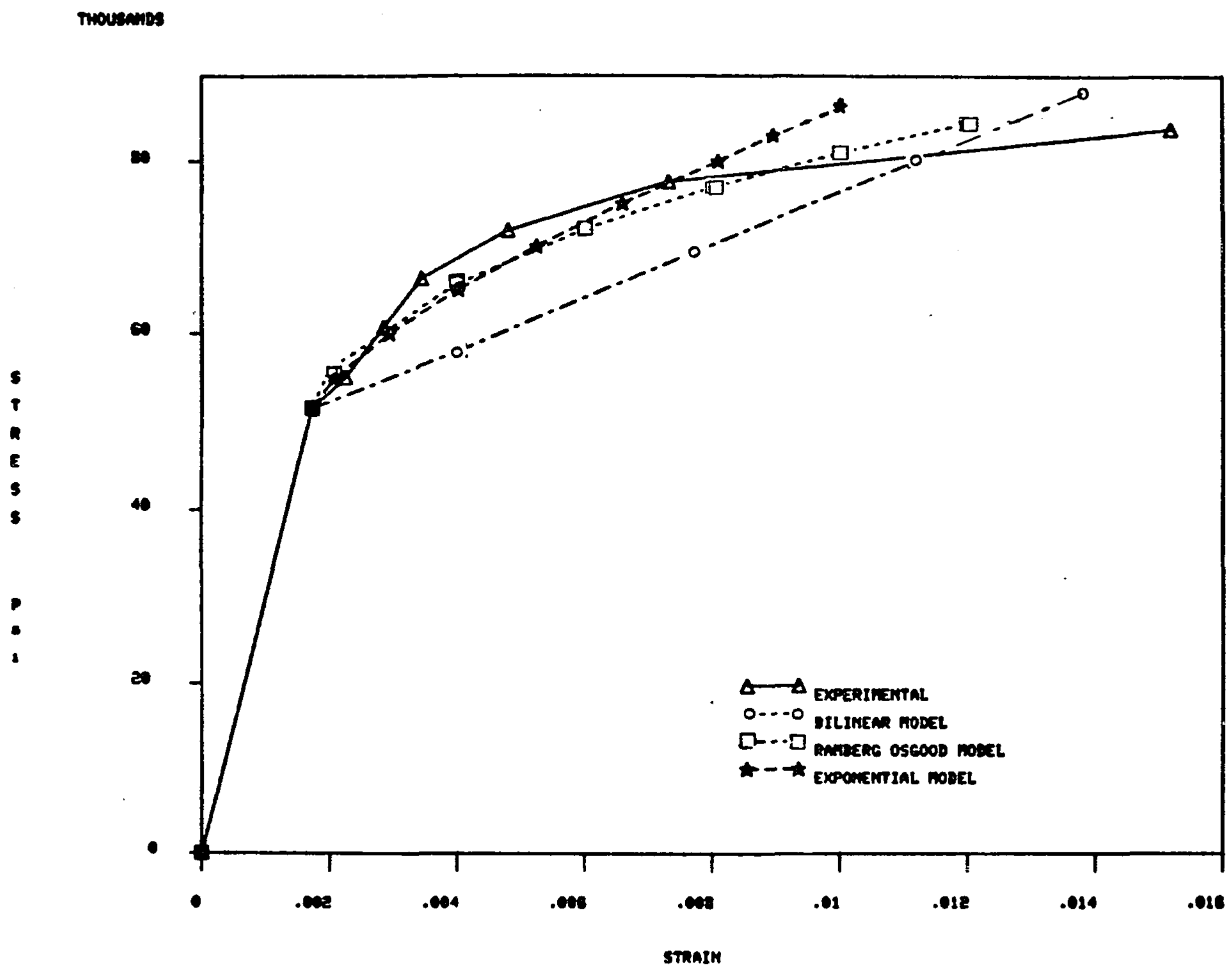

Figure 37 Comparison of material models.

Stability Analysis Under Single Loads

Buckling loads were first determined by applying one type of load only. The loads studied were external pressure and bending moments. Table 13 lists the dimensions and mesh sizes of the models used. The dimensions are the same as those used in Battelle's study [43].

Table 13. Specifications of Models Used in Nonlinear Analysis

		Model 30	Model 31	Model 32
	Dimensions			
1.	Outside dia/thickness ratio	16	20	40
2.	Length/dia. ratio	11.2	11.4	20.3
3.	Midsurface dia., D(in)	1.339	1.32	1.28
4.	Shell thickness (in)	0.089	0.0695	0.033
5.	Length (in)	15	15	26
	Section Properties			
6.	Area, in^2	0.374	0.288	0.133
7.	Moment of area, in^4	0.084	0.163	0.0274
	Mesh			
8.	Circumferential elements	4	4	4
9.	Elements along length	6	6	8
10.	No. of nodes	80	80	104
11.	No. of elements	24	24	32
12.	Multiplying factor (See Appendix A)	1.	1.	1.

Since computation times on the VAX-750 were very high (about one hour per loadstep), all models are fairly coarse. Also, if longer cylinders were to be analyzed, the number of elements would have to be increased to keep the aspect ratio the same. The aspect ratio of Models 30 and 31 is obtained from eq. (7.1) as

$$\frac{a_1}{a_2} = \frac{\pi D/NC}{L/NL}$$

$$= \frac{\pi(1.339) \times 6}{15 \times 4}$$

$$= 0.42$$

For Model 32

$$\frac{a_1}{a_2} = \frac{\pi(1.28) \times 8}{26 \times 4}$$

$$= 0.31$$

These ratios are in the acceptable range but for larger cylinders it would be difficult to maintain these ratios without increasing the number of elements considerably. The displacement solution in the linear range for these aspect ratios indicates that the conclusions of the linear study are still valid.

Unless otherwise stated, 3 x 3 x 2 Gauss quadrature was used with degenerated elements. For external pressure, IP2 was taken as 5 (consistent loading). Loads were applied in equal steps until the approach of the limit point.

Buckling Under External Pressure

External pressure was applied to the three models specified in the previous section. One end was fixed, the other was free to move axially. The restraints were applied in such a manner so as not to force ovalization at the ends, i.e. the nodes on opposite side of the cylinder were not restrained in the direction coincident with the line joining them.

The following procedure was followed for stability problems for single loads. Some estimate for the buckling load was obtained from either analytical or experimental studies. The load applied ranged from zero to twice this estimate. The total number of steps chosen was based largely on limitations on computer time. However, if difficulties were involved because of large step size, a higher number of steps was used in subsequent runs.

In order to reduce unnecessary computations, the following variables must be specified:

STAB1 = Linearity criterion

ICRIT = Critical stiffness parameter

NCRIT = Critical step number

Several stiffness parameters (stability indices) were defined in Chapter V. The user inputs a code to choose one of these in accordance with the procedure given in Appendix B. In order to reduce unwanted iterations in the linear range STAB1 is specified; as long as the critical parameter is below STAB1, the solution from the first iteration will be considered the final solution in that step. In this section, STAB1 was specified as 0.01. ST3 was taken as the critical index, although the variation in other indices was monitored also.

NCRIT is a number between 1 and NSTEP (the total number of steps). It is the load step in which some part of the structure is expected to go into the plastic range. By specifying this, time is saved in steps below NCRIT since the plasticity part of the program is by-passed. There is no harm in specifying a lower value of NCRIT (only additional computation time) but if a higher value is specified, the solution may be erroneous.

In RUN91F, p_{max} = 20,000 psi was used. The load was applied in 6 equal steps. However, since NCRIT = 4 was used, erroneous results were obtained (the determinant becomes negative before reaching ST2 or ST3 reach STAB2).

This situation was corrected in RUN91G. The load was applied in 8 steps. A rough calculation shows that NCRIT should be 3. Before any experience was gained with the program, there was no criterion available for selecting STAB2. Recall that STAB2 determines when displacement control should start. The following reasoning was used.

If the solution strategy is not altered, then at the limit point the following events may take place.

1) diagonal elements of the stiffness matrix approach zero (if execution is continued, the program would be terminated by a floating zero divide)
2) convergence cannot be achieved by a quasi Newton scheme. (the only reason one may obtain a solution is because of round-off errors)

3) the determinant of the stiffness matrix approaches zero and may even change sign (if the limit point is passed)

4) the lowest eigenvalue approaches zero

Some initial runs were made with no displacement control (STAB2 = 0.0). If the solution diverged or the determinant changed signs, the values of the stability indices was examined. In subsequent runs STAB2 was based on these values. For example, RUN91G did not converge in step 6 out of a total of 8 steps. The values of ST2 and ST3 were in the vicinity of 0.5. RUN91H was a repeat of RUN91G but with STAB2 = 0.5.

The values of ST2 and ST3 are plotted in Fig. 38 for RUN91H. Figure 39 shows the load-displacement curve for this run. In all load-displacement curves, D1 represents the start and D2 the end of displacement control. Table 14 shows the values of all the stability indices. ST1 was omitted because of numerical problems.

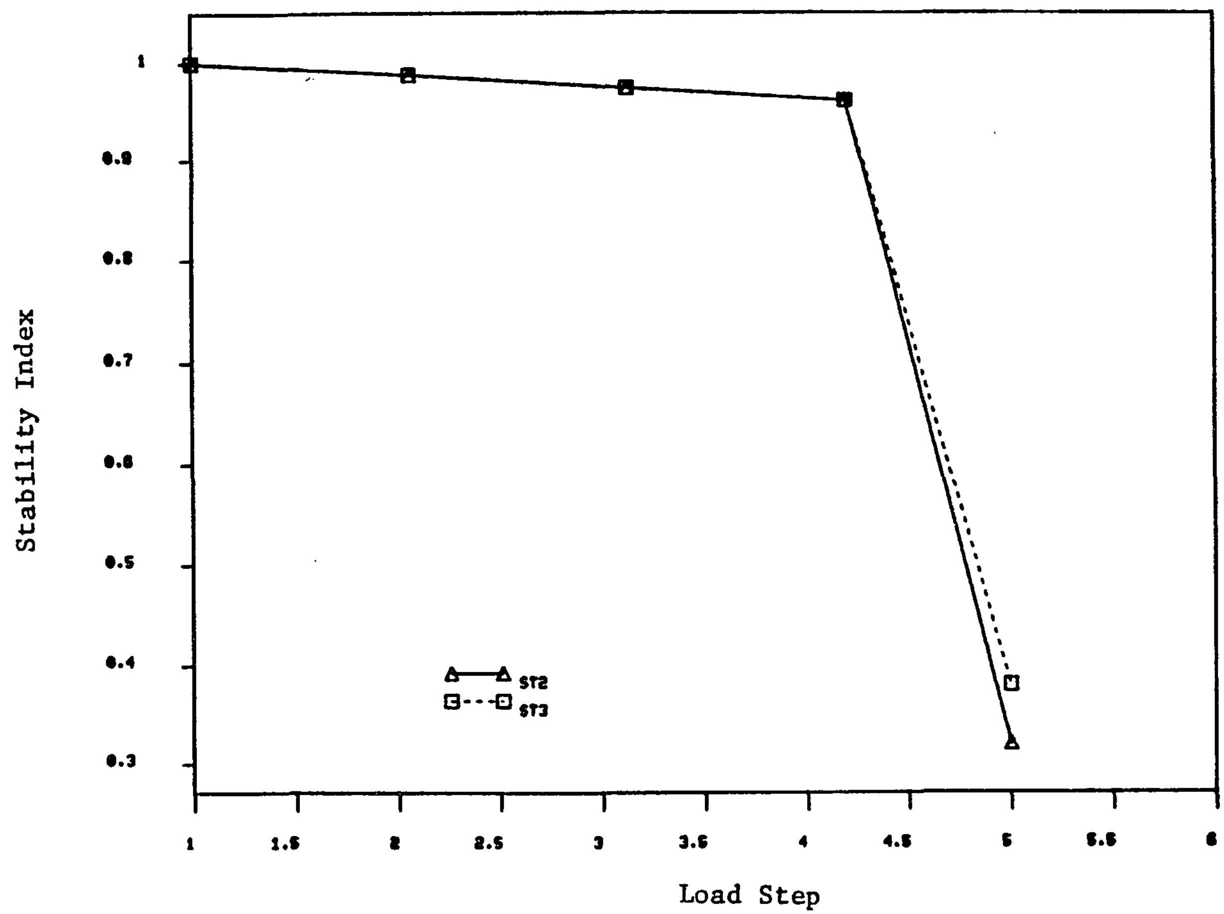

Figure 38 Variation of stability indices in RUN91H (pure pressure).

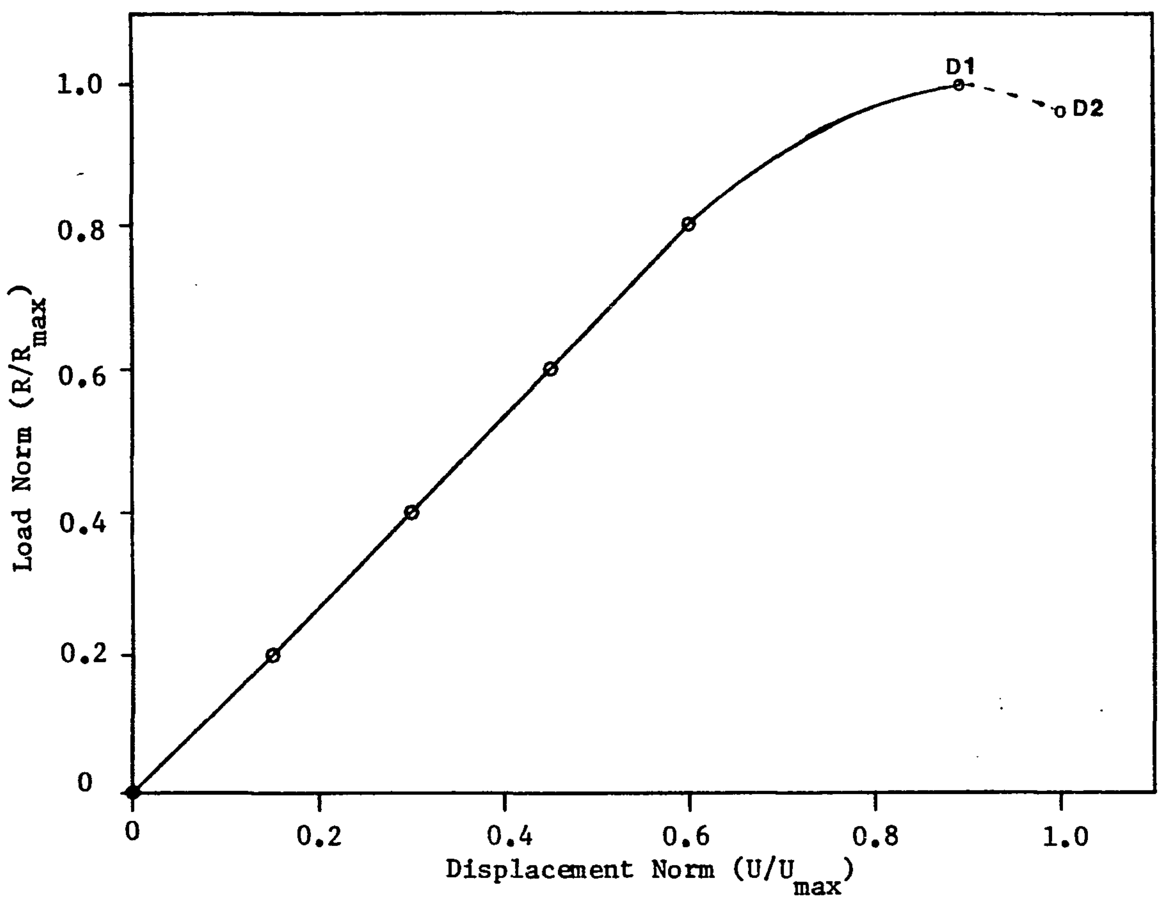

Figure 39 Load-displacement curve for RUN91H (pure pressure).

Table 14. Stability Indices in Last Step for External Pressure

INDEX	RUN91H (Model 30)	RUN102 (Model 31)	RUN204 (Model 32)
ST2	0.426	0.099	0.05
ST3	0.481	0.302	0.116
STOVL	1.01	1.02	1.09
STBND x 10^{-4}	0.295	0.539	0.168
STBRAZ	0.0	0.0	0.0
STEULR x 10^{-4}	0.113	0.851	0.699
STBNDA x 10^{-6}	0.0267	0.185	0.25

The next step is to determine the external pressure corresponding to the limit point. The load vector is printed out with the .RST file. However, because displacement control was used after step 5 there was no direct correspondence between the load vector and applied pressure: the solution deviates from the proportional load line. The method used was based on the average nodal loads at the three key points mentioned before. These are listed in Table 15.

Table 15. Average Nodal Loads for RUN91H

Node*	Load Step #1	Maximum	at Buckling+
Corner nodes	798	4990	3545
Circumfer. midnodes	3562	17,810	12,560
Lengthwise midnodes	2779	13,895	9,805

* excluding boundary nodes

\+ after crossing the limit point

The maximum loads correspond to an applied pressure of 12,500 psi (approximately).

The same procedure was used on models 31 and 32. The maximum pressure in RUN101 was 10,000 psi applied in 8 steps and NCRIT = 5. RUN101 was run without displacement control and it diverged in step 7. RUN102 used STAB2 = 0.4; it buckled in step 7 with ST3 = 0.302. The results are given in Table 14 and Figures 40 and 41. The equivalent nodal loads are given in Table 16.

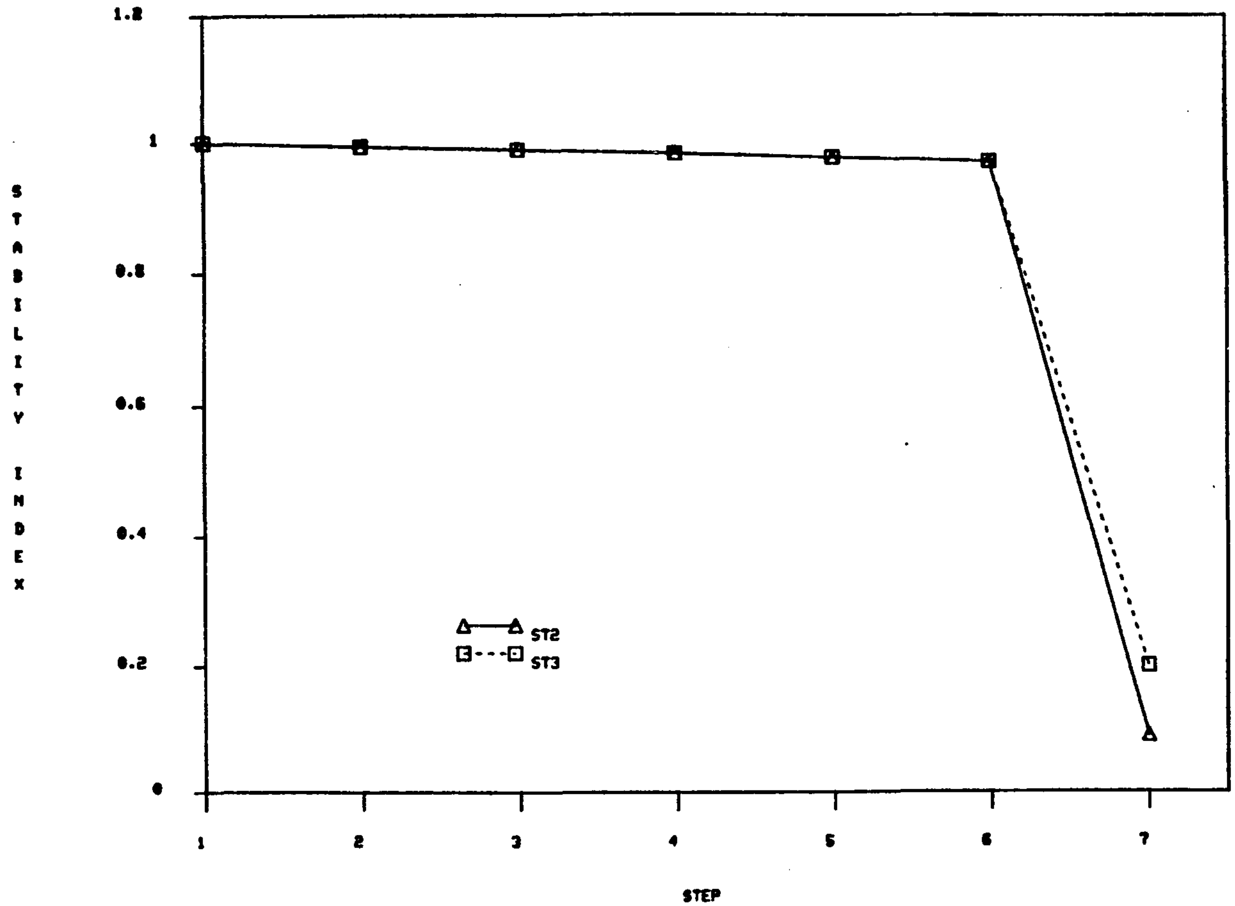

Figure 40 Variation of stability indices in RUN102 (pure pressure).

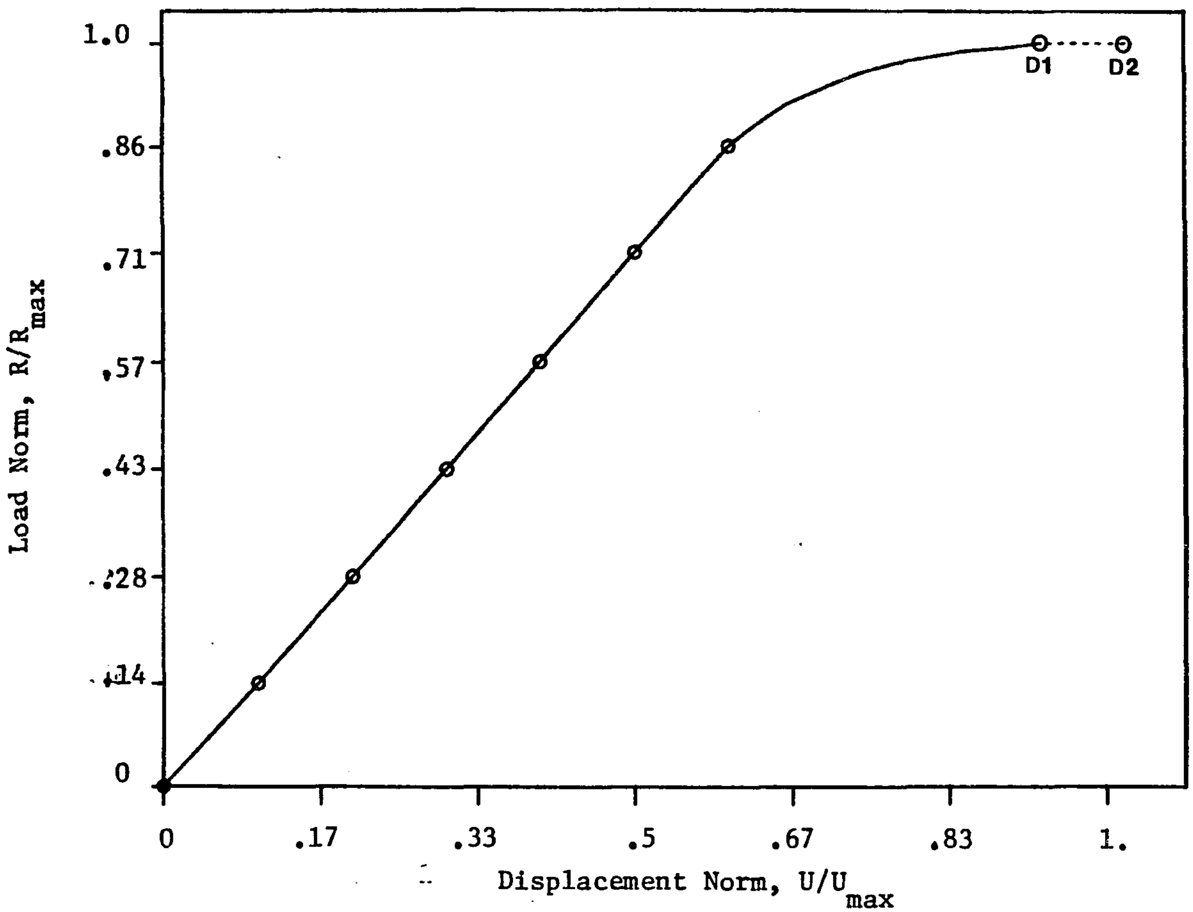

Figure 41 Load-displacement curve for RUN102 (pure pressure).

Table 16. Equivalent Nodal Loads for RUN102

Node*	Load Step #1	Maximum	At Buckling
Corner nodes	492	3444	2490
Circumf. midnodes	1756	12,292	10,020
Lengthwise midnodes	1370	9,590	7,500

* excluding boundary nodes

The maximum loads correspond to an applied pressure of 8750 psi.

In a similar manner, Model 32 was analyzed. The maximum load in RUN204 was 5000 psi applied in 10 steps. The determinant becomes negative in step 3. The stability indices are listed in Table 14. The critical loads correspond to an applied pressure of 1250 psi (step 3 is on the other side of the limit point).

Buckling Under Bending Load

As in linear analysis, pure bending moments are applied by means of end couples. However, there will be no shear forces in the pipe if the loads are applied in this manner. On the other hand, if two concentrated lateral loads of equal magnitude are applied at the same distance from each simple support one gets both bending moments and shear forces. However, concentrated loads cause excessive local deformation, and the structure may be predicted to buckle prematurely (since real loads are distributed over a finite area). It is felt that the two methods mentioned above represent two extremes.

Runs RUN94B to RUN94H used the former method for Model 30 while RUN97A and RUN97B used concentrated loads. A maximum bending moment of 15,000 in-lb was applied in equal steps. In RUN94E the total number of load steps was 6. The Ramberg-Osgood model was used with degenerated elements. The final values of the stability indices are given in Table 17. The variation in the major indices is shown in Fig. 42. The load-displacement curve is shown in Fig. 43. At buckling, the maximum moment was 12,500.

Using concentrated loads (RUN97B) the structure failed at 7500 in-lb with lowest ST3 value of 0.24, before displacement control.

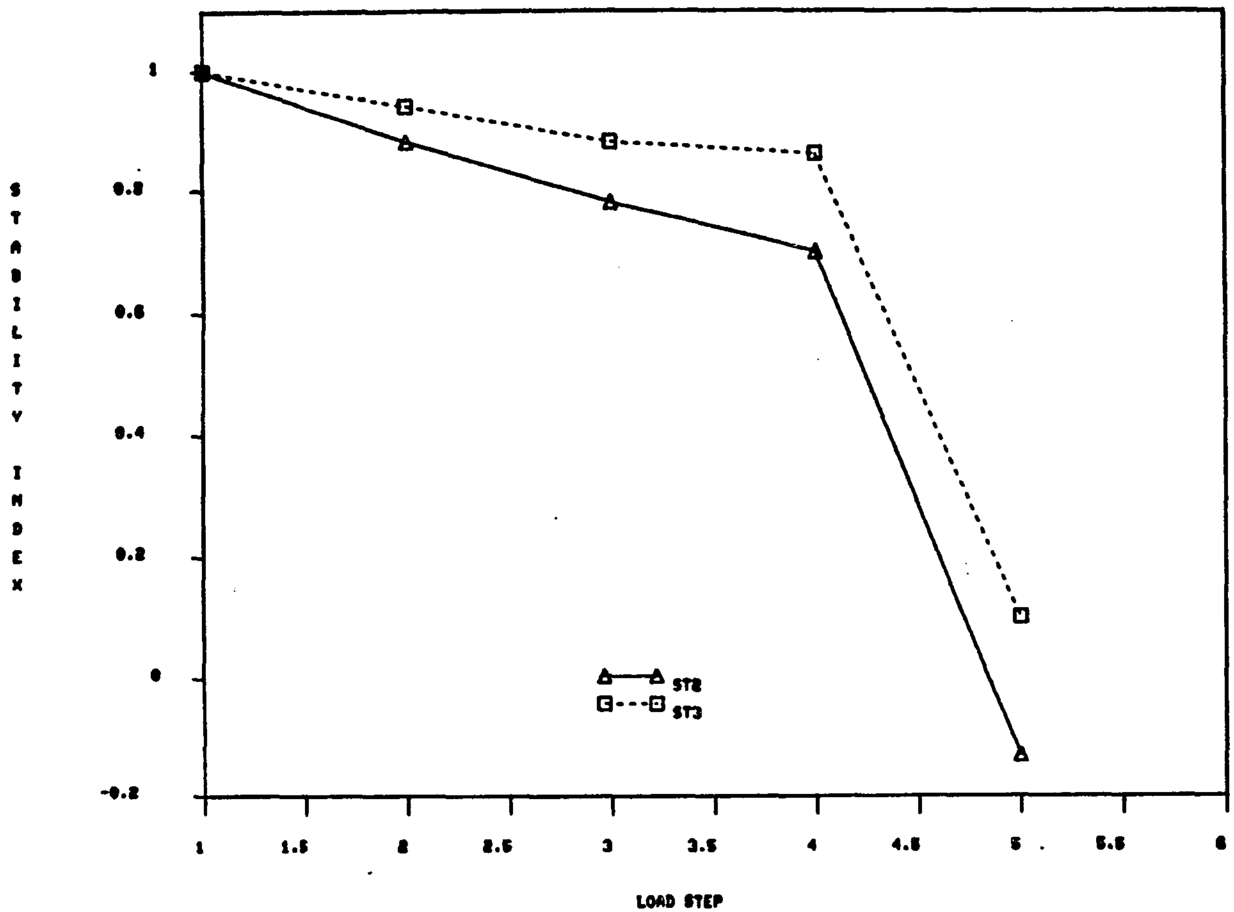

Figure 42 Stability indices for RUN94E (pure bending).

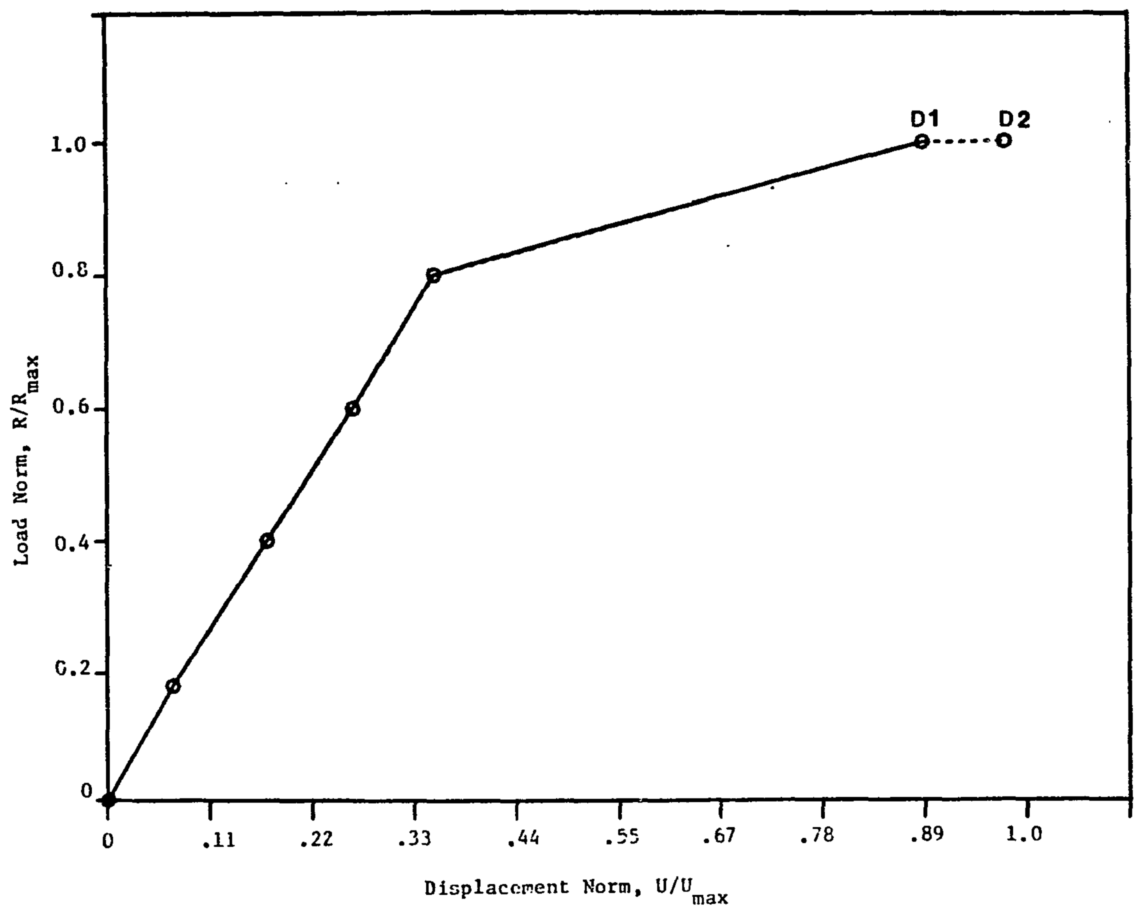

Figure 43 Load-displacement curve for RUN94E (pure bending).

Table 17 Stability Indices in Last Step for Bending

INDEX	RUN94E (Model 30)	RUN105 (Model 31)	RUN209 (Model 32)
ST1	0.89	0.89	1.00
ST2	-0.01	-0.043	0.40
ST3	0.10	0.207	0.22
STOVL	0.17	-0.32	0.57
STBND	0.10	0.21	2.2
STBRAZ	4.88	2.4	3.6
STEULR	0.101	0.06	0.12
STBNDA	0.024	0.012	.004

The same procedure was applied to Model 31 in RUN105 and to Model 32 in RUN209. The results for constant bending moments are compared to Model 30 in Table 17. Figures 44 and 45 show the variations in stability indices and the load-displacement curve for RUN105. The buckling load for RUN105 was 11,840 and for RUN209 was 3300 lb_f.

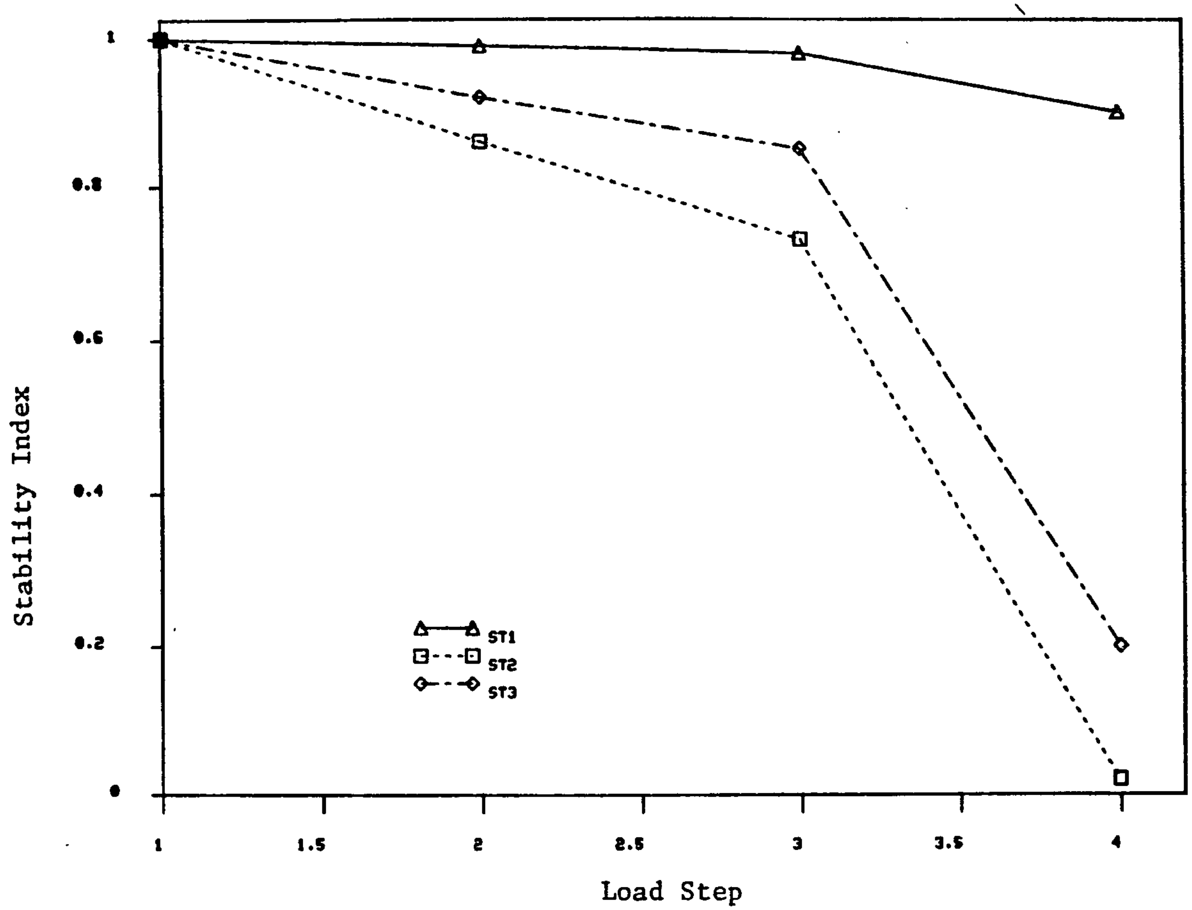

Figure 44 Stability indices for RUN105 (pure bending).

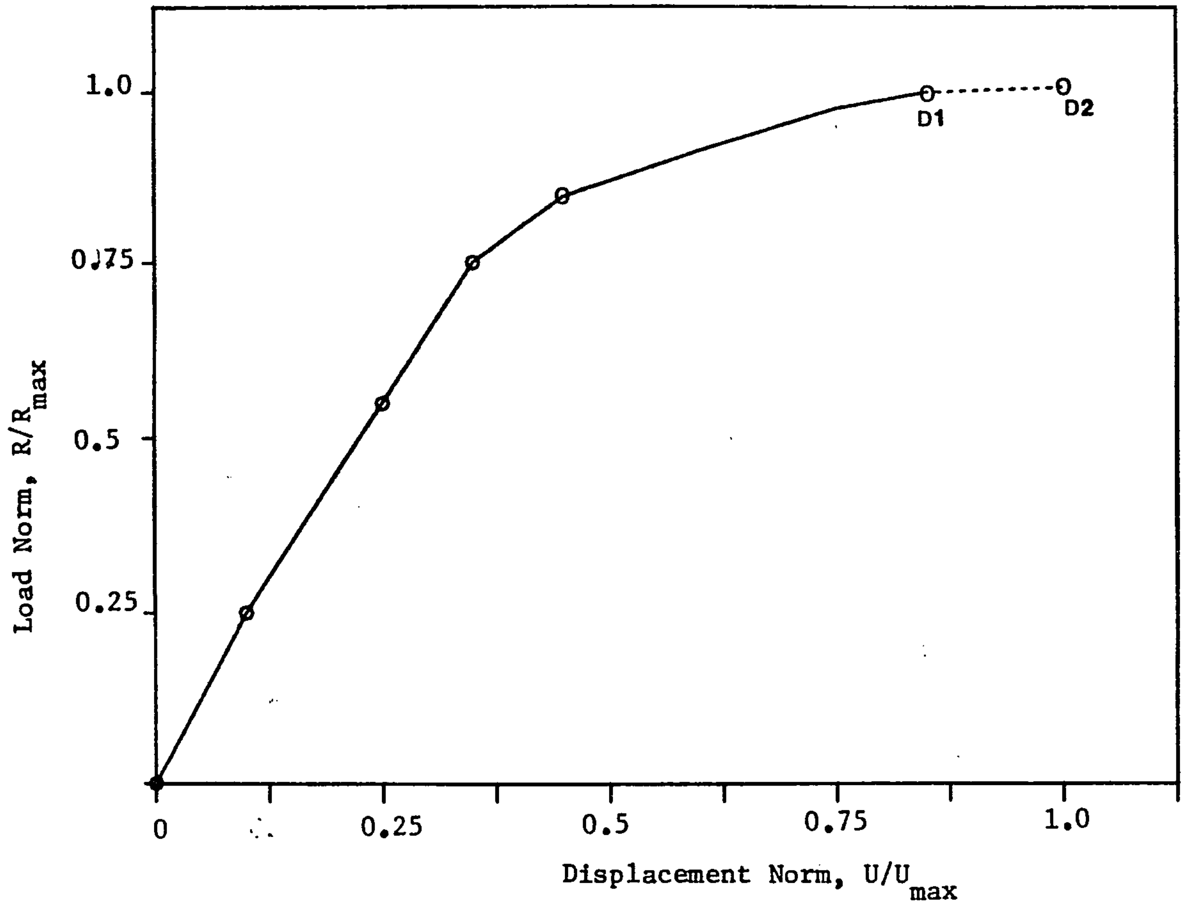

Figure 45 Load-displacement curve for RUN105 (pure bending).

Buckling Under Combined Loads

Some program runs were made using various combinations of bending moment and external pressure. In the first set of runs, the load was applied proportionately i.e. the ratio of the bending moment to pressure was the same in all load steps. In subsequent runs the influence of the order of loading was investigated. The results are discussed below.

In the first run of this type, designated RUN311, bending moment and pressure were applied to Model 30 in a 1 psi: 1 in-lb ratio. In each load step, 1000 psi of external pressure and 1000 in-lbs of moment were applied. The variation in stability index ST3 is shown in Figure 46 and the norm of the load vector is plotted against the displacement norm in Figure 47. Buckling occured after load step 7 in the first iteration of displacement control. In other runs, the pressure:moment ratio was changed to 2.5:1 (RUN322) and 1:2 (RUN301), etc. The results are plotted in Figure 48 using dimensionless ratios p/p_{cr} and M/M_{cr}, where p_{cr} and M_{cr} are the critical values of external pressure and bending moment respectively, when each is applied separately.

In the next set of runs, the influence of the order of loading was investigated as follows. The same loads as those used for proportional loading were applied but this time all of the moment was applied first, then the moment was kept constant and pressure increased to its maximum value or to the value at which buckling was detected. The loading history is shown in Figure 49. The critical values of the loads are plotted in Figure 50.

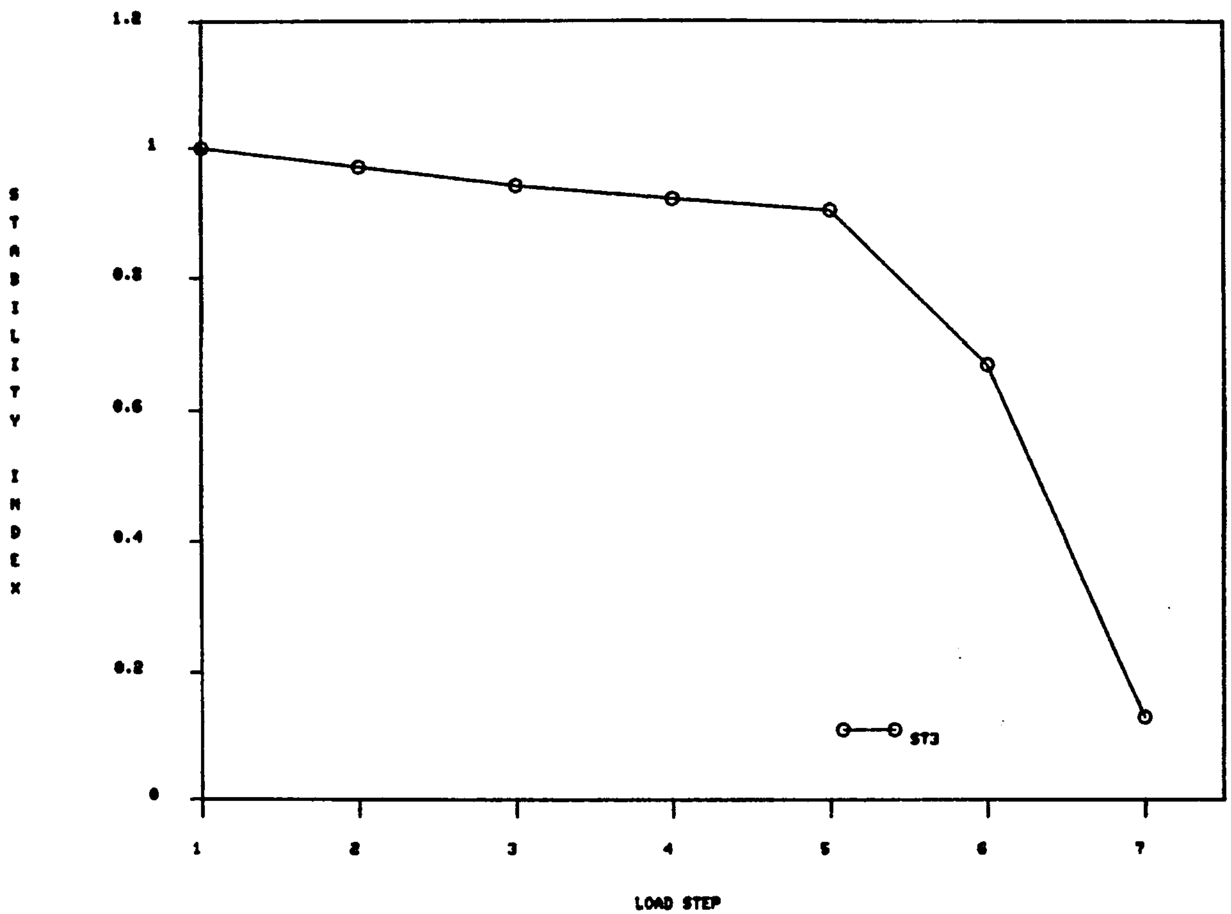

Figure 46 Variation of ST3 in RUN311 (combined load).

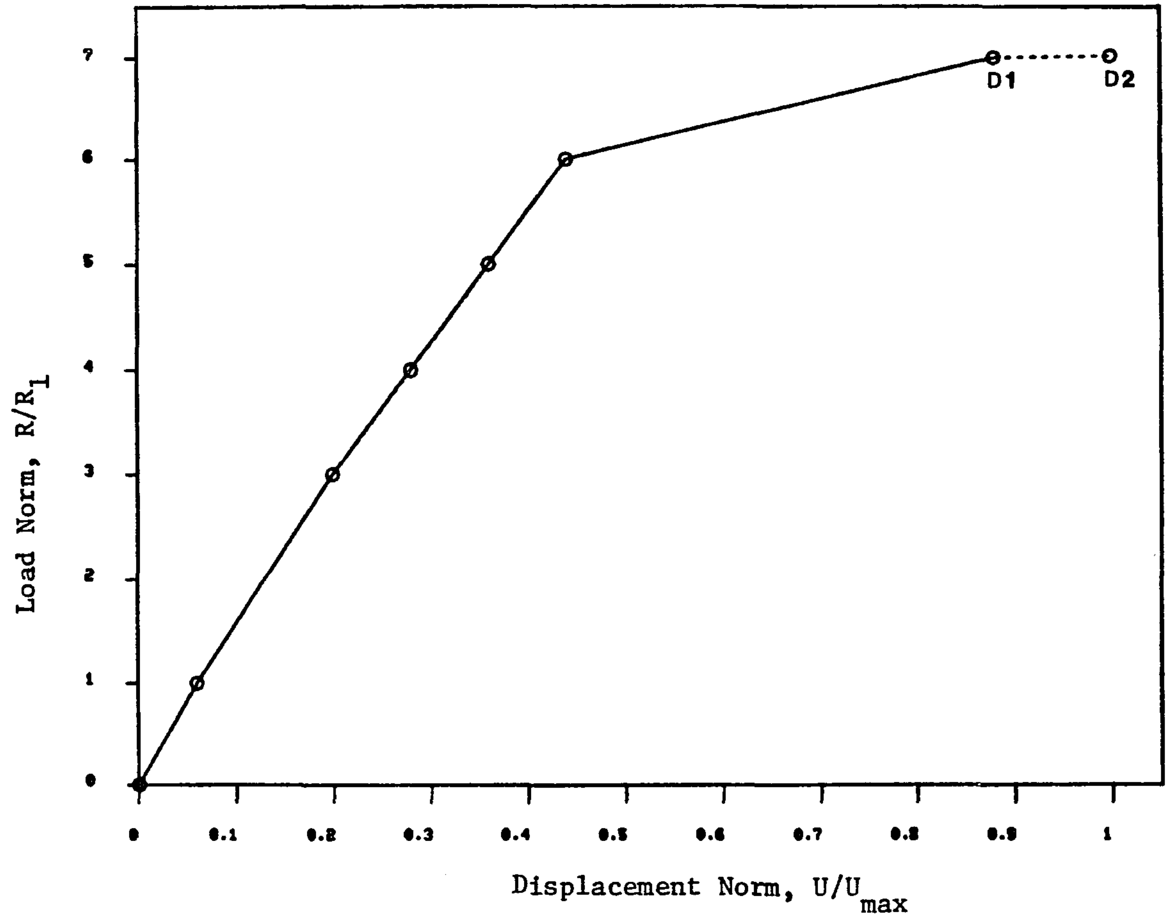

Figure 47 Load-displacement curve for RUN311 (combined load).

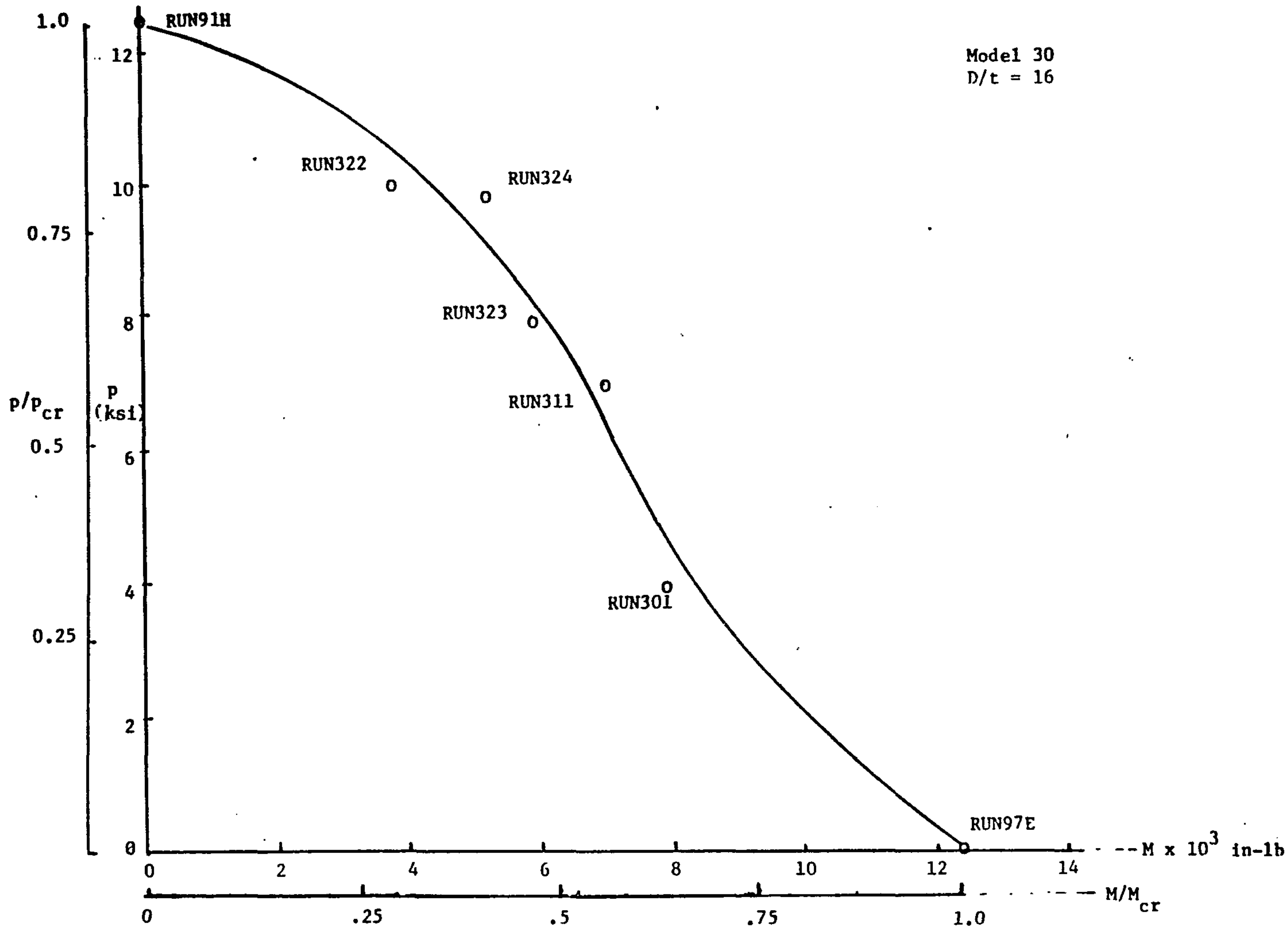

Figure 48 Failure curve for combined bending and pressure (proportional loading).

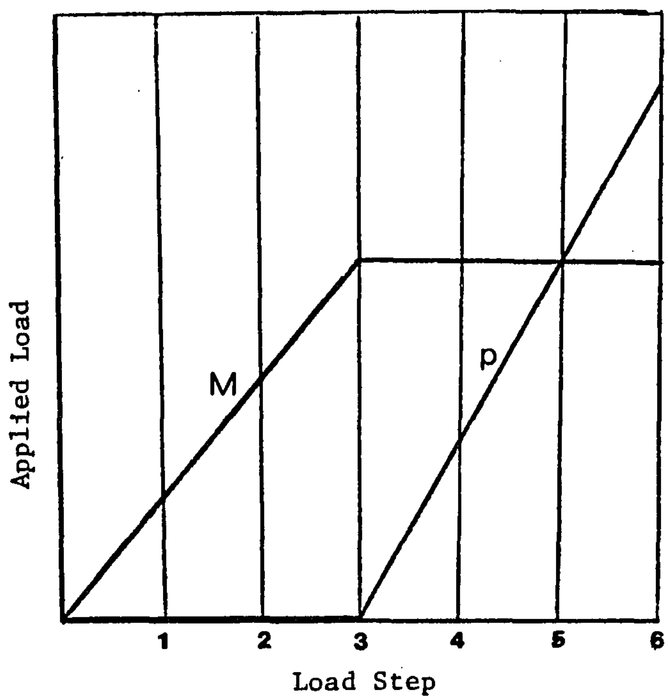

Figure 49 Variation of load when moment is applied first.

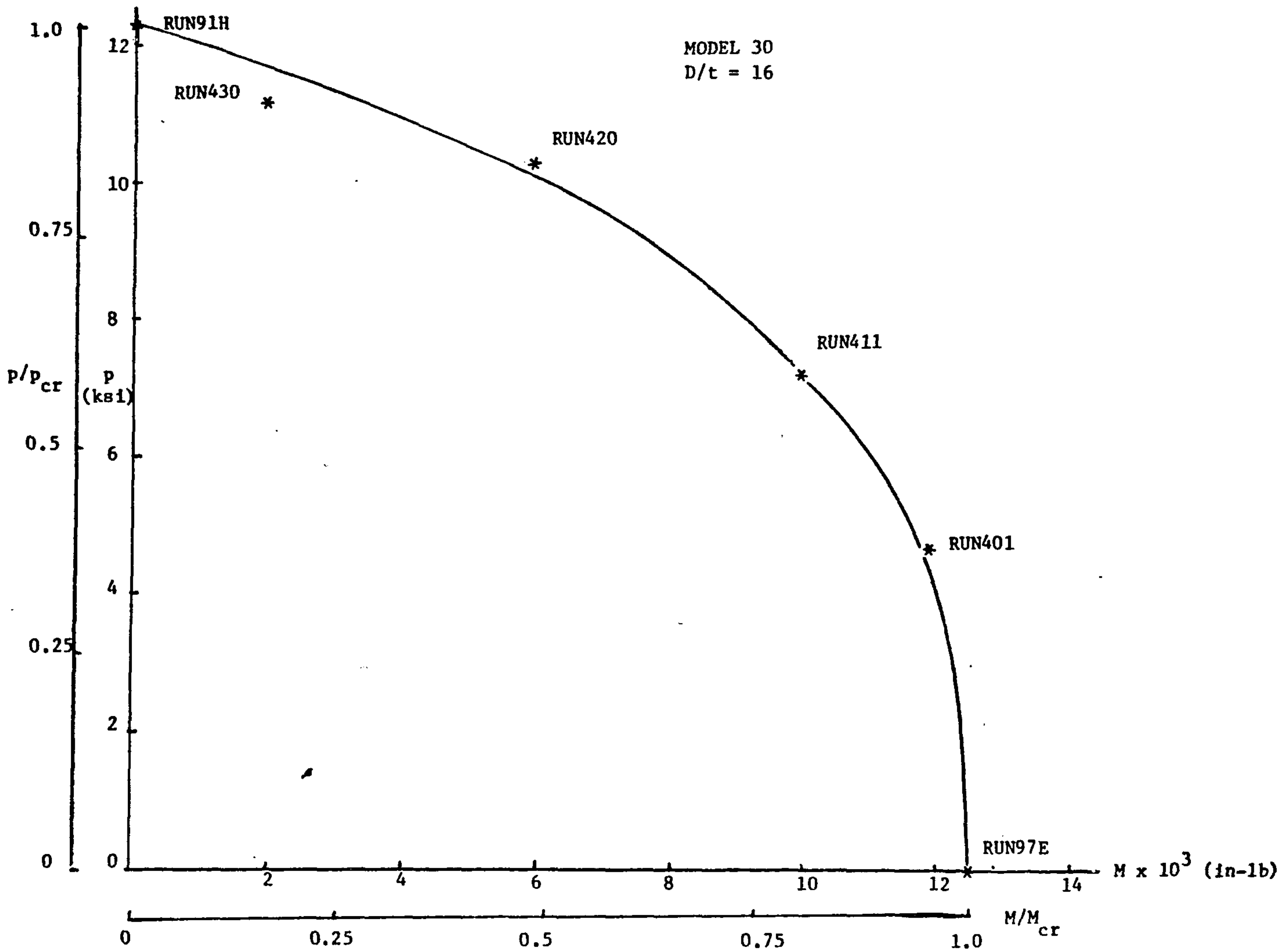

Figure 50 Failure surface for nonproportional bending and pressure; bending moment applied first.

In a similar manner, the pressure was applied first followed by the bending moment. The loading history is shown in Figure 51 and the results in Figure 52. Subroutine UNPROP makes it possible to apply loads in any manner desired.

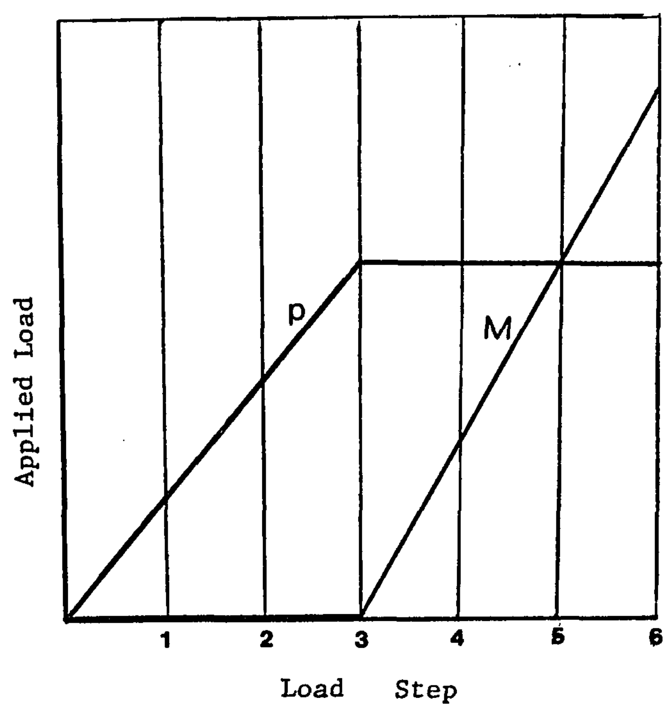

Figure 51 Variation of load when pressure is applied first.

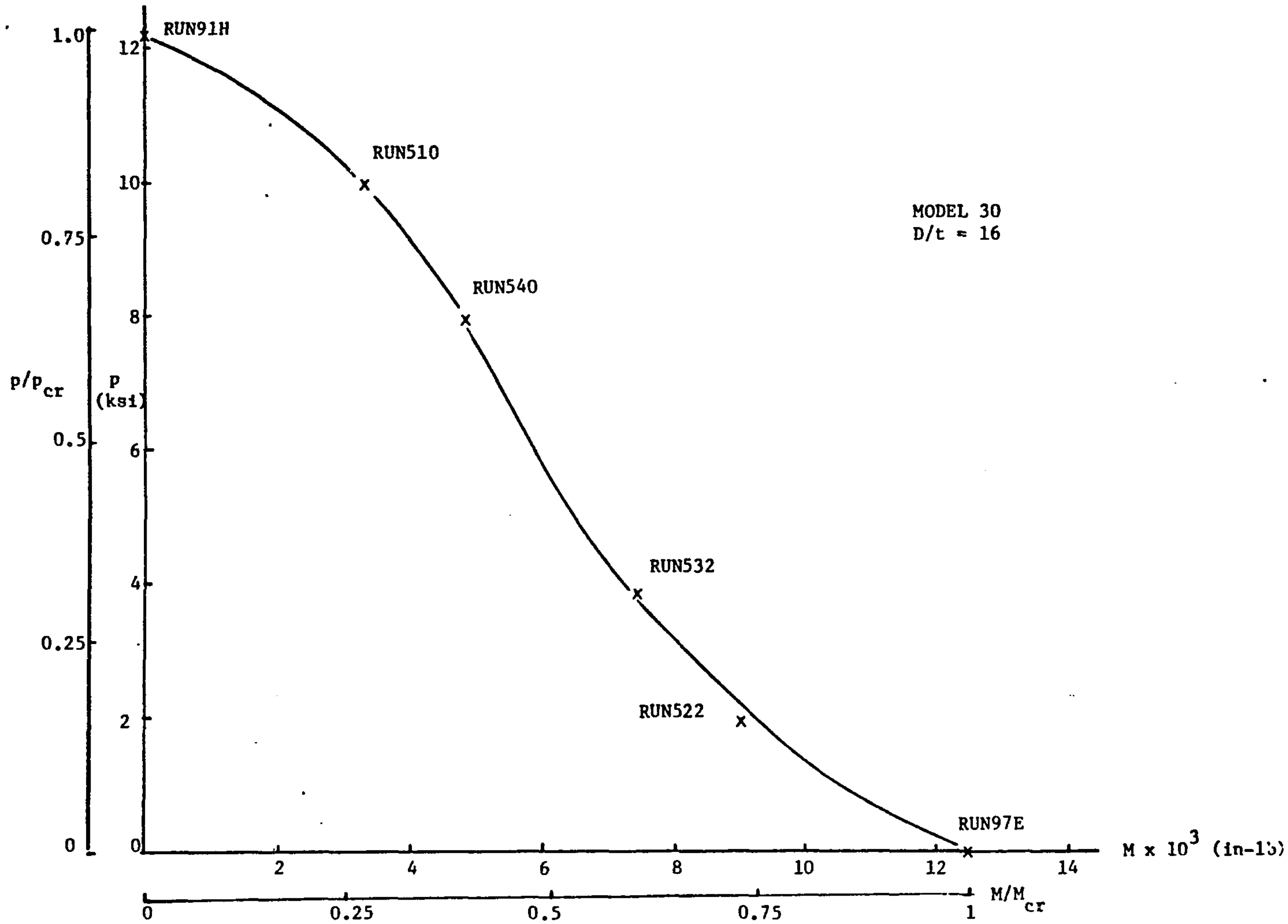

Figure 52 Failure surface for nonproportional bending and pressure; pressure applied first.

Conclusions

The results obtained from program BUCKS were compared to Battelle's experimental study, which used the same cylinder dimensions and same types of loads. The critical loads for pure pressure are plotted in Figure 53. The difference at D/t = 16 is fairly large (about 25%) but it is about 13% at D/t = 40. It should be mentioned here that the length of the D/t = 16 specimen was 15 inches compared to 26 inches for the D/t = 40 specimens. For such small cylinders the end conditions have a considerable influence on the stresses and a large difference in the buckling loads between the finite element study and experiments is not surprising. This is supported by the fact that the difference becomes smaller as the length is increased. It is not possible to simulate the end conditions exactly in the finite element program.

It should also be noted that the program assumes that the material is perfect and the loads are not eccentrically applied. Differences could also arise from the choice of parameters that affect the displacement solution. The following parameters are considered to belong to this class:

1. Size of loadstep (NSTEP)
2. Convergence criterion (CONV)
3. Choice of the stability index (ISTAB)
4. Stability criterion (STAB2)
5. Mesh size
6. Size of displacement vector, [ΔU], in displacement control

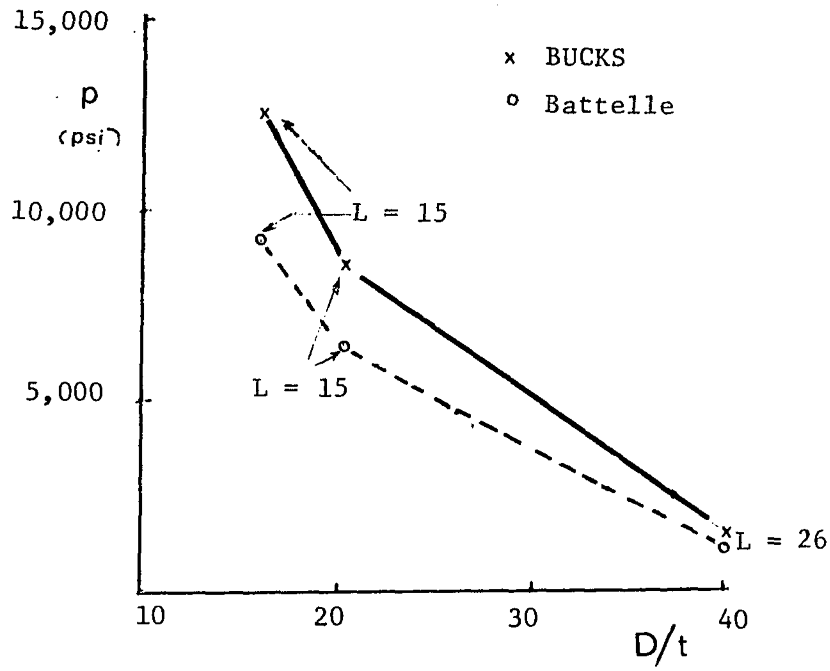

Figure 53 Comparison of critical pressures to Battelle's study [43].

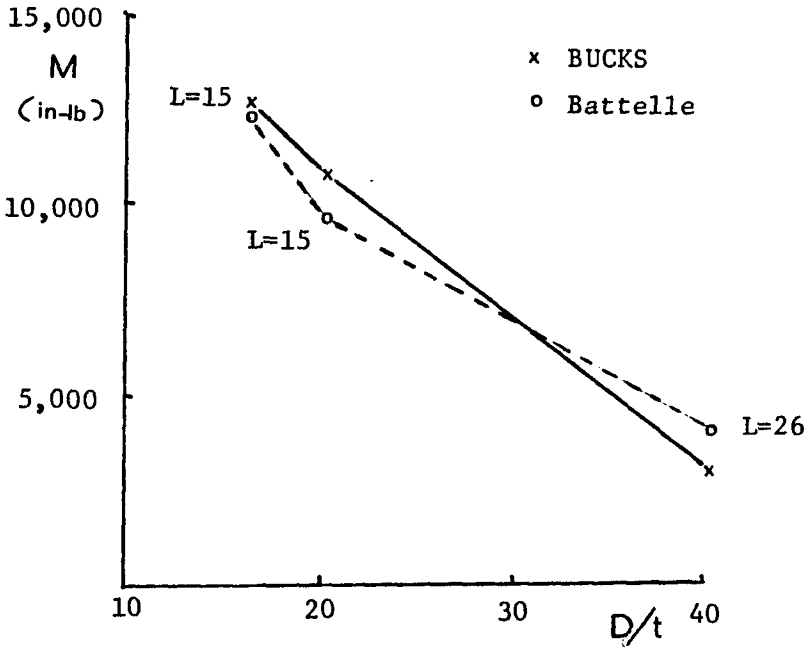

Figure 54 Comparison of critical moments to Battelle's study [43].

The results for pure moments are compared in Figure 54. The agreement is better than for pure pressure. The results for combined loads are compared in Figure 55.

It was seen that the order of loading influences the buckling loads significantly. This difference is much greater at the high moment-low pressure region than at the low moment-high pressure region. Thus, if the bending moments are small, the order of loading does not change the buckling load significantly. Also, it was observed that if external pressure is applied first, the moment carrying capacity of cylinders is reduced sharply from the value obtained if both loads increased proportionally or if moment was applied first. There was also a difference in the way the stiffness reduced in the two cases. If moment was applied first followed by pressure, the stiffness reduced gradually as ovalization increased until a limit point was reached. If the pressure was applied first, the stiffness reduced sharply as bending moment was applied. The extent of ovalization was small and the pipe collapsed suddenly without developing its full moment.

Finally, the stiffness of softening parameters were compared. From the plots of ST2 and ST3 included in this chapter it can be seen that either one could be used as a reliable indicator of stiffness. However, it is far simpler to calculate ST3 than it is to calculate ST2. In the case of nonproportional loading, the calculation of ST3 requires storage of additional arrays used in the matrix multiplication given in Chapter V. For these reasons, ST3 was found to be the simplest and reliable measure when the buckling mode is

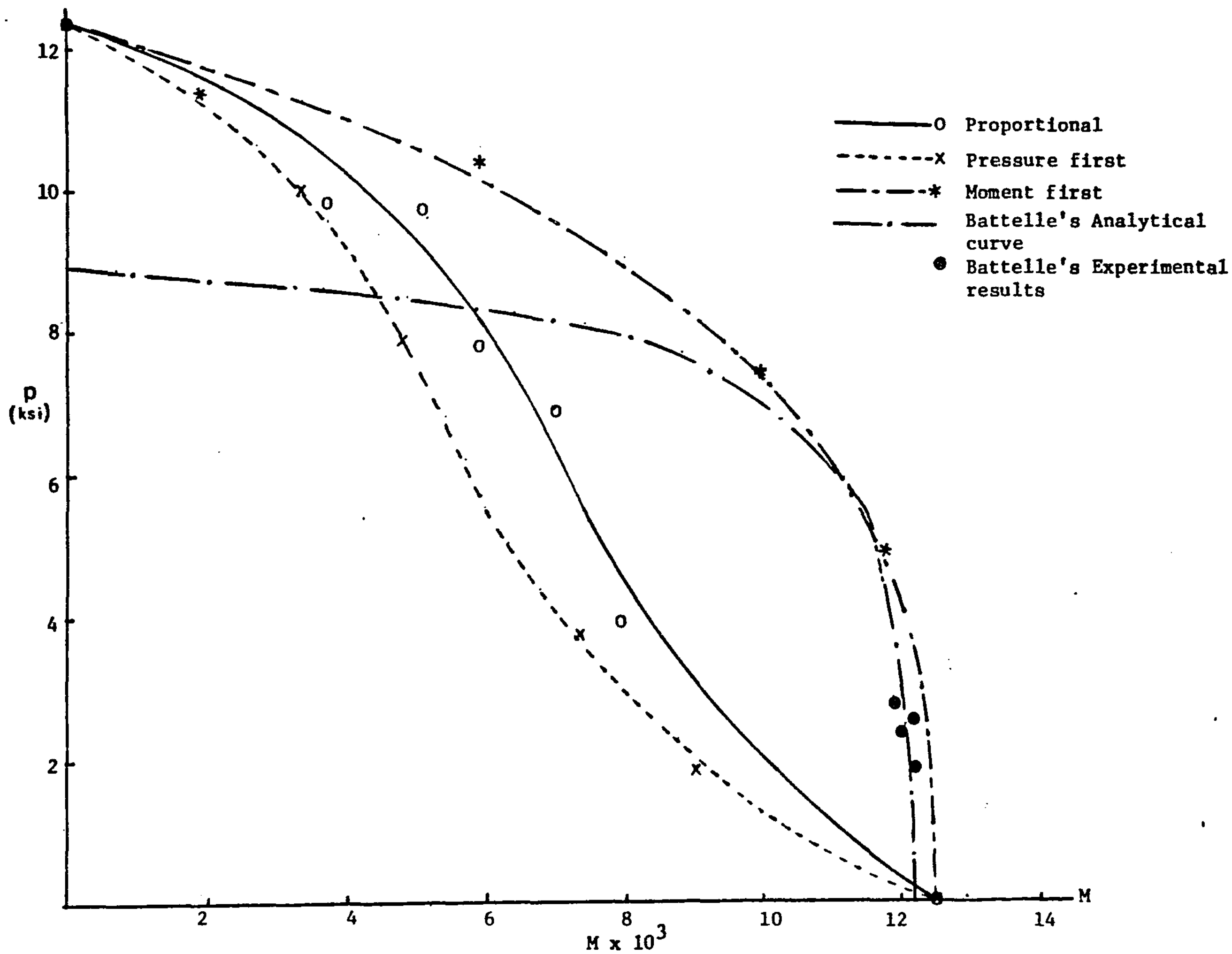

Figure 55 Comparison of failure curves.

unknown. However, neither ST2 nor ST3 give any indication of the buckling mode.

The performance of ST1 was poor; it did not reduce appreciably (minimum values were around 0.88) even just before limit points. Thus, if this measure were to be used as the basis for the decisions in the solution algorithm, numerical instability would be encountered.

Table 18 Comparison of Stiffness Indices

	Bending	Pressure	BM+P**	BM,P+	P, BM++
STOVL	0.17	0.0*	1.4	7.7	61.8
STBRAZ	4.8	0.	0.8	5.8	0.01
STBND	0.1	$.29\times10^{-4}$	.67	.19	.02
STBNDA	0.02	$.03\times10^{-6}$	.006	.02	.004
STEULR	0.1	$.11\times10^{-4}$	.003	.07	.02

* reset to 1 when below a minimum

** proportional ratio 1:2

\+ moment applied first

++ pressure applied first

Table 18 compares the mode dependent stiffness indicators, STOVL and STBND, along with the absolute measures of displacements. For proportional loads STOVL and STBND lie between 1 and 0. For pure bending it can be seen that STOVL and STBND could have been used as the critical indices with STAB2 = 0.2. However, one must be careful in using these measures. For example, in the case of pure pressure

STBND $\approx$ 0 would imply that failure takes place by bending. But when one looks at the absolute measures STBNDA and STEULR, it is seen that there is practically no bending. Therefore, STBNDA must be used in conjunction with STBNDA or STEULR.

For the case of proportional loading, one sees that ovalization has reached 80% of the Brazier value but the bending index STBND is still 0.67 and the absolute bending deflections are small. The structure will most likely fail by ovalization. This was also the case with moment applied first. But when pressure was applied first, STBRAZ reached a value of 0.01 only, even though STOVL is 61.8. This is because under pressure the ovalization is small and all subsequent steps compare deformations to the first step. Since STOVL and STBRAZ are used together, this does not present a problem. In the case of pressure applied first the pipe fails before considerable ovalization. Hence, the reduction in load carrying capacity.

More experience is needed with this program in order to establish numerical basis for predicting failure mode via these indices.

Research Contributions

The following are considered to be the major contributions of this study:

1. Prediction of buckling loads for cylinders under nonproportional and nonlinear loading.
2. Prediction of buckling modes via deformation based stiffness parameters.
3. Dependence of buckling loads and modes on the order of loading.
4. Extension of the Bathe shell element [71] to cylinderical degenerated shells undergoing elastic-plastic deformation.

Appendix A

Model Creation for BUCKS

Models can be created interactively using the special purpose mesh generation program "PREP". The advantage of using this program over general purpose packages, such as SUPERTAB, are as follows: (a) PREP can be run on any alphanumeric terminal (b) it takes only a couple of minutes of logon time to input, generate, and write model geometry compared to about 15 to 20 minutes for accessing and running SUPERTAB (c) the output file of PREP is compatible with BUCKS data input.

Only cylindrical shell mesh can be generated with PREP but the mesh can be varied as desired by the user. Using multiplying factors, the mesh can be finer in any direction. The user need only input the diameter thickness, length (or half length) of the cylinder and specify the number of elements along the circumference and length (or half length). If the multiplying factor is unity then all elements will be of equal length. The length of elements may be increased in going from one end of the cylinder to the other by using a multiplying factor greater than one and reduced by using a factor lower than one. This is shown in Figs. 56 and 57 respectively. If it is desired to change the element size in both directions from the center, as shown in Fig. 58, only half-length mesh should be generated and the model reflected.

DO YOU WANT TO ZOOM (Y/N)?

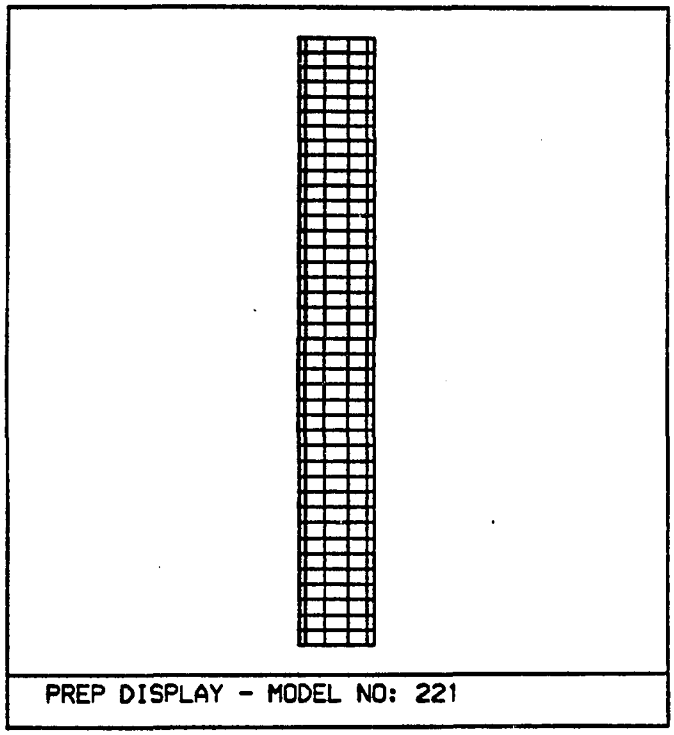

Figure 56 Front view of model generated with multiplying factor equal to unity.

DO YOU WANT TO ZOOM (Y/N)?

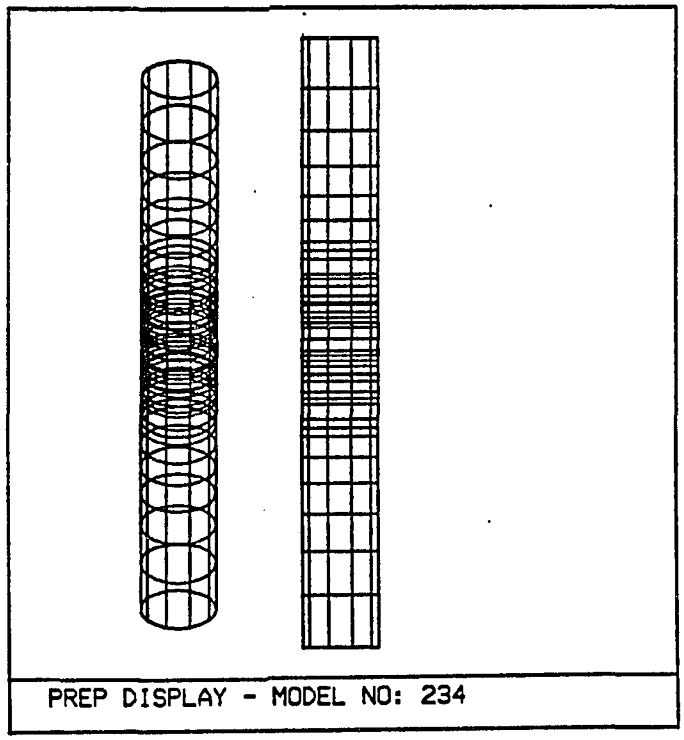

Figure 57 Symmetric increase of mesh size by reflection about center plane.* (Multiplying factor = 1.2)

* the rotated view has been superimposed.

DO YOU WANT TO ZOOM (Y/N)?

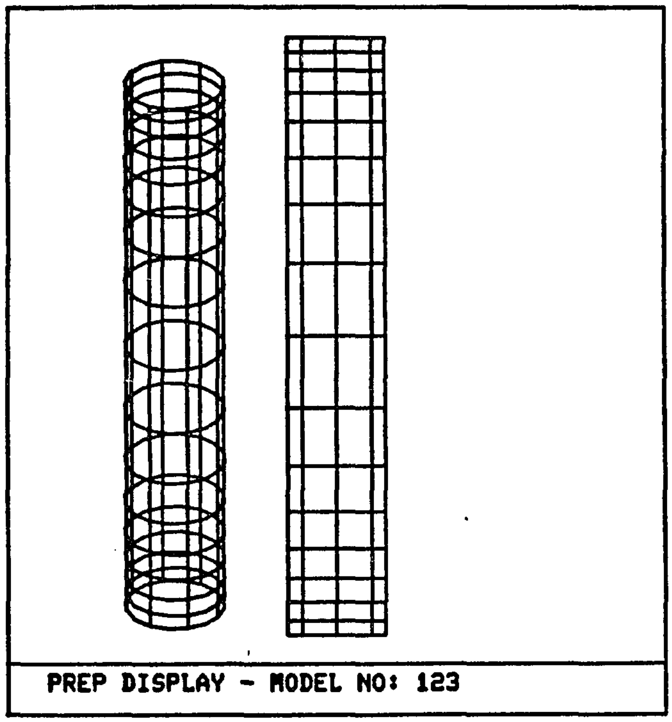

Figure 58 Symmetric reduction of mesh size by reflection about the center plane*. (Multiplying factor = 0.8)

* the rotated view has been superimposed.

The program outputs a named data file; the first line is the same as the second line given in Appendix B. It then outputs the coordinates of the nodes generated and element connectivities.

The generated mesh can be checked using the program "DSPLAY". This is not an essential part of model creation. It requires a graphics terminal compatible with TEKTRONIX graphics package PLOT10. Data is read from file named FOR001.DAT.

After the data has been read in, the program offers the user a menu of various viewing options. These include: rotation of the model about the three axes at any angle specified by the user; magnifying any given area of the model whose diagonal points are specified using the graphics cursor; displaying node numbers; displaying front and end views.

```
DO YOU WANT TO ZOOM AGAIN ? N
DO YOU WANT NODE NUMBERS (Y/N) ?Y
INPUT NODE START, END, INC. 1,10,1
NEED MORE NODES (Y/N)? Y
INPUT NODE START, END, INC. 11,20,1
NEED MORE NODES (Y/N)? Y
INPUT NODE START, END, INC. 21,30,1
NEED MORE NODES (Y/N)?
```

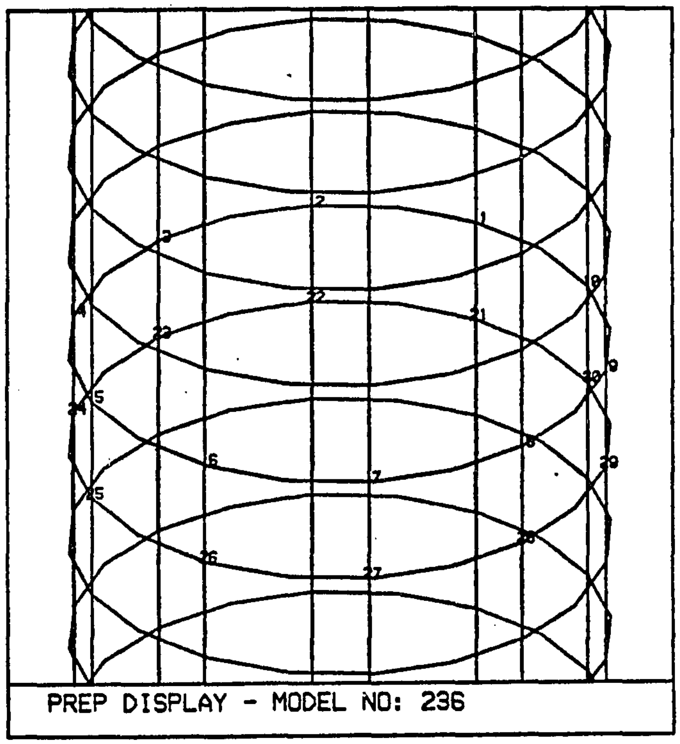

Figure 59 Viewing options offered by program DSPLAY.

Appendix B

Input File Format

The first line must be the debug code (explained later), followed by the cylinder mesh parameters, nodal coordinates and element connectivity, in that order. With the exception of the first line, these can be inserted directly from the output file of program PREP. After element connectivities, the data may appear in any order, as long as it is preceded by the proper header card. The 'ORDER OF LOADING' card must be placed before any load cards. All alphanumeric input must be left justified, all integers must be right justified, and all real neumonics can appear anywhere in their respective fields. The following pages describe the types of input, the options, and the required format.

Debug Code

Cols.	1–5	6–10	11–15	16–20	21–25	26–30	31–35
	DBG						

1. DBG = Debug Code for printing intermediate arrays (Format: A15)

   If not required leave the first line blank

   DBG can be any combination of the following alphanumeric characters which will print the respective arrays to the DBG file

   BO = Linear strain-displacement matrices BLO

   BL1 = Linear strain-displacement matrices BL1

   BL = Total linear strain-displacement matrices

   BNL = Nonlinear strain-displacement matrices

   STR = Stress matrix [SM] from SHELL1

   VEC = Vectors, V1, V2, V3, from VECTOR

   JAC = Jacobian matrix from JACOB

   SRN = Green-Lagrange strains from STRES1

   TCB = Matrices $[B_L]^T[C][B_L]$ and $[B_{NL}]^T[SM][B_{NL}]$

   LVC = Load vectors from DRIVER

   ASM = Assembled system matrix for each element

   SYS = System stiffness matrix [SK]

   EQN = System equations from EQSOLV

   DSB = Incremental displacement

TOT = Total displacements at end of iteration

SKY = Stiffness matrix Skyline

Cylinder Mesh Data

	NN	NE	NNOD	NDOF	RAD		XL		NL	NC
Cols.	1–5	6–10	11–15	16–20	21–25	26–30	31–35	36–40	41–45	46–50

1. NN = number of nodes (I5)*
2. NE = number of elements (I5)
3. NNOD = number of nodes per element (I5)
4. NDOF = number of degrees of freedom per node (I5)
5. RAD = radius of cylinder at midplane (F10)
6. XL = length of cylinder (F10)
7. NL = number of element along length (I5)
8. NC = number of elements along circumference (I5)

Nodal Coordinates

These are inserted directly by the preprocessor

Element Connectivity

Also inserted by the preprocessor

---

* numbers in parentheses give format

After this point, data may be input in any order. Any number of comments may be placed by putting a '#' in the first column

Case Title

	TITLE
	TIT
Cols.	1-60

In all the following cards, the first line gives the header, 'TITLE' in this case, followed by the corresponding data.

1. TIT = Case Title (A60)

Analysis Codes

ANALYSIS						
RATIO		D		IFK	IANY	ISTR
Cols. 1–5	6–10	11–15	16–20	21–25	26–30	31–35

1. RATIO = Maximum allowable ratio of incremental displacement to total displacements (F10)

2. D = Code for calculating stiffness index ST1 (F10)

   D = 0 ST1 not calculated

   D $\neq$ 0 ST1 is calculated

3. IFK = Force code (I5)

   IFK = 1 Spurious loads set to zero

   IFK $\neq$ 1 Spurious loads not set to zero

4. IANY = Element type (I5)

   IANY = 1 Continuum elements

   IANY = 2 Degenerated elements

5. ISTR = Stress code (I5)

   ISTR = 0 Use P/K stresses for yield criteria

   ISTR = 1 Use Cauchy stresses for yield criteria

Run Parameters

	MODEL						
	MOD	NSTEP	CONV		ITRMAX		
Cols.	1–5	6–10	11–15	16–20	21–25	26–30	31–35

1. MOD = Model number (I5)

2. NSTEP = Number of loadsteps to be used in incremental solution (I5)

3. CONV = Convergence criterion (F10)

4. ITRMAX = Maximum number of iterations per loadstep (I5)

Stability Parameters

STABILITY							
	STAB1		STAB2		NCRIT2	ISTAB	
Cols.	1–5	6–10	11–15	16–20	21–25	26–30	31–35

1. STAB1 = Linearity criterion (F10)

2. STAB2 = Stability criterion (F10)

3. NCRIT2 = Loadstep in which perterbation is to be caused (I5)

4. ISTAB = Select code for critical stiffness parameter (I5)

   ISTAB = 1 Select ST1

   ISTAB = 2 Select ST2

   ISTAB = 3 Select ST3

   ISTAB = 4 Select STOVL

   ISTAB = 5 Select STBND

   ISTAB = 6 Select STEVLR

   ISTAB = 7 Select STBNDA

   ISTAB = 8 Select STBRAZ

Note: STAB1 and STAB2 must be geared to ISTAB

Order of Loading

ORDER OF LOADING						
IOL						
Cols. 1–5	6–10	11–15	16–20	21–25	26–30	31–35

Continuation cards (optional)

IS	PINM(IS)		PINUC(IS)		PINUL(IS)	
Cols. 1–5	6–10	11–15	16–20	21–25	26–30	31–35

PINP(IS)					
Cols. 36–40	41–45	46–50	51–55	56–60	61–65

The order of Loading card must precede all load cards i.e. LOADS, PRESSURE, MOMENT, UDLC, and UDLC. The first card is required. Continuation cards are required only if IOL = 2; the number of continuation cards must be equal to NSTEP specified with the MODEL data.

Card 1

1. IOL = Order of loading code (I5)

   IOL = 1 proportional, linear loads

   IOL = 2 nonproportional/nonlinear loads

Continuation Cards

1. IS = Load step number (starts at 1 and ends at NSTEP); Format (I5)
2. PINM (IS) = Ratio of bending moment in step IS to reference load specified on MOMENT cards (F10)

3. PINUC (IS) = Ratio of uniformly distributed axial load to the reference load specified by UDLC cards (F10)

4. PINUL (IS) = Ratio of uniformly distributed lateral loads to reference loads specified by UDLL cards (F10)

5. PINP (IS) = Ratio of external/internal pressure in step IS to reference load specified by PRESSURE cards (F10)

External/Internal Pressure

PRESSURE									
IEL	IEN	INC	IP1	IP2	PRES			RKL	RKM
1–5	6–10	11–15	16–20	21–25	26–30	31–35	36–40	41–45	46–50

Cols. (bottom row)

1. IEL = Element start (I5)
2. IEN = Element end (I5)
3. INC = Increment from IEL to IEN
4. IP1 = Resultant load code (required for IP2=1 or 2); (I5)

   IP1 = use arc length

   IP2 = use chord length
5. IP2 = Code for calculating equivalent loads (I5)

   IP2 = 1 consistent loads based on flat rectangular elements

   IP2 = 2 equal loads on element basis

   IP2 = 3 equal loads on global basis

   IP2 = 4 user input ratios RKL and RKM for calculating equivalent loads

   IP2 = 5 consistent loads for curved elements
6. PRES = Value of element pressure; should be positive for external pressure and negative for internal pressure
7. RKL = Ratio of lengthwise midnode load to corner node load
8. RKM = Ratio of circumferential midnode load to corner node load

Uniformly Distributed Axial Load

Cols.	1–5	6–10	11–15	16–20	21–25	26–30	31–35	36–40	41–45	46–50
	UDLC									
	UD		IDR1	ICS1	ICE1	IC1	IMS1	TME1	IM1	

1. UD = Value of distributed load per unit length of circumference (F10)
2. IDR1 = Direction of load (I5)
3. ICS1 = Corner node start number (I5)
4. ICE1 = Corner node end number (I5)
5. IC1 = Corner node increment (I5)
6. IMS1 = Midnode start number (I5)
7. IME1 = Midnode end number (I5)
8. IM1 = Midnode increment (I5)

Uniformly Distributed Lateral Load

	UDLL									
		UW	IDR1	ICS2	ICE2	IC2	IMS2	IME2	IM2	
Cols.	1–5	6–10	11–15	16–20	21–25	26–30	31–35	36–40	41–45	46–50

1. UW = Value of lateral distributed load per unit length (F10)
2. IDR2 = Direction of load (I5)
3. ICS2 = Corner node start number (I5)
4. ICE2 = Corner node end number (I5)
5. IC2 = Corner node increment (I5)
6. IMS2 = Midnode start number (I5)
7. IME2 = Midnode end number (I5)
8. IM2 = Midnode increment (I5)

Constant Bending Moment

	MOMENT						
	BMOM			M1			
Cols.	1–5	6–10	11–15	16–20	21–25	26–30	31–35

1. BMOM = Value of the constant bending moment (F15)
2. M1 = Corner node (one of four) on which equivalent load is applied to create constant bending moment condition

Concentrated Loads

LOADS						
NODE	IEND	INC	IDIR		FORCE	
Cols. 1–5	6–10	11–15	16–20	21–25	26–30	31–35

1. NODE = Starting label of node group loaded (I5)
2. IEND = End label of node group loaded (I5)
3. INC = Node increment between NODE and IEND
4. IDIR = Direction of concentrated force or moment (from 1 to 5 corresponding to degrees of freedom); (I5)
5. FORCE = Value of concentrated load (F15)

Restraints

RESTRAINTS						
NODE	IEND	INC	IRST			
Cols. 1–5	6–10	11–15	16–20	21–25	26–30	31–35

1. NODE = Starting label of node group restrained (I5)
2. IEND = End label of node group restrained (I5)
3. INC = Node number increment between NODE and IEND (I5)
4. IRST = Restraint code (A5); any combination of the following

   1 - restrained in x-direction

   2 - restrained in y-direction

   3 - restrained in z-direction

   4 - rotation α restrained

   5 - rotation β restrained

Numerical Integration

	SHELL						
	INT1	INT2					
Cols.	1–5	6–10	11–15	16–20	21–25	26–30	31–35

1. INT1 = Order of integration in shell plane (I5)

2. INT2 = Order of integration in thickness direction (I5)

3. A = Shell thickness (assumed constant), (F10)

Output Options

	OUTPUT						
	IKOD						
Cols.	1–5	6–10	11–15	16–20	21–25	26–30	31–35

1. IKOD = Output code (I5)

   IKOD = 0 output final displacements to RST file

   IKOD = 1 output P/K stress in each iteration and final Cauchy stresses to RST file, and final displacements

   IKOD = 2 output final Cauchy stresses and final displacements

Note: The average stresses and the load vector obtained after displacement control are output regardless of IKOD value.

Material Properties

ELASTIC							
	EY		POIS				
Cols.	1–5	6–10	11–15	16–20	21–25	26–30	31–35

PLASTIC							
	NCRIT	IH	AP		BP		SY
Cols.	1–5	6–10	11–15	16–20	21–25	26–30	31–35

		ET				
Cols.	36–40	41–45	46–50	51–55	56–60	61–65

Elastic Properties (required)

1. EY = Young's modulus (F10)
2. POIS = Poisson's ratio (F5)

Plastic Properties (value of NCRIT is required if elastic analysis is done only)

1. NCRIT = Critical load step below which yield condition is not checked (I5)
2. IH = Hardening model used (I5)

   IH = 1 Bilinear model

   IH = 2 Exponential model

   IH = 3 Ramberg-Osgood model
3. AP = Hardening coefficient for IH = 2 or 3 (F10)
4. BP = Hardening exponent for IH = 2 or 3 (F10)
5. SY = Yield stress (F10)
6. ET = Tangent modulus for IH = 1 (F10)

Appendix C

List of Subroutines and Functions

1. BUCKS8$MAIN

   Main program serves the purpose of variable dimensioning only

2. DRIVER

   Controls the running of the entire program: input, computation, and output

3. INPUT

   Reads model geometry from input file and echoes input data

4. LOADIN

   Reads loads, pressures, restraints, material properties, etc. which are input in random order in the input file

5. BEGIN

   Initializes force, pressure, and restraint vectors

6. PRESUR

   Calculates equivalent nodal loads from element pressures: based on rectangular flat elements

7. PRSUR2

   Calculates equivalent nodal loads from element pressures for curved elements; consistent loads

8. SHELL1

   Calculates stiffness matrix and load vectors for degenerated and continuum, nonlinear parabolic shell elements

9. SHSTRS

   Initializes Piola-Kirchhoff stress matrices at Gauss points

10. INIT

    Calculates initial value of shell normal vectors and initializes displacements

11. ELAST

    Calculates the constitutive matrix for a linear-elastic, isotropic material (continuum)

12. ELAST2

    Calculates constitutive matrix for shells; must be used in conjunction with 'DEGEN'

13. PLAST

    Calculates the constitutive matrix of an isotropic, linear work-hardening material

14. PLAST2

    Calculates constitutive matrix for elastic-plastic shells (used with DEGEN)

15. VMISES

    Determines which constitutive matrix to use by testing for yielding

16. VECTOR

    Updates normal V3 vector and calculates reference vectors V1 and V2 for measuring shell rotations

17. ASSEM

    Assembles system matrix

18. ELEM1

    For each Gauss point of each element, it calculates the linear and nonlinear strain-displacement matrices

19. JACOB

    Calculates the Jacobian matrix, its determinant and inverse

20. SHAPE

Calculates shape functions and their derivatives for parabolic shell elements

21. STRES1

Updates the Piola-Kirchhoff stresses at Gauss points

22. CAUCHY

Transforms the Piola-Kirchhoff stresses to Cauchy stresss

23. NEWTON

Newton-Raphson scheme for solving nonlinear equations

24. EQSOL2

Active column skyline method for solving linear equations (reduced storage reqd; improved version of EQSOLV)

25. SKYLIN

Calculates the skyline of stiffness matrix

26. UPDATE

Updates coodinates and displacements in total Lagrangian system

27. NULOAD

Calculates the current load in each load step

28. OUTPUT

Outputs results of BUCKS (displacements and Cauchy stresses) in the last iteration

29. STROUT

Outputs P/K stresses (optional - used only when debugging the program)

30. RSTRNT

Interprets restraint code and removes equations corresponding to the restrained degrees of freedom

31. RSTRN2

Removes elements in load vector alone; used in quasi Newton scheme when stiffness is not updated

32. SHUFL

Recovers full displacement vectors by re-inserting equations removed by RSTRNT

33. CONVRT

Extracts a smaller square matrix from a larger one

34. BUCKLE

Detects the onset of buckling limit points using 'stiffness ratios'

35. DEGEN

Degenerates the constitutve matrix by applying Kirchhoff assumptions of shell theory

36. ERRBAC

Outputs error messages

37. MULTIP

Multiplies two matrices

38. TRPMUL

Multiplies the transpose of a matrix by the second matrix

39. ADD

Adds two matrices

40. ADD2

Adds two matrices and stores result in the first matrix

41. MATRIX

Calculates the determinant and inverse of a 3 x 3 matrix

42. TRANSP

Finds the transpose of a square matrix of arbitrary size

43. FORCE3

When convergence is achieved in a load step the load vector increment is set to zero

44. AVGSTR

Calculates average element stresses

45. CAUCH2

Transforms Kirchhoff stresses to Cauchy stress called from SHELL1, more specific than Cauchy

46. UNPROP

Calculates new loads for non-proportional, nonlinear loads

47. UDLL

Calculates equivalent nodal loads for uniformly distributed lateral loads

48. UDLC

Calculates equivalent nodal loads for uniformly distributed axial loads

49. MOMENT

Calculates equivalent nodal loads for constant bending moment condition

50. FORCE2

Sets spurious stresses to zero

51. OVAL

Calculates amount of ovalization and softening based on ovalization buckling

52. BEND

Calculates softening based on Euler buckling mode

53. XNORM

Calculates the root mean square norm of given vector

54. XNORM2

Calculates the sum of an array

55. SMAX

Calculates the maximum in a one-dimensional array

LIST OF REFERENCES

1. Timoshenko and Goodier, "Theory of Elasticity," McGraw-Hill Book Co., Second Edition, 1951.

2. Timoshenko and Gere, "Theory of Elastic Stability," McGraw-Hill Book Co., Second Edition, 1961.

3. Brush, D.O. and Almroth, B.O., "Buckling of Bars, Plates, and Shells," McGraw-Hill Book Co., 1975.

4. Bleich, F., "Buckling Strength of Metal Structures," McGraw-Hill Book Co., 1952.

5. Budiansky, B., "Theory of Buckling and Post-Buckling Behaviour of Elastic Structures," Advances in Appl. Mech., Vol. 14.

6. Hutchinson, J.W., "Plastic Buckling", U.S. Air Force Technical Report No. AFOSR-TR-73-2083, July, 1973.

7. Popelar, C.H., "Inelastic Collapse and Buckling of Long Cylindrical Shells," Final Report to Battelle Columbus Laboratories, June 1975.

8. Brazier, L.G., "On the Flexure of Thin Cylindrical Shells and Other Thin Sections," Proceedings of the Royal Soc., Series A, V116, 1927.

9. Almroth, B.O. and Starnes, J.H., "The Computer in Shell Stability Analysis," J. of Eng. Mech. Div., Dec. 1975, pp. 873-888.

10. Flugge, W., "Stresses in Shell," Springer-Verlag, Berlin, 1962.

11. Croll, J.L.A., "Elastic-Plastic Buckling of Pressure and Axial Loaded Cylinders," Proceedings of Inst. of Civil Engineers, Part 2, Sept. 1982, pp. 633-652.

12. Weiner, P.D. and Smith, S.A., "Maximum Moment Capability of Pipe with Various D/T Ratios," J. of Eng. for Industry, Aug. 1976, pp. 1107-1111.

13. Lee, L.H., "Inelastic Buckling of Initially Imperfect Cylindrical Shells Subject to Axial Compression," J. Aero Sci., V29, pp. 87-95, 1962.

14. Shanley, F.R., "Inelastic Column Theory," J. of Aero. Sciences, Vol. 14, no. 5, May 1947.

15. Reddy, B.D., "Plastic Buckling of a Cylindrical Shell in Pure Bending," Int. J. of Mechanical Sciences, Vol. 21, No. 11, 1979, pp. 671-680.

16. Korol, R.M., "Critical Buckling Strains of Round Tubes in Flexure," Int. J. of Mechanical Sciences, Vol. 21, No. 12, 1979, pp. 719-730.

17. Sobel, L.H. and Newman, S.Z., "Plastic Buckling of Cylindrical Shells Under Axial Compression," J. of Pressure Vessel Tech., Vol. 102, p. 40, Feb. 1980.

18. Donnel, L.H., "Beams, Plates, and Shells," McGraw-Hill, Inc., 1976.

19. Tamano, T., et al, "A New Empirical Formula for Collapse Resistance of Commercial Casings," Offshore Tech./Arctic Eng. Conf., Houston, Texas, Jan. 1982.

20. Bernitas, M.M. and Kokkins, T., "Buckling of Risers in Tension Due to Internal Pressure: Nonmovable Boundaries," Offshore Tech/ Arctic Eng. Conf., Houston, Texas, Jan. 1982.

21. Szymczak, C., "Buckling and Initial Post-Buckling Behavior of Thin-Walled I Columns," Computers and Structures, Vol. 11, pp. 481-487, 1980.

22. Sobel, L.H. and Newman, S.Z., "Plastic Buckling of Cylindrical Shells Under Axial Compression," J. of Pressure Vessel Tech., Vol. 102, Feb. 1980, pp. 40-48.

23. Malik, Z., Morton, J., and Ruiz, C., "Buckling Under Normal Pressure of Cylindrical Shells with Various End Conditions," J. of Pressure Vessel Technology, Vol. 102, Feb. 1980, pp. 107-111.

24. Shanely, F.R., "The Column Paradox," J. of Aeronautical Sciences, Vol. 13, No. 12, Dec. 1946.

25. von Karman, T., "Untersuchungen uber Knic festigkiet," Mitt. U. Forschungsarb, Heft 81, Berlin 1909.

26. Gerard, G., "Compressive and Torsional Buckling of Thin-Walled Cylinders in Yield Region," NACA TN-3726, Aug. 1956.

27. Batterman, S.C., "Plastic Buckling of Axially Compressed Cylindrical Shells," AIAA Journal, Vol. 3, No. 2, Feb. 1965.

28. Bynum, D., "Buckling Considerations for Subsea Pipeline Design," Ocean Resources Engg., April 1977.

29. Tvergaard, V., "Buckling of Elastic-Plastic Oval Cylindrical Shells Under Axial Compression," Int. J. of Solids and Structures, Vol. 12, 1976.

30. Wilhout, J.C. and Merwin, J.E., "Critical Plastic Buckling Parameters for Tubing in Bending Under Axial Tension", Fifth Offshore Tech. Conference, Houston, Texas, April 1973.

31. Small, N.C., "Plastic Collapse of Oval Straight Tubes Under External Pressure," ASME Energy Tech. Conf., Houston, Sept. 1977.

32. Tugcu, P. and Schroeder, J., "Plastic Deformation and Stability of Pipes Exposed to External Pipes."

33. Ades, C.S., "Bending Strength of Tubing in the Plastic Range," J. of Aero. Sci., Aug. 1957.

34. Schilling, C.G., "Buckling Strength of Circular Tubes," J. of Struc. Div., Proc., of ASCE," Oct. 1965.

35. Budiansky, B. and Hutchinson, J.W., "Buckling: Progress and Challenge", Proceedings of the Symposium dedicated to the 65th Birthday of Koiter, June 1979. Report entitled "Trends in Solid Mechanics 1979", ed. Bessling and Heijdan.

36. Krysko, V.A. and Kolomoets, A.A., "Stability of Local Loading of a Cylindrical Shell," Soviet Applied Mechanics, Vol. 17, No. 10, Oct. 1981.

37. Ramsey, H., "Localized Plastic Buckling Deformation in Axially Compressed Cylindrical Shells," J. of Engineering Mathematics, Vol. 47, Sept. 1980.

38. Tvergaard, V. and Needleman, A., "On the Localization of Buckling Patterns," J. of Applied Mech., Trans. ASME, Vol. 47, Sept. 1980.

39. Ramsey, H., "Buckling Deformation in Axially Compressed Elastic-Plastic Cylinderical Shells Initiated by Local Axisymmetric Imperfections," J. of Engg. Math., Vol. 15, No. 3, July 1981.

40. Row, D.G., et al, "Local Buckling Analysis of Pipelines," Int. Offshore Mechanics/Arctic Engg. Symposium, Jan. 1982, Houston.

41. Kyriakides, S., Babcock, C.D. and Elyada, D., "Initiation of Propagating Buckles from Local Pipeline Damages," Int. Offshore Mech./Arctic Engg. Symposium, Jan. 1982, Houston.

42. Mesloh, R. et.al., "The Propagating Buckle," BOSS 76, (Proc. Int. Conf. on Behaviour of Offshore Structures), Norwegian Inst. of Tech., 1976.

43. Kinzel, G.L., et. al., "The Inelastic Collapse and Buckling of Deep Water Pipelines under Combined Moment, Pressure and Axial Tension," Research Report to the Deep Water Offshore Pipeline Group, Battelle Columbus Labs, Mar. 1976.

44. Mesloh, R.E., Sorenson, J.E., and Atterbury, T.J., "Buckling - and Offshore Pipelines," The Gas Magazine, July, 1973.

45. Johns, T.G. and Tamm, M.A., "Local Buckling of Cylinderical Columns Under Combined Loads," Offshore Tech. Conf. Houston, May 1977.

46. Bathe, K.J., "Finite Element Procedures in Engineering Analysis," Prentice-Hall, Inc., New Jersey, 1982.

47. Zienkiewicz, O.C., "The Finite Element Method," McGraw-Hill.

48. Norrie, D.H. and DeVries, G., "An Introduction to Finite Element Method," Academic Press, Inc., New York, 1978.

49. Bathe, K.J. and Wilson, E.L., "Numerical Methods in Finite Element Analaysis," Prentice-Hall, Inc., New Jersey, 1976.

50. Segerlind, L.J., "Applied Finite Element Analysis," J. Wiley and Sons, Inc., New York, 1976.

51. Besseling, J.F., "Finite Element Methods," Proc. of the Symp. on 'Trends in Solid Mechanics 1979', editors Besseling, J.F. and Van der Heijden, June, 1979.

52. Weinstock, R., "Calculus of Variations," Dover Pub., New York.

53. Lipschutz, S., "Linear Algebra," McGraw-Hill, Schaum Series.

54. Stricklin, J.A., et. al., "Formulation, Computation, and Solution Procedures for Material and/or Geometric Nonlinear Structural Analysis by the Finite Element Method," Sandia Lab., Contract Report SC-CR-72-3102, July 1972.

55. Gerald, C.E., "Numerical Analysis," Addison-Wesley.

56. Synge and Schild, "Tensor Calculus," Dover Publ., Inc., New York.

57. Kasar, T., "Finite Element Formulation for Inelastic Equilibrium and Buckling of Thin-Walled Structural Systems," Ph.D. Dissertation, U. of Minnesota 1975.

58. Glancy, J., "Determination of the Lowest Critical Buckling Stress of Various Shaped Plates by Finite Elements," Ph.D. Dissertation Arizona State Univ., 1973.

59. Akkoush, E.A., et.al., "Bifurcation, Pre-and Post-Buckling Analysis of Frame Structures," J. of Computers and Structures, Vol. 8, pp. 667-678.

60. Brendl, B. and Ramm, E., "Linear and Nonlinear Stability Analysis of Cylinderical Shells," J. of Computers and Structures, Vol. 12, pp. 549-558.

61. Maier, G. and Andreuzz, F., "Elastic and Elasto-Plastic Analysis of Submarine Pipelines as Unilateral Contact Problems," J. of Computers and Structures, Vol. 8, pp. 421-431.

62. Noor, A.K. and Peters, J.M., "Bifurcation and Post-Buckling Analysis of Laminated Composite Plates via Reduced Basis Technique," ASME Applied Mech. Div. Conference, 'New Concepts in F.E. Analysis,' Boulder, Colorado, June 1981.

63. Gallagher, R.H., "Geometrically Nonlinear Shell Analysis," Proc. of Int. Conf. on Finite Elements in Nonlinear Mech., Geilo, Norway, Aug. 1977.

64. Kraikeland, B., "Nonlinear Analysis of Shells Using Degenerate Isoparametric Elements," Proc. of Int. Conf. on Finite Elements in Nonlinear Mech., Geilo, Norway, Aug, 1977.

65. Frey, F. and Cesscotto, S., "Some New Aspects of the Incremental Total Lagrangian Description in Nonlinear Analysis," Proc. of Conf. on Finite Elements in Nonlinear Mechanics, Geilo, Norway, Aug. 1977.

66. Mau, S.T. and Gallagher, R.H., "A Finite Element Procedure for Nonlinear Prebuckling and Initial Postbuckling Analysis," NASA Contractor Report CR-1936, Jan. 1972.

67. Mendelson, A., "Plasticity: Theory and Applications," Macmillan Co., New York, 1968.

68. Mroz, Z., "Mathematical Models of Inelastic Material Behaviour," U. of Waterloo, Canada, 1973.

69. Budiansky, B., "A Reassessment of Deformation Theories of Plasticity," J. of Appl. Mech., June 1959.

70. Anand, S.C. and Shaw, R.H., "Mesh Refinement and Substructuring Techniques in Elastic-Plastic Finite Element Analysis," J. of Computers and Structures, Vol. 11, pp. 13-21.

71. Bathe, K.J. and Bolourchi, S., "A Geometric and Material Nonlinear Plate and Shell Element," J. of Comp. and Struc., Vol. 11, pp. 23-48.

72. Bergan, P.G., et.al., "Solution Techniques for Nonlinear Finite Element Problems," Int. J. for Numerical Methods in Engg., Vol. 12, 1978.

73. Horrigmoe, G., "Hybrid Stress Finite Element Model for Nonlinear Shell Problems," Int. J. for Num. Meth. in Engg., Vol. 12, 1978.

74. Yamada, Y., "Constitutive Modeling of Inelastic Behaviour and Numerical Solution of Nonlinear Problems by the Finite Element Method," J. of Computers and Strucs., Vol. 8, pp. 533-543.

75. Timoshenko and Woinosky-Krieger, "Theory of Plates and Shells," McGraw-Hill Book Co., New York, 1959.

76. Wunderlich, W., "Incremental Formulations for Geometrically Non-linear Problems," Formulations and Comp Algorithms in F.E. Analysis, MIT Press, 1977.

77. Ramm, E., "A Plate/Shell Element for Large Deflections and Rotations," Formulations and Comp. Algorithms in F.E. Analysis, MIT Press, 1977.

78. Reissner, E., "On Stresses and Deformations in Toroidal Shells of Circular Cross-section which are Acted Upon by Uniform Normal Pressure," Qtr. Appl. Math, V 21, No. 3, 1963.

79. Prager, W., "Introduction to the Mechanics of Continua," Dover, 1973.

80. Vlasov, V.Z. and Leontev, N.N., "Beams, Plates and Shells on Elastic Foundations," NASA TT-F-357.

81. Haydl, H.M. and Sherbourne, A.N., "Elastic Buckling of Columns by Initial Parameter Method," Comp. and Struc., V. 6, 1976.

82. Fletcher, R. and Powell, M.J.D., "A Rapidly Convergent Descent Method for Minimization," Computer J., V. 6, 1963, pp. 163-168.

83. Irons, B. and Elsawaf, "The Conjugate Newton Algorithm for Solving Finite Element Equations," Formulations and Comp Algorithms in F.E. Analysis, MIT Press, 1977.

84. Bushnell, D., "BOSOR5 - Program for Buckling of Elastic-Plastic Complex Shells of Revolution Including Large Deflections and Creep," Comp and Struc., V. 6, pp. 221-239, 1976.

85. Bushnell, D., "Comparison of Test and Theory for Nonsymmetric Elastic-Plastic Buckling of Shells of Revolution," Int. J. Solids and Strucs, 1974, V. 10, pp. 1271-1286.

86. Fletcher, R. and Reeves, M., "Function Minimizations by Conjugate Gradients," Computer J., V. 7, 1964, pp. 149-154.

87. Jones, R.E. and Strome, D.R., "A Survey of Analysis of Shells by the Displacement Method," Proc. Conf. Matrix Meth in Struc Mech, Wright-Patterson Base, Oct. 1965.

88. Martin, H.C., "On the Derivation of Stiffness Matrices for the Analysis of Large Deflection and Stability Problems," Proc. Conf. Matrix Meth in Struc Mech, Wright-Patterson Base, Oct. 1965.

89. Kosko, E., "The Equivalence of Force and Displacement Methods in the Matrix Analysis of Elastic Structures," Proc. Conf. Matrix Meth in Struc. Mech., Wright-Patterson Base, Oct. 1965.

90. Pian, T.H., "Element Stiffness-Matrices for Boundary Compatibility and for Prescribed Boundary Stresses," Proc. Conf. Matrix Meth in Struc Mech., Wright-Patterson Base, Oct. 1965.

91. Koiter, W.T., "Elastic Stability and Post-buckling Behaviour," Proc. Symp. Nonlinear Probs. Ed. R.E. Langer, U. of Wisconsin, 1963.

92. Oden, J.T., "F.E. in Nonlinear Continua," McGraw-Hill, 1972.

93. Yaghmai, S., "Incremental Analysis of Deformation in Mechanics of Solids with Applications of Axisymmetric Shells of Revolution," Ph.D. Thesis, U. of Cal., Berkeley, 1968.

94. Altman, W. and Igut, F., "A Thin Cylinderical Shell Finite Element Based on a Mixed Formulation," Comp. and Struc., V 6, 1976, pp. 149-155.

95. Tong, P., "An Assumed Stress Hybrid Finite Element Method for an Incompressible Material," Int. J. Solids and Strucs., V. 5, pp. 455-461.

96. Reissner, E., "On Finite Bending of Pressurized Tubes," J. of Appl. Mech., Trans. ASME, V. 25, 1959.

97. Drucker, D.C., "A Discussion of the Theories of Plasticity," J. Aero Sci., V. 16, 1949.

98. Pian, T.H., "Derivation of Element Stiffness Matrices by Assumed Stress Distributions," AIAA Journal, V. 2, 1964.

99. Atluri, S.N. and Marakawa, H., "On Hybrid Finite Element Models in Nonlinear Solid Mechanics," Int. Conf. F.E. Nonlinear Solid and Struc Mech., Norway, 1977.

100. Bushnell, D., "Bifurcation Buckling of Shells of Revolution Including Large Deflections, Plasticity and Creep," Int. J. Solids and Strucs, V. 10, 1974, pp. 1287-1305.

101. Horrigmoe, G. and Eidsheim, O.M., "Hybrid Stress Finite Element Model for Elastic-Plastic Analysis," Int. Conf. F.E. Nonlinear Solid and Struc. Mech., Norway, 1977.

102. Washizu, K., "Variational Methods in Elasticity and Plasticity," Pergamon Press, 1968.

103. Tong, P. and Rossettos, J.N., "Finite Element Method," MIT Press, 1978.

104. Barnard, A.J. and Sharman, P.W., "Elastic Plastis Analysis Using Hybrid Stress Finite Elements," Int. Conf. F.E. Nonlinear Solid and Struc Mech., Norway, 1977.

105. Siddal, J.N., "Analytical Decision - Making in Engineering Design," Prentice-Hall, 1972.

106. Ramm, E. and Stegmuller, H., "The Displacement Finite Element in Nonlinear Buckling Analysis of Shells," Proc. of Colloquium on Buckling of Shells, Stuttgart, 1982. (Publ. Springer-Verlag, Ed. E. Ramm).

107. Kratzig, W.B. et.al., "Nonlinear Behaviour and Elastic Stability of Shells," Proc. of Colloquium on Buckling of Shells, Stuttgart, 1982. (Publ. Springer-Verlag, Ed.E. Ramm).

108. Resinger, F. and Greiner, R, "Buckling of Wind Loaded Cylinderical Shells ...," Proc. of Colloquium on Buckling of Shells, Stuttgart, 1982. (Publ. Springer-Verlag, Ed. E. Ramm).

109. Sall, H., "Bucking of Long Liquid-Filled Cylinderical Shells," Proc. of Colloquium on Buckling of Shells, Stuttgart, 1982, (Publ. Springer-Verlag, Ed. E. Ramm).

110. Pian, T.H. and Boland, P.L.," Formulation of Large Deflection Shell Analysis by Assumed Stress Finite Element Method," Formulations and Comp Algorithms in F.E. Analysis, ed. Bathe, Oden, Wunderlich, MIT Press, 1977.

111. Wennerstrom, H., "Nonlinear Shell Analysis Performed with Flat Elements," Int. Conf. Finite Elements in Nonlinear Mech., V. 1, Norwegian Inst. of Tech., Trondheim, 1977.

112. Yamada, Y. et.al., "Analysis of Large Deformation and Bifurcation in Plasticity Problems by the F.E. Method," Int. Conf. Finite Elements in Nonlinear Mech., V. 1, Norwegian Inst. of Tech., Trondheim, 1977.

113. Hangai, Y. and Kawamata, S., "Perturbation Method in the Analysis of Geometrically Nonlinear and Stability Problems," Adv. in Comp. Meth. in Struc Mech and Design, Ed. Oden, Clough, Yamamato, Univ. Alabama, Huntsville Press, 1972.

114. Stricklen, J.A., et.al., "Static Geometric and Material Nonlinear Analysis," Adv. in Comp. Meth in Struc Mech and Design, Ed. Oden, Clough, Yamamato, Univ. Alabama, Huntsville Press, 1972.

115. Yamada, Y., "Incremental Formulations for Problems with Geometric and Material Nonlinearity," Adv in Comp Meth in Struc Mech and Design, Ed. Oden, Clough, Yamamato, Univ. Alabama, Huntsville Press, 1972.

116. Oden, J.T., "Some Aspects of the Mathematical Theory of Finite Elements," Adv in Comp Meth in Struc Mech and Design, Ed. Oden, Clough, Yamamato, Univ. Alabama, Huntsville Press, 1972.

117. Washizu, K, "Some Considerations on Basic Theory of the Finite Element Method," Adv in Comp Meth in Struc Mech and Design, Ed. Oden, Clough, Yamamato, Univ. Alabama, Huntsville Press, 1972.

118. Felippa, C.A., "Basis for Formulation of Finite Element Models," Adv in Comp Meth in Struc Mech and Design, Ed. Oden, Clough, Yamamato, Univ. Alabama, Huntsville Press, 1972.

119. Cowper, G.R., "Variational Procedures and Convergence of Finite Element Methods," Num and Comp Meth in Struc Mech, ed. Fenves, Perrone, et.al., Academic Press, 1973.

120. Zienkiewicz, O.C., "Isoparametric and Allied Numerically Integrated Elements - A Review," Num and Comp Meth in Struc Mech, Ed., Fenves, Perrone, et.al., Academic Press, 1973.

121. Wilson, E.L., et.al., "Incompatible Displacement Models," Num and Comp Meth in Struc Mech, Ed., Fenves, Perrone, et.al., Academic Press, 1973.

122. Pian, T.H., "Hybrid Models," Num and Comp Meth in Struc Mech, Ed. Fenves, Perrone, et.al., Academic Press, 1973.

123. Argyris, J., et.al., "On the Large Displacement - SMall Strain Analysis of Strucs with Rotational dof," Comp Meth Appl Mech Eng, V. 14, 1978.

124. Pian, T.H. and Mau, S.T., "Some Recent Studies in Assumed Stress Hybrid Models," Adv in Comp Methods in Struc Mech and Design, Eds. Oden, Clough, Yamamato, Univ. of Albama, Huntsville Press, 1973.

125. Yokouchi, Y., et.al., "Finite Difference Solutions for Large Deformations of Cylinderical Shells - A Comparison with F.E. Solutions," Adv in Comp Methods in Struc Mech and Design, Eds. Oden, Clough, Yamamato, Univ. of Alabama, Huntsville Press, 1973.

126. Sander, G. and Carnoy, E., "Equilibrium and Mixed Formulations in Stability Analysis," Int. Conf. on F.E. in Nonlinear Solids and Struct. Mech., Norway, 1977.

127. Kroplin, B.H., "Postbuckling Instability of Shells using the Mixed Method," Proc. Colloq Buckling of Shells, Stuttgart, 1982.

128. Ramm, E., "Geometrisch Nichtlineare Elastostatik Und Finite Elemente," Bericht Nr 76-2, Univ. of Stuttgart, 1976.

129. Bornscheuer, F.W., "Case Studies of Shell Structures," Bericht Nr 79-3, U of Stuttgart, 1979.

130. Bergan and Clough, "Large Deflection of Plates and Shallow Shells using the Finite Element Method," Int J of Num Meth in Engg., V. 5, pp. 543-556, 1973.

131. Murray and Wilson, "Finite Element Deflection Analysis of Plates," J of Engg Mech Div., ASCE, V. 95, pp. 143-165, 1969.

132. Ramberg, W. and Osgood, W.R., "Description of Stress-Strain Curves by Three Parameters," TN 902, NACA, 1943.

133. Wilkinson, J.H., "Some Recent Advances in Numerical Algebra," Proc Conf on State of the Art in Num Analysis, A.P. Press, 1977, (ed. D. Jacobs).

134. Brodlie, K.W., "Unconstrained Minimization," Proc Conf on State of the Art in Num Analysis, A.P. Press, 1977. (ed. D. Jacobs).

135. Fletcher, R., "Methods for Solving Non-linearly Constrained Optimization Problems," Proc Conf on State of the Art in Num Analysis, A.P. Press, 1977. (ed. D. Jacobs).

136. Fox, L., "Finite Difference for Elliptic Boundary-Value Problems," Proc Conf on State of the Art in Num Analysis, A.P. Press, 1977. (ed. D. Jacobs).

137. Sandhu, R., "EM 839 Class Notes," OSU Spring 1983.

138. Bushnell, D., "Finite Difference Energy Models versus Finite Element Models," Num and Computer Meths in Struc Mech, Ed. Fenves, Perrone, Robinson, Schnobrich, Academic Press, 1973.

139. Argyris, J.H., et.al., "Elasto-Plastic Analysis of Finite Deformation Problems," Formulation of Large Deflection Shell Analysis by Assumed Stress Finite Element Method," Formulations and Comp Algorithms in F.E. Analysis, ed. Bathe, Oden, Wunderlich, MIT Press, 1977.

140. Crisfield, M.A., "Incremental/Iterative Solution Procedures for Nonlinear Struc Analysis," Num Meth for Non-Linear Problems, Pineridge, Swansea, 1980, pp. 261-290.

141. Brebbia, "The Boundary Element Method,".

142. Wood, J.D., "The Flexure of a Uniformly Pressurized Circular Cylindrical Shell," Report GM-TR-224(A), Contract No. AF18(600)-1190, The Ramo-Wooldridge Corporation, 1957.

143. Zopkres, W., Voce, S.J., Strickler, C.T., "Design Buckling Criteria for Cylinders and Truncated Cones of Small Semivertex Angle in the Low R/t and Z Parameter Ranges", Report EM 14-9, TRW Space Technology Lab, 1964.

144. Irons, B. and Ahmad, S., "Techniques of Finite Elements," J. Wiley, 1980.

145. Crisfield, M.A., "A Fast Incremental/Iterative Solution Procedure that Handles Snap-Through," Comp & Struc, Vo. 13, pp. 55-62.

146. Haisler, W.E., Stricklin, J.A., and Key, J.E., "Displacement Incrementation in Nonlinear Structural Analysis by the Self-Correcting Method," Int. J. Num. Meth. Engg., Vol. 11, pp. 3-10, 1977.

147. Wang, C., "Applied Elasticity," McGraw-Hill, 1953.

148. Housner, G.W. and Vreeland, T., "The Analysis of Stress and Deformation," Macmillan Press, 1966.

149. Ugural, A.C. and Fenster, S.K., "Advanced Strength and Applied Elasticity," Elsevier, 1979.